NOTE TO USERS

Simplified Decoding for a Quasi-Orthogonal Space-Time Code Family

Yunfei Deng

Department of Electrical & Computer Engineering
McGill University
Montreal, Canada

June 2004

A thesis submitted to the Faculty of Graduate Studies and Research in partial fulfillment to the requirements for the degree of Master of Engineering.

Your file Votre référence
ISBN: 0-494-06551-6
Our file Notre référence
ISBN: 0-494-06551-6

Abstract

This thesis considers simplified decoding for a type of full-rate non-orthogonal complex space-time block codes (STBCs) over Rayleigh fading channels. More precisely, we propose a decision feedback symbol-by-symbol decoding algorithm for the Quasi-Orthogonal code family, that comprises the Quasi-Orthogonal code and the Improved Quasi-Orthogonal code, by using the QR decomposition. Compared to optimal joint decoding, this algorithm significantly reduces complexity. For performance evaluations of the simplified decoding algorithm for the Quasi-Orthogonal code family over Rayleigh fading channels, we derive upper and lower bounds for symbol error rate. Furthermore, by using high SNR asymptotics we investigate the diversity orders provided by different decoding algorithms. The analysis shows that because of the relative constellation rotation, the diversity order provided by optimal decoding for the Improved Quasi-Orthogonal code is 4. Also, because of the error propagation in the decision feedback, the diversity order provided by the simplified decoding for the Improved Quasi-Orthogonal code is reduced to 2. All analytical results match well the associated computer simulations. Finally, we compare the performances of the simplified and optimal decoding for the Improved Quasi-Orthogonal code over correlated Rayleigh fading channels by using the "one-ring" channel model. Through computer simulations we show that the relative performance loss between the simplified and optimal decoding decreases as channel correlation increases. Therefore, the simplified decoding algorithm is suitable for highly spatially correlated Rayleigh fading channels.

Sommaire

Le sujet proposé dans cette thèse concerne le décodage simplifié d'un type de codes spatio-temporels en bloc pour des canaux à évanouissements de Rayleigh. Les codes spatio-temporels en considération sont complexes, à rendement plein ("full rate") et non orthogonaux. Plus précisément, nous proposons un algorithme de décodage symbole-par-symbole de rétroaction de décision pour la famille de codes quasi-orthogonaux comprenant le code quasi-orthogonal et le code quasi-orthogonal amélioré, et ce en utilisant une décomposition QR. Comparé à un décodage conjoint optimal, cet algorithme résulte en une réduction significative de complexité. Afin d'évaluer la performance de l'algorithme de décodage simplifié pour la famille de codes quasi-orthogonaux pour des canaux à évanouissements de Rayleigh, nous dérivons des bornes inférieures et supérieures pour le taux d'erreur par symbole. En outre, nous présentons une analyse des ordres de diversité fournis par les différents algorithmes de décodage moyennant une étude asymptotique avec un rapport signal-sur-bruit élevé. L'analyse des résultats montre qu'à cause de la rotation relative de la constellation, l'ordre de diversité obtenu par décodage optimal du code quasi-orthogonal amélioré est de 4. Par ailleurs, à cause de la propagation d'erreur dans la rétroaction de décision, l'ordre de diversité obtenu par décodage simplifié du code quasi-orthogonal amélioré se réduit à 2. La totalité des résultats analytiques coïncident bien avec ceux obtenus par simulations numériques. Finalement, nous comparons la performance des algorithmes de décodage simplifié et optimal pour codes quasi-orthogonaux améliorés pour des canaux à évanouissements de Rayleigh corrélés utilisant un modéle de canal "one-ring". Les simulations numériques montrent que la perte de performance relative entre le décodage simplifié et optimal diminue lorsque le niveau de corrélations dans le canal augmente. Par conséquent, l'algorithme de décodage simplifié est approprié pour les canaux à évanouissements de Rayleigh ayant un niveau élevé de corrélations spatiales.

Acknowledgments

Writing this thesis was a challenge to me. For a lot of times, it was thought as a mission impossible. I was so lucky that I met Prof. Harry Leib and completed the research and the thesis under his supervision. I can remember clearly the nights we spent together in discussing the problems like "the close form of error performance" and "the expression of upper and lower bounds". I owe my best thanks to him for his encouragements, supports, patience and understanding not only as a teacher but also as a good friend.

I am also grateful to Marine, Usa, Frederic, Marthe and all other wireless guys for providing helps in my graduate studies. Marthe 's translation of the abstract is greatly appreciated.

Specially, thanks are due to my parents and my fiancee. It is their love that help me survive the bitter and sweet years I spent at McGill University.

Notation

The following notation is used throughout the thesis.

- $j = \sqrt{-1}$.
- x^* is the complex conjugate of the variable x
- $\mathbf{x}^*$ is the complex conjugate of the vector $\mathbf{x}$
- $\mathbf{X}^*$ is the complex conjugate of the matrix $\mathbf{X}$
- $\mathrm{Re}(x)$ is the real part of the variable x
- $\mathrm{Im}(x)$ is the imaginary part of the variable x
- $\mathbf{X}^T$ is the transpose of the matrix $\mathbf{X}$
- $\mathbf{x}^T$ is the transpose of the vector $\mathbf{x}$
- $\mathbf{X}^H$ is the conjugate transpose of the matrix $\mathbf{X}$
- $\mathbf{x}^H$ is the conjugate transpose of the vector $\mathbf{x}$
- $\mathbf{I}$ is the identity matrix
- $\mathbf{0}$ is the zero matrix

Contents

List of Figures

List of Tables

List of Abbreviations

BER	Bit Error Rate
BS	Base Station
FER	Frame Error Rate
iff	if and only if
i.i.d	Independent identically distributed
LMMSE	Least Minimum Mean Square Error
MGF	Moment Generating Function
ML	Maximum Likelihood
MS	Mobile Station
MRRC	Maximal-Ration Receiver Combining
OD	Orthogonal Design
pdf	Probability density function
PSK	Phase-Shift Keying
QAM	Quadrature Amplitude Modulation
SEP	Symbol Error Probability
SER	Symbol Error Rate
SNR	Signal to Noise Ratio
STBC	Space-Time Block Code *or* Space-Time Block Coding
STTC	Space-Time Trellis Code *or* Space-Time Trellis Coding

Chapter 1

Introduction

1.1 Literature Review

In the past years, the world witnessed a significant progress in wireless communication technologies [1]-[9]. Among these technologies, *space-time coding* [5] [7], which provides reliable communications over fading channels by using multiple antennas, attracted much research interest [10]-[15]. It has been shown by Telatar [16], Foschini and Gans [17] that in rich scattering environments, the capacity of a multi-antenna communication system increases linearly with the minimum number of transmit and receive antennas when the signal to noise ratio (SNR) is sufficiently large. This indicates the possibility of significant capacity gains for multi-antenna systems, when compared to single-antenna systems. Furthermore, it provides the reason for exploring new channel coding schemes for multi-antenna systems.

Generally speaking, there are two types of space-time coding schemes, which are termed as *space-time trellis coding* (STTC) [5] and *space-time block coding* (STBC) [7]. In [5], Tarokh *et al* proposed STTC as an effective anti-fading technique for Rayleigh and Rician fading channels. Performance criteria, *coding* and *diversity gain*, for designing STTC over slow fading and frequency non-selective channels were derived in [5]. Alamouti [18] introduced a remarkable

simple coding scheme that employs two transmit antennas, and not only achieves full diversity gain, but also allows simple symbol-by-symbol maximum likelihood (ML) decoding. A generalization of Alamouti's scheme in form of STBCs were presented later in [7]. Using the *theory of orthogonal designs* [19] for code constructions of STBCs, Tarokh *et al* [7] proposed orthogonal STBCs for more than two transmit antennas. For orthogonal STBCs, the transmitted symbols can be decoded independently, thus the decoding complexity is comparable to un-coded system. For STTCs, the transmitted symbols are estimated jointly at the decoder, which leads to a higher decoding complexity when compared to un-coded system. Because of the lower decoding complexity at the mobile, we are more interested in code designs of orthogonal STBCs.

Two classes of orthogonal STBCs have been proposed: real orthogonal STBCs and complex orthogonal STBCs [7]. Real orthogonal STBCs are based on real orthogonal designs. The code matrices of real orthogonal STBCs are order N orthogonal designs with entries $\{\pm s_i,\ i = 1, ..., N\}$ taken from real (one dimensional) constellations such as PAM and BPSK. Complex orthogonal STBCs are based on complex orthogonal designs. The code matrices of complex orthogonal STBCs are order N orthogonal designs with entries $\{0, \pm s_i,\ i = 1, ..., N\}$ taken from complex (two dimensional) constellations such as QAM and MPSK ($M > 2$) or their conjugates $\{\pm s_i^*,\ i = 1, ..., N\}$ and products of these indeterminates with $j = \sqrt{-1}$. As illustrated in [7], orthogonal STBCs have the advantages of providing full code rate, full diversity order and simple symbol-by-symbol ML decoding. As far as bandwidth efficiency is concerned, complex orthogonal STBCs are more efficient than real STBCs. We define code rate as the ratio of the number of information bearing symbols in a codeword to the number of channel usages required to transmit a codeword. Complex orthogonal STBCs achieve higher bandwidth efficiency than real orthogonal STBCs assuming they have the same code rate. In modern wireless communications, we are seeking bandwidth efficient technologies, and hence we are more interested in complex orthogonal STBCs.

The existence of code designs for orthogonal STBCs was considered in [7] by using Radon

and Hurwitz theorem [21]. According to the *theory of existence of complex orthogonal designs*, a complex orthogonal STBC exists if and only if (iff) the order of the code matrix is 2. In other words, Alamouti's scheme is the unique complex orthogonal STBC. In order to explore new complex orthogonal STBCs, Tarokh *et al* [7] introduced coding schemes allowing linear processing, with which the entries of code matrix may be the linear combinations of $\{s_i, s_i^* \; i = 1, ..., N\}$ or products of these indeterminates with $j = \sqrt{-1}$. Later, Ganesan and Stoica [23] connected the complex orthogonal STBC designs with the *theory of amicable orthogonal designs*.

As proved by [7], a complex orthogonal STBC exists iff the order of code matrix is 2, i.e., only Alamouti's scheme exists. In the design of complex STBC other than Alamouti's scheme, we can not satisfy the requirements of full code rate and full orthogonality (which results in full diversity and symbol-by-symbol ML decoding) at the same time. In [24], Tirkkonen *et al* presented novel constructions for STBCs based on multi-modulation techniques that increase bandwidth efficiency. Such STBCs were then used as components in concatenated schemes. In [7], Tarokh *et al* introduced *generalized complex orthogonal designs*, which allow non-square code matrices. Furthermore, Tarokh *et al* [7] extended generalized complex orthogonal designs to *generalized complex linear processing orthogonal designs*, which allow the entries of code matrix to be linear combination of $\{s_i, s_i^* \; i = 1, ..., N\}$ or products of these indeterminates with $j = \sqrt{-1}$. It has been proved by Tarokh *et al* [7] that there exists full code rate generalized complex linear processing orthogonal designs for two transmit antennas. But whether or not there exists full code rate generalized complex linear processing orthogonal designs for more than two transmit antennas was unknown. In [25], Liang proved the nonexistence of full code rate complex orthogonal designs for more than two transmit antennas. Later, Liang and Xia [26] further demonstrated that no such full code rate generalized complex linear processing orthogonal designs exists for more than two transmit antennas. Through examples, Tarokh *et al* [7] proved that for any number of transmit antennas code rate 0.5 can be achieved with generalized complex orthogonal designs. In [7], by using generalized complex linear processing orthogonal designs, coding schemes for

3 and 4 transmit antennas that achieve code rate $3/4$ were proposed. Later in [23], Ganesan and Stoica, presented another coding scheme achieving code rate $3/4$ by employing *amicable orthogonal designs*.

As aforementioned, if we are going to ensure full code rate in a complex STBC design, besides Alamouti's scheme, the feature of full orthogonality must be sacrificed. In an effort of keeping full code rate, Tirkkonen *et al* [27] and Jafarkhani [28] proposed two types of full-rate and order-four non-orthogonal complex STBCs independently. Both of these two codes use Alamouti's scheme as construction blocks and provide diversity order of two in the one receive antenna system with ML decoding. Recently, Sharma and Papadias [29] improved the Quasi-Orthogonal code [28] through constellation rotations for some transmitted symbols. With this improvement, the diversity order provided by the code with ML decoding increases to four for one receive antenna.

Because of the loss of full orthogonality, optimal decoding of non-orthogonal complex STBCs can not be as simple as symbol-by-symbol decoding. Therefore, reduced-complexity decoding schemes for non-orthogonal complex STBCs are worth being developed. In [27], Tirkkonen *et al* proposed an easily implementable decoding scheme. This decoding scheme is based on iterative interference cancellation between parts of the code. The decoding scheme also employs a least minimum mean square error (LMMSE) technique when it constructs the decorrelation matrix inside the decoder. In [30], the sphere decoding algorithm was first introduced as a method for finding lattice vectors of short length. In [31], sphere decoding was presented as a near optimum method for space-time coded system. In this thesis, we will focus on the decoding of full-rate non-orthogonal complex STBC. A technique for simplified decoder will be proposed and the corresponding error performance will be analyzed.

1.2 Outline and Main Contributions of This Thesis

The remainder of this thesis is organized as follows.

Chapter 2 presents the background and rationale of space-time block coding. The system model, the decoding scheme and diversity criteria, the application of orthogonal designs to space-time block coding and the existence of complex orthogonal STBCs are addressed in this chapter. In chapter 3, we present a simplified decoding scheme for the Quasi-Orthogonal code family [28] [29]. Performances of the simplified and optimal decoding are evaluated analytically and are verified by computer simulations. In chapter 4, we consider the performances of the simplified decoding scheme over spatial-correlated channels by using the one-ring channel model [42]. We compare the performances of different decoding schemes over the channels with different correlation coefficients by computer simulations. Finally in chapter 5, we present conclusions. The main contributions of this thesis are:

1. We propose a simplified decoding scheme for Quasi-Orthogonal STBC family. By the use of the QR decomposition, this simplified decoding scheme realizes symbol-by-symbol with decision feedback decoding. The complexity of the simplified decoding, which is measured in terms of number of comparisons over all possible values after linear combinations, increases linearly with the size of modulation constellation size.

2. We evaluate the performances of simplified and optimal decoding over independent Rayleigh fading channels though mathematical analysis and computer simulations. By using asymptotical mathematical analysis, we proved that the diversity orders provided by optimal decoding of Quasi-Orthogonal and Improved Quasi-Orthogonal code are 2 and 4, respectively. The diversity orders provided by simplified decoding of Quasi-Orthogonal and Improved Quasi-Orthogonal code are both 2.

3. We compare the performances of different decoding schemes over spatially correlated channels by using the "one-ring" channel model [42]. It is shown that the performance gap

between optimal and simplified decoding decreases as channel correlation increases. Based on the comparisons, we conclude that the simplified decoding scheme is more suitable for the highly correlated channels.

Chapter 2

Space-Time Block Coding: Background and Rationale

2.1 Space-Time Block Coding

2.1.1 System Model and Coding Scheme

The system model of the STBC system proposed by Tarokh *et al* [7] is presented in Fig.2.1. All the descriptions and the analysis in the following chapters are based on this model unless specified. As shown in Fig.2.1, the transmitter is equipped with N antennas and the receiver is

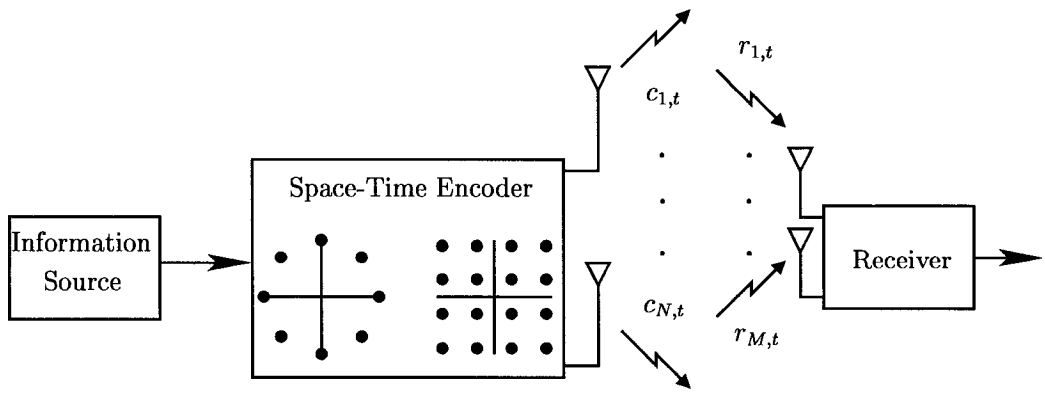

Fig. 2.1 Space-Time Block Coding

equipped with M antennas. We assume the duration of each codeword is D channel uses and the constellation employed by the space-time encoder is of size 2^Y. We also assume each codeword is made up of K symbols $\{s_1, ..., s_K\}$, which can be real or complex. The coding scheme is expressed as follows. In each period of D time slots, KY bits enter the space-time encoder and select symbols $\{s_1, ..., s_K\}$ from the constellation. Using these selected symbols, the space-time encoder generates an $N \times D$ code matrix

$$\mathbf{C} = \begin{pmatrix} c_{1,1} & c_{1,2} & \cdots & c_{1,D} \\ c_{2,1} & c_{2,2} & \cdots & c_{2,D} \\ \vdots & \vdots & \vdots & \vdots \\ c_{N,1} & c_{N,2} & \cdots & c_{N,D} \end{pmatrix} \tag{2.1}$$

For real STBC, the entries of the code matrix of (2.1) are linear combinations of zero and the real symbols $\{s_1, ..., s_K\}$. For complex STBC, the entries of the code matrix (2.1) are linear combinations of zero and complex symbols $\{s_1, ..., s_K, s_1^*, ..., s_K^*\}$ or products of these with $j = \sqrt{-1}$. At the t^{th} $(t = 1, ..., D)$ slot, the entries $c_{i,t}$'s $(i = 1, ..., N)$ of (2.1) are transmitted simultaneously from antennas $1, ..., N$. The code rate is defined as (Information Symbols)/(Channel Uses).

The transmission environment of space-time block codes is modeled as a quasi-static and flat fading wireless channel [7]. As shown in Fig.2.2, the whole system is described by

$$\mathbf{R} = \mathbf{AC} + \mathbf{N} \tag{2.2}$$

In (2.2), **R**, **A**, **C** and **N** denote the received signal, the channel coefficients, the code matrix and the noise over D time slots corresponding to a frame, respectively. The i^{th} row of **C** represents the symbols transmitted from the i^{th} transmit antenna and the t^{th} column of **C** represents the symbols

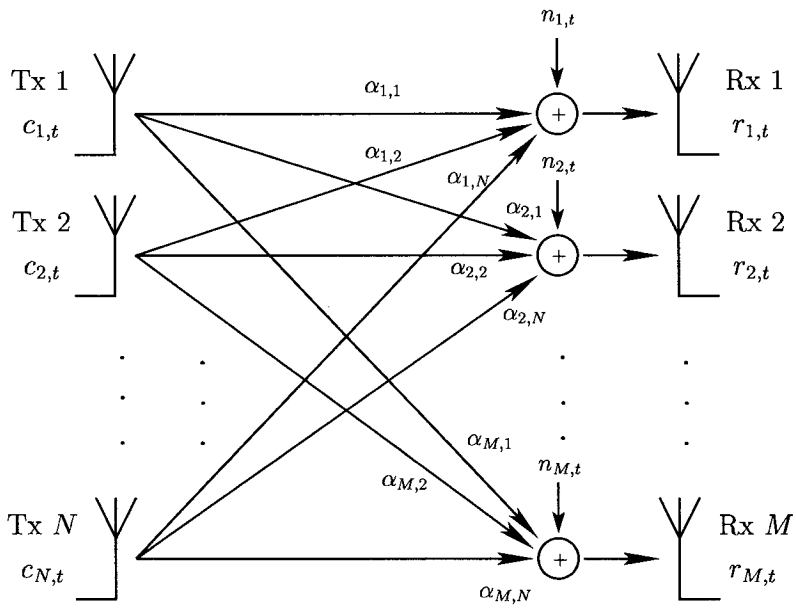

Fig. 2.2 Transmission Model of Space-Time Block Codes

transmitted at the t^{th} time slot. The channel coefficient matrix $\mathbf{A}$ is defined as

$$\mathbf{A} = \begin{pmatrix} \alpha_{1,1} & \alpha_{1,2} & \dots & \alpha_{1,N} \\ \alpha_{2,1} & \alpha_{2,2} & \dots & \alpha_{2,N} \\ \vdots & \vdots & \vdots & \vdots \\ \alpha_{M,1} & \alpha_{M,2} & \dots & \alpha_{M,N} \end{pmatrix} \tag{2.3}$$

where $\alpha_{j,i}$ $(j = 1, ..., M;\ i = 1, ..., N)$ denotes the channel fading coefficient from the i^{th} transmit antenna to the j^{th} receive antenna. The wireless channel is assumed to be quasi-static, i.e., the channel fading coefficients remain constant over a frame of length D and vary independently from one frame to another. The channel fading coefficients are modeled as i.i.d circularly symmetric complex Gaussian with zero mean and variance 0.5 for each component.

According to the previous definitions , we conclude that the received signal matrix $\mathbf{R}$ is an

$M \times D$ matrix

$$\mathbf{R} = \begin{pmatrix} r_{1,1} & r_{1,2} & \dots & r_{1,D} \\ r_{2,1} & r_{2,2} & \dots & r_{2,D} \\ \vdots & \vdots & \vdots & \vdots \\ r_{M,1} & r_{M,2} & \dots & r_{M,D} \end{pmatrix} \tag{2.4}$$

where the $(j,t)^{\text{th}}$ element of $\mathbf{R}$ represents the signal received by the j^{th} antenna at the t^{th} time slot and it is given by

$$r_{j,t} = \sum_{i=1}^{N} \alpha_{j,i} c_{i,t} + n_{j,t} \tag{2.5}$$

In (2.5), $n_{j,t}$ denotes the $(j,t)^{\text{th}}$ $(j = 1, ..., M;\ t = 1, ..., D)$ element of the noise matrix

$$\mathbf{N} = \begin{pmatrix} n_{1,1} & n_{1,2} & \dots & n_{1,D} \\ n_{2,1} & n_{2,2} & \dots & n_{2,D} \\ \vdots & \vdots & \vdots & \vdots \\ n_{M,1} & n_{M,2} & \dots & n_{M,D} \end{pmatrix} \tag{2.6}$$

and it represents the additive noise affecting the j^{th} receive antenna at the t^{th} time slot. The elements of $\mathbf{N}$ are modeled as independent samples of circularly symmetric complex Gaussian random variables with zero mean and variance $N_0/2$ for each component.

2.1.2 Decoding Scheme with Known Channel

Assuming that the channel state information is available, i.e., the receiver knows $\alpha_{1,i}$ $(i = 1, 2, 3, 4)$, by using ML decoding, the decoder computes the decision metric [7]

$$||\mathbf{R} - \mathbf{A}\tilde{\mathbf{C}}||^2 = \sum_{t=1}^{D} \sum_{j=1}^{M} \left| r_{j,t} - \sum_{i=1}^{N} \alpha_{j,i} \tilde{c_{i,t}} \right|^2 \tag{2.7}$$

over all possible codewords $\tilde{\mathbf{C}}$ and decides in favor of codeword $\hat{\mathbf{C}}$ that minimizes (2.7).

2.1.3 Diversity Advantage and Coding Advantage

When channel coefficients $\alpha_{1,i}$ $(i = 1, 2, 3, 4)$ are known at the receiver, the probability that the transmitted codeword C is decoded as $\hat{\mathbf{C}}$, where $\hat{\mathbf{C}} \neq \mathbf{C}$, over a Rayleigh channel is bounded by [5]

$$P(\mathbf{C} \rightarrow \hat{\mathbf{C}}; \hat{\mathbf{C}} \neq \mathbf{C}) \leq \Big(\prod_{i=1}^{R} \lambda_i\Big)^{-M} (E_s/4N_0)^{-RM} \tag{2.8}$$

In (2.8), R is the rank of the matrix $(\mathbf{C} - \hat{\mathbf{C}})(\mathbf{C} - \hat{\mathbf{C}})^H$ and $\{\lambda_i;\ i = 1, ..., R\}$ are none-zero eigenvalues of the matrix $(\mathbf{C} - \hat{\mathbf{C}})(\mathbf{C} - \hat{\mathbf{C}})^H$. By taking the logarithm on both sides of (2.8), we get

$$\log P(\mathbf{C} \rightarrow \hat{\mathbf{C}}; \hat{\mathbf{C}} \neq \mathbf{C}) \leq -RM\Big\{\log\big(\frac{E_s}{4N_0}\big) + \log\big(\prod_{i=1}^{R} \lambda_i\big)^{-\frac{1}{R}}\Big\} \tag{2.9}$$

In (2.9), RM is defined as diversity advantage and $\big(\prod_{i=1}^{R} \lambda_i\big)^{-\frac{1}{R}}$ is defined as coding advantage [5]. Assuming $R_{\min}$ is the minimum rank of $\mathbf{C} - \hat{\mathbf{C}}$ over any pair of distinct codewords, then from (2.9), the STBC achieves a diversity of $MR_{\min}$. From (2.9), we know that if we plot the decoding error probability curve in logarithm scale versus SNR (in dB). The slope of the curve indicates the diversity advantage and horizonal shift indicates the coding advantage.

2.2 Orthogonal Designs and Space-Time Block Codes

2.2.1 Definitions of Orthogonal Designs

A *real orthogonal design* [19] of order N and type $t_1, ..., t_L$, where t_i's are positive integers, is an $N \times N$ matrix $\mathbf{X_R}$ with entries from $\{0, \pm s_1, ..., \pm s_L\}$ satisfying

$$\mathbf{X_R}\mathbf{X_R}^T = \mathbf{X_R}^T\mathbf{X_R} = \Big(\sum_{i=1}^{L} t_i s_i^2\Big)\mathbf{I} \tag{2.10}$$

Alternatively, each row or each column of $\mathbf{X_R}$ has t_i entries of $\pm s_i$ and the rows or columns are orthogonal under the Euclidean inner product.

A *complex orthogonal design* $\mathbf{X_C}$ of order N and type $t_1, ..., t_L$ is an $N \times N$ matrix from $\{\pm s_1, ..., \pm s_L\}$, and their conjugates $\{\pm s_1^*, ..., \pm s_L^*\}$ or products of these indeterminates with $j = \sqrt{-1}$ satisfying

$$\mathbf{X_C}\mathbf{X_C}^H = \mathbf{X_C}^H\mathbf{X_C} = (\sum_{i=1}^{L} t_i|s_i|^2)\mathbf{I} \tag{2.11}$$

In the following discussions, we will take full code rate orthogonal designs, i.e. $L = N$, as examples unless specified.

2.2.2 Constructions of Real Orthogonal Designs

Let $\{\mathbf{X}_i;\ i = 1, ..., N\}$ be a set of $N \times N$ real matrices and let $\{s_i;\ i = 1, ..., N\}$ be a set of N real scalars, then we seek to represent a real orthogonal design $\mathbf{X_R}$ as

$$\mathbf{X_R} = \sum_{i=1}^{N} \mathbf{X}_i s_i \tag{2.12}$$

by deriving the required properties of $\{\mathbf{X}_i;\ i = 1, ..., N\}$ to enable such a representation. From (2.10) and (2.12), we have

$$\Big(\sum_{i=1}^{N} \mathbf{X}_i s_i\Big)^T \Big(\sum_{l=1}^{N} \mathbf{X}_l s_l\Big) = \sum_{i,l=1}^{N} \mathbf{X}_i^T \mathbf{X}_l s_i s_l = (\sum_{i=1}^{N} t_i s_i^2)\mathbf{I} \tag{2.13}$$

and

$$\Big(\sum_{i=1}^{N} \mathbf{X}_i s_i\Big)\Big(\sum_{l=1}^{N} \mathbf{X}_l s_l\Big)^T = \sum_{i,l=1}^{N} \mathbf{X}_i \mathbf{X}_l^T s_i s_l = (\sum_{i=1}^{N} t_i s_i^2)\mathbf{I} \tag{2.14}$$

For (2.13) and (2.14) to hold, the $\mathbf{X}_i$'s $(i = 1, ..., N)$ in (2.12) must satisfy

$$\mathbf{X}_i\mathbf{X}_l^T = \begin{cases} t_i\mathbf{I}; & \forall\ i = l \\ -\mathbf{X}_l\mathbf{X}_i^T; & \forall\ i \neq l. \end{cases} \quad \text{and} \quad \mathbf{X}_i^T\mathbf{X}_l = \begin{cases} t_i\mathbf{I}; & \forall\ i = l \\ -\mathbf{X}_l^T\mathbf{X}_i; & \forall\ i \neq l. \end{cases} \tag{2.15}$$

In other words, if we can find a group of $\mathbf{X}_i$'s satisfying the constraints listed in (2.15), we can easily construct a real orthogonal design by using (2.12). The existence of $\mathbf{X}_i$'s will be discussed lately by using theorem of Radon.

2.2.3 Constructions of Complex Orthogonal Designs

Let $\mathbf{A}_k$'s and $\mathbf{B}_k$'s $(k = 1, ..., N)$ be complex $N \times N$ matrices satisfying the requirements that will be derived later, we seek to represent a complex orthogonal design $\mathbf{X_C}$ as

$$\mathbf{X_C} = \sum_{k=1}^{N} \mathbf{A}_k s_k + \sum_{k=1}^{N} \mathbf{B}_k s_k^* \tag{2.16}$$

According to the definition, a complex orthogonal design $\mathbf{X_C}$ satisfies

$$\mathbf{X_C}^H\mathbf{X_C} = \mathbf{X_C}\mathbf{X_C}^H = \Big(\sum_{k=1}^{N} t_k|s_k|^2\Big)\mathbf{I} \tag{2.17}$$

From (2.16) and (2.17), we have

$$\begin{aligned} \mathbf{X_C}^H\mathbf{X_C} &= \Big(\sum_{k=1}^{N} \mathbf{A}_k s_k + \sum_{k=1}^{N} \mathbf{B}_k s_k^*\Big)^H \Big(\sum_{l=1}^{N} \mathbf{A}_l s_l + \sum_{l=1}^{N} \mathbf{B}_l s_l^*\Big) \\ &= \sum_{k,l=1}^{N} \big(\mathbf{A}_k^H\mathbf{A}_l + \mathbf{B}_l^H\mathbf{B}_k\big)s_k^* s_l + \sum_{k,l=1}^{N} \mathbf{A}_k^H\mathbf{B}_l s_k^* s_l^* + \sum_{k,l=1}^{N} \mathbf{B}_k^H\mathbf{A}_l s_k s_l \\ &= \Big(\sum_{k=1}^{N} t_k|s_k|^2\Big)\mathbf{I} \end{aligned} \tag{2.18}$$

and

$$\begin{aligned}\mathbf{X_C X_C}^H &= \Big(\sum_{k=1}^{N}\mathbf{A}_k s_k + \sum_{k=1}^{N}\mathbf{B}_k s_k^*\Big)\Big(\sum_{l=1}^{N}\mathbf{A}_l s_l + \sum_{l=1}^{N}\mathbf{B}_l s_l^*\Big)^H \\ &= \sum_{k,l=1}^{N}\big(\mathbf{A}_k\mathbf{A}_l^H + \mathbf{B}_l\mathbf{B}_k^H\big)s_k s_l^* + \sum_{k,l=1}^{N}\mathbf{A}_k\mathbf{B}_l^H s_k s_l + \sum_{k,l=1}^{N}\mathbf{B}_k\mathbf{A}_l^H s_k^* s_l^* \\ &= \Big(\sum_{k=1}^{N} t_k|s_k|^2\Big)\mathbf{I} \qquad (2.19)\end{aligned}$$

For (2.18) and (2.19) to hold, $\mathbf{A}_k$'s and $\mathbf{B}_k$'s in (2.16) must satisfy the following constrains

$$\mathbf{A}_k^H\mathbf{A}_l + \mathbf{B}_l^H\mathbf{B}_k = t_k\mathbf{I} \quad \mathbf{A}_k\mathbf{A}_l^H + \mathbf{B}_l\mathbf{B}_k^H = t_k\mathbf{I} \quad \forall\, k = l \qquad (2.20)$$

$$\mathbf{A}_k^H\mathbf{A}_l + \mathbf{B}_l^H\mathbf{B}_k = \mathbf{0} \quad \mathbf{A}_k\mathbf{A}_l^H + \mathbf{B}_l\mathbf{B}_k^H = \mathbf{0} \quad \forall\, k \neq l \qquad (2.21)$$

$$\mathbf{A}_k^H\mathbf{B}_l = -\mathbf{A}_l^H\mathbf{B}_k \forall\, k, l \qquad (2.22)$$

$$\mathbf{B}_k\mathbf{A}_l^H = -\mathbf{B}_l\mathbf{A}_k^H \quad \forall\, k, l \qquad (2.23)$$

If we have $\mathbf{A}_k$'s and $\mathbf{B}_k$'s satisfying the constraints listed in (2.20)-(2.23), we can construct a complex orthogonal design by using (2.16).

2.2.4 Application of Orthogonal Designs to STBCs

In [7], Tarokh *et al* applied orthogonal designs to the constructions of STBCs. In this application, the code matrix (2.1) is an orthogonal matrix of order N with entries from $\{\pm s_1, ..., \pm s_N\}$ for real orthogonal STBC, or an orthogonal matrix of order N with entries from $\{\pm s_1, ..., \pm s_N; \pm s_1^*, ..., \pm s_N^*\}$ or products of these with $\pm j$ for complex orthogonal STBC. Furthermore, all the types t_i's were assumed to be equal to t.

In describing the decoding algorithms of orthogonal STBCs, we consider a system with N transmit and one receive antenna for simplicity. In the decoding of real orthogonal STBCs,

according to (2.2) and (2.12), the received sample vector corresponding to the transmission of codeword $\mathbf{C}$ is given by

$$\begin{aligned}\mathbf{r}^T &= \mathbf{a}^T\mathbf{C} + \mathbf{n}^T = \sum_{i=1}^{N} s_i \mathbf{a}^T\mathbf{X}_i + \mathbf{n}^T = (s_1, ..., s_N)\begin{pmatrix} \mathbf{a}^T\mathbf{X}_1 \\ \vdots \\ \mathbf{a}^T\mathbf{X}_N \end{pmatrix} + \mathbf{n}^T \\ &= \mathbf{s}^T\mathbf{H} + \mathbf{n}^T \end{aligned} \tag{2.24}$$

where

$$\mathbf{H} = \begin{pmatrix} \mathbf{a}^T\mathbf{X}_1 \\ \vdots \\ \mathbf{a}^T\mathbf{X}_N \end{pmatrix} \tag{2.25}$$

By taking conjugates of both sides of (2.24), we get

$$\mathbf{r}^H = \mathbf{s}^T\mathbf{H}^* + \mathbf{n}^H \tag{2.26}$$

From(2.24) and (2.26), we have

$$\mathbf{r}^T\mathbf{H}^H + \mathbf{r}^H\mathbf{H}^T = \mathbf{s}^T(\mathbf{H}\mathbf{H}^H + \mathbf{H}^*\mathbf{H}^T) + \mathbf{n}^T\mathbf{H}^H + \mathbf{n}^H\mathbf{H}^T \tag{2.27}$$

We can write (2.27) in the form

$$\breve{\mathbf{r}}^T = \mathbf{s}^T\breve{\mathbf{H}} + \breve{\mathbf{n}}^T \tag{2.28}$$

where

$$\breve{\mathbf{r}}^T = \mathbf{r}^T\mathbf{H}^H + \mathbf{r}^H\mathbf{H}^T \tag{2.29}$$

$$\breve{\mathbf{H}} = \mathbf{H}\mathbf{H}^H + \mathbf{H}^*\mathbf{H}^T \tag{2.30}$$

and

$$\breve{\mathbf{n}}^T = \mathbf{n}^T\mathbf{H}^H + \mathbf{n}^H\mathbf{H}^T \tag{2.31}$$

The purpose of the operations in (2.27) is to make a preparation for symbol-by-symbol decoding. As we will prove later, the realization of symbol-by-symbol decoding depends on the construction features of real orthogonal designs as listed in (2.15). According to (2.15), (2.30) and (2.31), when the channel coefficients $\alpha_{1,n}$'s $(n = 1, 2, 3, 4)$ are known, the $(i, j)^{\text{th}}$ element of $\breve{\mathbf{H}}$ is

$$\begin{aligned}\breve{\mathbf{H}}(i,j) &= \mathbf{a}^T\mathbf{X}_i(\mathbf{a}^T\mathbf{X}_j)^H + \mathbf{a}^H\mathbf{X}_i(\mathbf{a}^T\mathbf{X}_j)^T = \mathbf{a}^T\left(\mathbf{X}_i\mathbf{X}_j^T + \mathbf{X}_j\mathbf{X}_i^T\right)\mathbf{a}^* \\ &= \begin{cases} 2t\sum_{n=1}^{N}|\alpha_{1,n}|^2; & \forall\ i = j \\ 0; & \forall\ i \neq j. \end{cases}\end{aligned} \tag{2.32}$$

and the covariance matrix of the noise $\breve{\mathbf{n}}$ is

$$\begin{aligned}&E\left\{\left(\mathbf{n}^T\mathbf{H}^H + \mathbf{n}^H\mathbf{H}^T\right)^H\left(\mathbf{n}^T\mathbf{H}^H + \mathbf{n}^H\mathbf{H}^T\right)\Big|\ \alpha_{1,n}\ n = 1, ..., N\right\} \\ = \ &\mathbf{H}E\left\{\mathbf{n}^*\mathbf{n}^T\right\}\mathbf{H}^H + \mathbf{H}^*E\left\{\mathbf{n}\mathbf{n}^H\right\}\mathbf{H}^T + \mathbf{H}^*E\left\{\mathbf{n}\mathbf{n}^T\right\}\mathbf{H}^H + \mathbf{H}E\left\{\mathbf{n}^*\mathbf{n}^H\right\}\mathbf{H}^T\end{aligned} \tag{2.33}$$

We know that the real and the imaginary parts of the elements in $\mathbf{n}$ are modeled as independent samples of zero-mean Gaussian with variance σ^2 per complex dimension, so

$$E\left\{\mathbf{n}\mathbf{n}^T\right\} = E\left\{\mathbf{n}^*\mathbf{n}^H\right\} = 0 \tag{2.34}$$

From (2.33) and (2.34), we have

$$\begin{aligned} & E\Big\{\left(\mathbf{n}^T\mathbf{H}^H+\mathbf{n}^H\mathbf{H}^T\right)^H\left(\mathbf{n}^T\mathbf{H}^H+\mathbf{n}^H\mathbf{H}^T\right)\Big|\ \alpha_{1,n}\ \ n=1,...,N\Big\} \\ = \ & \mathbf{H}E\Big\{\mathbf{n}^*\mathbf{n}^T\Big\}\mathbf{H}^H+\mathbf{H}^*E\Big\{\mathbf{n}\mathbf{n}^H\Big\}\mathbf{H}^T \\ = \ & \begin{cases} 4\sigma^2 t\sum_{n=1}^{N}|\alpha_{1,n}|^2; & \forall\ i=j \\ 0; & \forall\ i\neq j. \end{cases} \end{aligned} \tag{2.35}$$

which is a diagonal matrix with identical diagonal elements. So the elements of $\breve{\mathbf{n}}$ are i.i.d complex Gaussian. From (2.32) and (2.35), ML decoding of real orthogonal STBCs can be decoupled into symbol-by-symbol decoding. In decoding the symbol s_i $(i=1,...,N)$, the receiver chooses the value for $\tilde{s}_i$ that minimizes

$$\left|\breve{r}_{i,1}-2t\sum_{n=1}^{N}|\alpha_{1,n}|^2\tilde{s}_i\right|^2 \tag{2.36}$$

For complex orthogonal STBCs, we have from (2.2) and (2.16)

$$\begin{aligned} \mathbf{r}^T &= \mathbf{a}^T\mathbf{C}+\mathbf{n}^T \\ &= \sum_{i=1}^{N}s_i\mathbf{a}^T\mathbf{A}_i+\sum_{i=1}^{N}s_i^*\mathbf{a}^T\mathbf{B}_i+\mathbf{n}^T=(s_1,...,s_N)\begin{pmatrix}\mathbf{a}^T\mathbf{A}_1\\ \vdots\\ \mathbf{a}^T\mathbf{A}_N\end{pmatrix}+(s_1^*,...,s_N^*)\begin{pmatrix}\mathbf{a}^T\mathbf{B}_1\\ \vdots\\ \mathbf{a}^T\mathbf{B}_N\end{pmatrix}+\mathbf{n}^T \\ &= \mathbf{s}^T\mathbf{H}_\mathbf{A}+\mathbf{s}^H\mathbf{H}_\mathbf{B}+\mathbf{n}^T \end{aligned} \tag{2.37}$$

where

$$\mathbf{H}_\mathbf{A}=\begin{pmatrix}\mathbf{a}^T\mathbf{A}_1\\ \vdots\\ \mathbf{a}^T\mathbf{A}_N\end{pmatrix} \tag{2.38}$$

and

$$\mathbf{H_B} = \begin{pmatrix} \mathbf{a}^T\mathbf{B}_1 \\ \vdots \\ \mathbf{a}^T\mathbf{B}_N \end{pmatrix} \tag{2.39}$$

By conjugating both sides of (2.37), we get

$$\mathbf{r}^H = \mathbf{s}^T\mathbf{H_B}^* + \mathbf{s}^H\mathbf{H_A}^* + \mathbf{n}^H \tag{2.40}$$

From (2.37) and (2.40), we let

$$\begin{aligned} \breve{\mathbf{r}}^T &= \mathbf{r}^T\mathbf{H_A}^H + \mathbf{r}^H\mathbf{H_B}^T \\ &= \mathbf{s}^T(\mathbf{H_A}\mathbf{H_A}^H + \mathbf{H_B}^*\mathbf{H_B}^T) + \mathbf{s}^H(\mathbf{H_B}\mathbf{H_A}^H + \mathbf{H_A}^*\mathbf{H_B}^T) + \mathbf{n}^T\mathbf{H_A}^H + \mathbf{n}^H\mathbf{H_B}^T \\ &= \mathbf{s}^T\mathbf{H_C} + \mathbf{s}^H\mathbf{H_D} + \mathbf{n_C}^T \end{aligned} \tag{2.41}$$

From (2.20)-(2.23) and (2.41), the $(i,j)^{\text{th}}$ element of $\mathbf{H_C}$ is

$$\begin{aligned} \mathbf{H_C}(i,j) &= \mathbf{a}^T\mathbf{A}_i(\mathbf{a}^T\mathbf{A}_j)^H + \mathbf{a}^H\mathbf{B}_i^*(\mathbf{a}^T\mathbf{B}_j)^T = \mathbf{a}^T(\mathbf{A}_i\mathbf{A}_j^H + \mathbf{B}_j\mathbf{B}_i^H)\mathbf{a}^* \\ &= \begin{cases} t\sum_{n=1}^{N}|\alpha_{1,n}|^2; & \forall\ i=j \\ 0; & \forall\ i\neq j. \end{cases} \end{aligned} \tag{2.42}$$

and the $(i,j)^{\text{th}}$ element of $\mathbf{H_D}$ is

$$\begin{aligned} \mathbf{H_D}(i,j) &= \mathbf{a}^T\mathbf{B}_i(\mathbf{a}^T\mathbf{A}_j)^H + \mathbf{a}^H\mathbf{A}_i^*(\mathbf{a}^T\mathbf{B}_j)^T = \mathbf{a}^T(\mathbf{B}_i\mathbf{A}_j^H + \mathbf{B}_j\mathbf{A}_i^H)\mathbf{a}^* \\ &= 0 \qquad \forall\ i,j \end{aligned} \tag{2.43}$$

Also, the covariance matrix of $\mathbf{n_C}$ is

$$\begin{aligned} & E\Big\{\left(\mathbf{n}^T\mathbf{H_A}^H+\mathbf{n}^H\mathbf{H_B}^T\right)^H\left(\mathbf{n}^T\mathbf{H_A}^H+\mathbf{n}^H\mathbf{H_B}^T\right)\Big|\ \alpha_{1,n}\ \ n=1,...,N\Big\} \\ = \ & \mathbf{H_A}E\Big\{\mathbf{n}^*\mathbf{n}^T\Big\}\mathbf{H_A}^H+\mathbf{H_B}^*E\Big\{\mathbf{n}\mathbf{n}^H\Big\}\mathbf{H_B}^T \\ = \ & \begin{cases} 2\sigma^2 t\sum_{n=1}^{N}|\alpha_{1,n}|^2; & \forall\ i=j \\ 0; & \forall\ i\neq j. \end{cases} \end{aligned} \tag{2.44}$$

which is a diagonal matrix with identical diagonal elements, so the elements of $\mathbf{n_C}$ are i.i.d complex Gaussian. From (2.42)-(2.44), ML decoding of complex orthogonal STBCs can be decoupled into symbol-by-symbol decoding. In the decoding of symbol s_i $(i=1,...,N)$, the receiver chooses the value for $\tilde{s}_i$ that minimizes

$$\left|\breve{r}_{i,1}-t\sum_{n=1}^{N}|\alpha_{1,n}|^2\tilde{s}_i\right|^2 \tag{2.45}$$

as the decoding result. It will be proven later that for complex orthogonal STBCs, the symbol-by-symbol decoding algorithm presented above is optimal. The analysis of real orthogonal code is similar and simpler, and therefore will be omitted.

Theorem: For Complex Orthogonal STBCs, the Symbol-by-Symbol Decoding Algorithm is Optimal

Proof: We take the STBC with entries $\{s_i, s_i^*;\ i=1,...,N\}$ or products of these indeterminates with $j=\sqrt{-1}$. Assuming the transmitted codeword is $\mathbf{C}$, from (2.7), an ML receiver selects value for $\tilde{\mathbf{C}}$ over all possible codewords that minimizes

$$\left|\left|\,\mathbf{r}^T-\mathbf{a}^T\tilde{\mathbf{C}}\,\right|\right|^2 \tag{2.46}$$

We know that

$$||\mathbf{r}^T - \mathbf{a}^T\tilde{\mathbf{C}}||^2 = ||\mathbf{a}^T(\mathbf{C} - \tilde{\mathbf{C}}) + \mathbf{n}^T||^2$$
$$= \mathbf{a}^T(\mathbf{C} - \tilde{\mathbf{C}})(\mathbf{C} - \tilde{\mathbf{C}})^H\mathbf{a}^* + \mathbf{n}^T\mathbf{n}^* + \mathbf{a}^T(\mathbf{C} - \tilde{\mathbf{C}})\mathbf{n}^* + \mathbf{n}^T(\mathbf{C} - \tilde{\mathbf{C}})^H\mathbf{a}^* \quad (2.47)$$

From (2.17), we have

$$\mathbf{a}^T(\mathbf{C} - \tilde{\mathbf{C}})(\mathbf{C} - \tilde{\mathbf{C}})^H\mathbf{a}^* = \Big(t\sum_{n=1}^{N}|\alpha_{1,n}|^2\Big)\Big(\sum_{k=1}^{N}|s_k - \tilde{s_k}|^2\Big) \quad (2.48)$$

From (2.37), we have

$$\mathbf{a}^T(\mathbf{C} - \tilde{\mathbf{C}})\mathbf{n}^* = \Big[(\mathbf{s} - \tilde{\mathbf{s}})^T\mathbf{H_A} + (\mathbf{s} - \tilde{\mathbf{s}})^H\mathbf{H_B}\Big]\mathbf{n}^* \quad (2.49)$$

and

$$\mathbf{n}^T(\mathbf{C} - \tilde{\mathbf{C}})^H\mathbf{a}^* = (\mathbf{a}^T(\mathbf{C} - \tilde{\mathbf{C}})\mathbf{n}^*)^H = \mathbf{n}^T\Big[\mathbf{H_A}^H(\mathbf{s} - \tilde{\mathbf{s}})^* + \mathbf{H_B}^H(\mathbf{s} - \tilde{\mathbf{s}})\Big] \quad (2.50)$$

Combining (2.48), (2.49) and (2.50) results in

$$\Big(t\sum_{n=1}^{N}|\alpha_{1,n}|^2\Big)\Big(\sum_{k=1}^{N}|s_k - \tilde{s_k}|^2\Big) + \mathbf{n}^T\mathbf{n}^* + \Big[(\mathbf{s} - \tilde{\mathbf{s}})^T\mathbf{H_A} + (\mathbf{s} - \tilde{\mathbf{s}})^H\mathbf{H_B}\Big]\mathbf{n}^*$$
$$+\mathbf{n}^T\Big[\mathbf{H_A}^H(\mathbf{s} - \tilde{\mathbf{s}})^* + \mathbf{H_B}^H(\mathbf{s} - \tilde{\mathbf{s}})\Big] \quad (2.51)$$

According to (2.45), for complex orthogonal codes, symbol-by-symbol decoding can be considered as taking the vector $\hat{\mathbf{s}}$ made up of symbols $\hat{s_k}$ $(k = 1, ..., N)$ for $\tilde{\mathbf{s}}$ that minimizes the metric

$$||\mathbf{r_C}^T - \tilde{\mathbf{s}}^T\mathbf{H_C}||^2 = ||(\mathbf{s} - \tilde{\mathbf{s}})^T\mathbf{H_C} + \mathbf{n_C}^T||^2 \quad (2.52)$$

as the decoding result. Because

$$
\begin{aligned}
& ||(\mathbf{s}-\tilde{\mathbf{s}})^T\mathbf{H_C}+\mathbf{n_C}^T||^2 \\
= & \Big((\mathbf{s}-\tilde{\mathbf{s}})^T\mathbf{H_C}+\mathbf{n_C}^T\Big)\Big(\mathbf{H_C}^H(\mathbf{s}-\tilde{\mathbf{s}})^*+\mathbf{n_C}^*\Big) \\
= & \Big(t\sum_{n=1}^{N}|\alpha_{1,n}|^2\Big)^2\sum_{k=1}^{K}|s_k-\tilde{s_k}|^2+t\sum_{n=1}^{N}|\alpha_{1,n}|^2\mathbf{n}^T\mathbf{n}^*+t\sum_{n=1}^{N}|\alpha_{1,n}|^2\big(\mathbf{n_C}^T(\mathbf{s}-\tilde{\mathbf{s}})^*+(\mathbf{s}-\tilde{\mathbf{s}})^T\mathbf{n_C}^*\big) \\
= & \Big(t\sum_{n=1}^{N}|\alpha_{1,n}|^2\Big)^2\sum_{k=1}^{K}|s_k-\tilde{s_k}|^2+t\sum_{n=1}^{N}|\alpha_{1,n}|^2\mathbf{n}^T\mathbf{n}^*+t\sum_{n=1}^{N}|\alpha_{1,n}|^2\Big(\Big[(\mathbf{s}-\tilde{\mathbf{s}})^T\mathbf{H_A} \\
& +(\mathbf{s}-\tilde{\mathbf{s}})^H\mathbf{H_B}\Big]\mathbf{n}^*+\mathbf{n}^T\Big[\mathbf{H_A}^H(\mathbf{s}-\tilde{\mathbf{s}})^*+\mathbf{H_B}^H(\mathbf{s}-\tilde{\mathbf{s}})\Big]\Big) \\
= & \ t\sum_{n=1}^{N}|\alpha_{1,n}|^2\Big(||\mathbf{r}^T-\mathbf{a}^T\tilde{\mathbf{C}}||^2\Big)
\end{aligned}
\tag{2.53}
$$

so minimizing the metric (2.52) is equivalent to minimizing the metric (2.46). Then we conclude that for complex orthogonal codes, the results obtained from symbol-by-symbol decoding are optimal. Q.E.D.

According to the diversity criterion mentioned in section 2.1.3, in order to achieve maximal diversity over the Rayleigh fading channel, the difference matrix of orthogonal design $\mathbf{X}$ from two distinct groups of symbols as $(\tilde{s_1},...,\tilde{s_N})$ and $(s_1,...,s_N)$ should be non-singular. Because $\mathbf{X}(\tilde{s_1},...,\tilde{s_N})-\mathbf{X}(s_1,...,s_N)=\mathbf{X}(\tilde{s_1}-s_1,...,\tilde{s_N}-s_N)$ [7] , where $\mathbf{X}(\tilde{s_1}-s_1,...,\tilde{s_N}-s_N)$ is constructed from $\mathbf{X}$ by replacing s_i with $\tilde{s_i}-s_i$ for all i. From the definition of orthogonal designs,

$$
\det(\mathbf{X}\mathbf{X}^H)^{1/2}=\Big(\sum_{i=1}^{N}t_i|s_i|^2\Big)^{N/2} \tag{2.54}
$$

Accordingly,

$$
\det\Big(\mathbf{X}(\tilde{s_1}-s_1,...,\tilde{s_N}-s_N)\mathbf{X}(\tilde{s_1}-s_1,...,\tilde{s_N}-s_N)^H\Big)^{1/2}=\Big(\sum_{i=1}^{N}t_i|\tilde{s_i}-s_i|^2\Big)^{N/2} \tag{2.55}
$$

which is non-zero. That means $\mathbf{X}(\tilde{s_1}-s_1,...,\tilde{s_N}-s_N)$ is nonsingular and the maximum diversity

order is achieved.

2.2.5 Alamouti's Scheme: A Brief Review

In [18], Alamouti proposed a remarkable coding scheme which has been cited frequently for its simplicity and good performance. Here, we take a brief review of Alamouti's scheme as an example of complex orthogonal STBC.

Alamouti's scheme employs two transmit antennas and the code matrix is presented as

$$\begin{pmatrix} s_1 & -s_2^* \\ s_2 & s_1^* \end{pmatrix} \tag{2.56}$$

This scheme also assumes that the channel is quasi-static, i.e., the channel fading coefficients remain constant over 2 time slots. We assume that the receiver employs one antenna. The result can be easily extended to a multiple receiver antenna system. From (2.2), the system model is written as

$$\begin{aligned} \mathbf{r_A}^T = \begin{pmatrix} r_{1,1} & r_{1,2} \end{pmatrix} &= \begin{pmatrix} \alpha_{1,1} & \alpha_{1,2} \end{pmatrix} \begin{pmatrix} s_1 & -s_2^* \\ s_2 & s_1^* \end{pmatrix} + \begin{pmatrix} n_{1,1} & n_{1,2} \end{pmatrix} \\ &= \begin{pmatrix} s_1 & s_2 \end{pmatrix} \begin{pmatrix} \alpha_{1,1} & 0 \\ \alpha_{1,2} & 0 \end{pmatrix} + \begin{pmatrix} s_1^* & s_2^* \end{pmatrix} \begin{pmatrix} 0 & \alpha_{1,2} \\ 0 & -\alpha_{1,1} \end{pmatrix} + \begin{pmatrix} n_{1,1} & n_{1,2} \end{pmatrix} \\ &= \mathbf{s}^T \mathbf{H_E} + \mathbf{s}^H \mathbf{H_F} + \mathbf{n}^T \end{aligned} \tag{2.57}$$

where

$$\mathbf{H_E} = \begin{pmatrix} \alpha_{1,1} & 0 \\ \alpha_{1,2} & 0 \end{pmatrix} \tag{2.58}$$

and

$$\mathbf{H_F} = \begin{pmatrix} 0 & \alpha_{1,2} \\ 0 & -\alpha_{1,1} \end{pmatrix} \tag{2.59}$$

By conjugating both sides of (2.57), we have

$$\mathbf{r_A}^H = \begin{pmatrix} r_{1,1}^* & r_{1,2}^* \end{pmatrix} = \begin{pmatrix} s_1 & s_2 \end{pmatrix} \begin{pmatrix} 0 & \alpha_{1,2}^* \\ 0 & -\alpha_{1,1}^* \end{pmatrix} + \begin{pmatrix} s_1^* & s_2^* \end{pmatrix} \begin{pmatrix} \alpha_{1,1}^* & 0 \\ \alpha_{1,2}^* & 0 \end{pmatrix} + \begin{pmatrix} n_{1,1}^* & n_{1,2}^* \end{pmatrix} \tag{2.60}$$

Then

$$\begin{aligned} \mathbf{r_A}^T \mathbf{H_E}^H + \mathbf{r_A}^H \mathbf{H_F}^T &= \Big(\sum_{i=1}^{2} |\alpha_{1,i}|^2\Big)\begin{pmatrix} s_1 & s_2 \end{pmatrix} + \begin{pmatrix} \alpha_{1,1}^* n_{1,1} + \alpha_{1,2} n_{1,2}^* & \alpha_{1,2}^* n_{1,1} - \alpha_{1,1} n_{1,2}^* \end{pmatrix} \\ &= \sum_{i=1}^{2} |\alpha_{1,i}|^2 \mathbf{s}^T + \mathbf{n_A}^T \end{aligned} \tag{2.61}$$

The covariance matrix of $\mathbf{n_A}$ is

$$E\big(\mathbf{n_A}\mathbf{n_A}^H\big) = 2\sigma^2 \sum_{i=1}^{2} |\alpha_{1,i}|^2 \mathbf{I} \tag{2.62}$$

which means the elements of $\mathbf{n_A}$ are i.i.d complex Gaussian. From (2.61) and (2.62), we define

$$\breve{\mathbf{r}}_\mathbf{A} = \mathbf{r_A}^T \mathbf{H_E}^H + \mathbf{r_A}^H \mathbf{H_F}^T \tag{2.63}$$

and re-write (2.61) as

$$\begin{pmatrix} \breve{r}_{A\,1,1} \\ \breve{r}_{A\,2,1} \end{pmatrix} = \begin{pmatrix} \sum_{i=1}^{2} |\alpha_{1,i}|^2 & 0 \\ 0 & \sum_{i=1}^{2} |\alpha_{1,i}|^2 \end{pmatrix} \begin{pmatrix} s_1 \\ s_2 \end{pmatrix} + \begin{pmatrix} n_{A\,1,1} \\ n_{A\,2,1} \end{pmatrix} \tag{2.64}$$

From (2.64), we have

$$\breve{r}_{A\,1,1} = \sum_{i=1}^{2} |\alpha_{1,i}|^2 s_1 + n_{A\,1,1} \tag{2.65}$$

and

$$\breve{r}_{A\,2,1} = \sum_{i=1}^{2} |\alpha_{1,i}|^2 s_2 + n_{A\,2,1} \tag{2.66}$$

By using ML decoding for s_1, the receiver chooses the value for $\tilde{s_1}$ that minimizes

$$d^2(\breve{r}_{A\,1,1}, \tilde{s_1}) \tag{2.67}$$

In decoding s_2, the receiver chooses the value for $\tilde{s_2}$ that minimizes

$$d^2(\breve{r}_{A\,2,1}, \tilde{s_2}) \tag{2.68}$$

2.3 Existence of Full Code Rate Orthogonal Designs

In discussing the existence of full code rate orthogonal designs, we introduce Hurwitz-Radon numbers $\rho(N)$ defined as follows.

If $N = 2^a(2b+1)$ and $a = 4c + d$, where a, b, c, and d are integers with $0 \leq d < 4$, then $\rho(N) = 8c + 2^d$. The equivalent and more convenient way to describe Hurwitz-Radon numbers is:

$$\rho(N) = \rho[2^a(2b+1)] = \begin{cases} 2a+1; & \text{if } a \equiv 0(\text{mod}4) \\ 2a; & \text{if } a \equiv 1(\text{mod}4) \\ 2a; & \text{if } a \equiv 2(\text{mod}4) \\ 2a+2; & \text{if } a \equiv 3(\text{mod}4) \end{cases} \tag{2.69}$$

We denote a set of $N \times N$ matrices $\{\mathrm{M}_i | i = 1, ..., K\}$ have the property that the linear

combinations

$$\kappa_1 \mathbf{M}_1 + \kappa_2 \mathbf{M}_2 + ... + \kappa_K \mathbf{M}_K \tag{2.70}$$

with real coefficients κ_i are nonsingular matrices except when all coefficients κ_i are zeros. We also denote $R(N)$ and $C(N)$ as the maximum K for which there exists such a real or complex matrix set with the above property, respectively.

The following Adams-Lax-Philips Theorem [20] determines the number for $R(N)$ and $C(N)$ by using Hurwitz-Radon numbers.

Adams-Lax-Philips Theorem: We have

$$R(N) = \rho(N) \tag{2.71}$$

$$C(N) = C[2^a(2b+1)] = 2a+2 \tag{2.72}$$

From Adams-Lax-Philips Theorem, we can get the maximal order of real and complex orthogonal designs that achieve full code rate. Actually, Adams-Lax-Philips Theorem is based on the corollaries obtained by Radon[21] and Hurwitz [22] by using a detail matrix analysis.

Corollary 1[21]: The maximum number L with the property that the $N \times N$ real matrix expressed by

$$\mathbf{X_R} = \sum_{i=1}^{L} \mathbf{X}_i s_i \tag{2.73}$$

where $\mathbf{X}_i$'s are order N real matrices, satisfies (2.10) is $R(N) = \rho(N)$.

Corollary 2[22]: The maximum number L with the property that the $N \times N$ complex matrix expressed by

$$\mathbf{X_C} = \sum_{i=1}^{L} \mathbf{A}_i s_i + \sum_{i=1}^{L} \mathbf{B}_i s_i^* \tag{2.74}$$

where $\mathbf{A}_i$'s and $\mathbf{B}_i$'s are order N complex matrices, satisfies (2.11) is $C(N)/2 = a+1$.

From Corollaries 1 and 2, we can see that the nonsingularity, implied by the orthogonality,

determines the maximum number L in the real and complex orthogonal designs of order N.

With the aid of Corollaries 1 and 2, we generate the table illustrating the relationship among N, $R(N)$, and $C(N)$ as the following. From Table.2.1, we can conclude that the full code rate

N	$R(N) = \rho(N)$	a	b	c	d	$C(N)/2 = a + 1$
2	2	1	0	0	1	2
4	4	2	0	0	2	3
8	8	3	0	0	3	4
16	9	4	0	1	0	5

Table 2.1 Relationship Among N, $R(N)$ and $C(N)$

real orthogonal design exists when the matrix order is 2, 4 and 8. The full code rate complex orthogonal design exists if and only if the matrix order is 2.

Chapter 3

Simplified Decoding for a Family of Quasi-Orthogonal Codes

As we showed previously in section 2.3, a complex orthogonal design of order N exists if and only if $N = 2$. In other words, Alamouti's scheme is the unique complex orthogonal STBC. Besides Alamouti's STBC scheme, full code rate and full orthogonality can not be satisfied at the same time. If we choose to keep full code rate, full orthogonality has to be sacrificed. In [28], a *Quasi-Orthogonal code* was introduced as a full-rate, non-orthogonal complex STBC. In [29], another full-rate, non-orthogonal complex STBC named *Improved Quasi-Orthogonal code* was presented. The code matrix construction of Improved Quasi-Orthogonal code is the same as that of Quasi-Orthogonal code. By employing rotated signal constellations, as will be shown later, the Improved Quasi-Orthogonal code provides diversity order of 4 compared to the diversity order of 2 provided by the Quasi-Orthogonal code in one receive antenna system employing ML decoding. As a result of the loss of full orthogonality, ML decoding of these two codes cannot be as simple as symbol-by-symbol decoding. We measure the complexity of decoding in terms of the number of comparisons among the possible values in the ML detector. Here, we consider the decoding of an order four full-rate STBC with MPSK modulation as example.

If it is an orthogonal STBC, ML decoding is decoupled into symbol-by-symbol decoding. The decoder selects one of the M possible symbols in the MPSK constellation that minimizes the decoding metric. Totally, there are $4M$ comparisons in decoding each codeword. If it is a non-orthogonal STBC such as Quasi-Orthogonal code or Improved Quasi-Orthogonal code, by using ML algorithm, the four information bearing symbols from a codeword are decoded jointly instead of independently. Therefore, the number of comparisons in the ML detector is M^4 compared to $4M$ comparisons for the orthogonal code. This indicates the need of reducing the decoding complexity of non-orthogonal STBC. In the following sections, we will propose a simplified decoding algorithm for the family of Quasi-Orthogonal and Improved Quasi-Orthogonal codes. The corresponding performance will be evaluated as well.

3.1 Code Constructions and Signal Constellations for the Quasi-Orthogonal Code Family

Let

$$\mathbf{C}_{12} = \begin{pmatrix} s_1 & -s_2^* \\ s_2 & s_1^* \end{pmatrix} \quad \text{and} \quad \mathbf{C}_{34} = \begin{pmatrix} s_3 & -s_4^* \\ s_4 & s_3^* \end{pmatrix} \tag{3.1}$$

and The code matrix of the Quasi-Orthogonal code family is constructed as

$$\mathbf{C} = \begin{pmatrix} \mathbf{C}_{12} & -\mathbf{C}_{34}^* \\ \mathbf{C}_{34} & \mathbf{C}_{12}^* \end{pmatrix} = \begin{pmatrix} s_1 & -s_2^* & -s_3^* & s_4 \\ s_2 & s_1^* & -s_4^* & -s_3 \\ s_3 & -s_4^* & s_1^* & -s_2 \\ s_4 & s_3^* & s_2^* & s_1 \end{pmatrix} \tag{3.2}$$

The difference between the Quasi-Orthogonal code and the Improved Quasi-Orthogonal code

lies in the choice of the signal constellations. For the Quasi-Orthogonal code, all symbols are

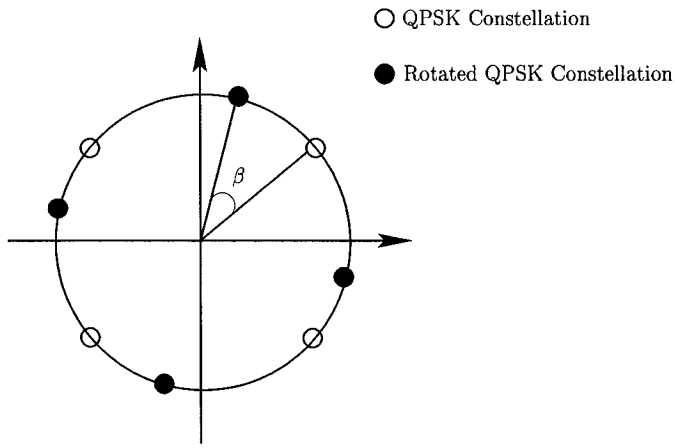

Fig. 3.1 QPSK and Rotated QPSK Constellations

taken from a QPSK constellation. For the Improved Quasi-Orthogonal code, s_1, s_2 are taken from a QPSK constellation and s_3, s_4 are taken from a rotated QPSK constellation specified in Fig.3.1, where $\beta = \frac{\pi}{6}$ denotes the relative rotation angle between the two constellations.

3.2 Simplified Decoding Algorithm for the Quasi-Orthogonal Code Family

3.2.1 Step One: Symbol Pair Joint Decoding

For the Quasi-Orthogonal code family, from (2.2), the one receive antenna system model is described by

$$\mathbf{r}^T = \mathbf{a}^T\mathbf{C} + \mathbf{n}^T = (\alpha_{1,1}, \alpha_{1,2}, \alpha_{1,3}, \alpha_{1,4}) \begin{pmatrix} s_1 & -s_2^* & -s_3^* & s_4 \\ s_2 & s_1^* & -s_4^* & -s_3 \\ s_3 & -s_4^* & s_1^* & -s_2 \\ s_4 & s_3^* & s_2^* & s_1 \end{pmatrix} + (n_{1,1}, n_{1,2}, n_{1,3}, n_{1,4}) \tag{3.3}$$

From section 2.1.2, when the channel state is known, the receiver calculates the decision metric

$$||\mathbf{r}^T - \mathbf{a}^T\tilde{\mathbf{C}}||^2 = \sum_{t=1}^{4} \left| r_{1,t} - \sum_{i=1}^{4} \alpha_{1,i}\tilde{c_{i,t}} \right|^2 \tag{3.4}$$

over all possible codewords $\tilde{\mathbf{C}}$ and decides in favorite of the codeword $\hat{\mathbf{C}}$ that minimizes (3.4). By complex conjugating the second and the third elements of $\mathbf{r}^T$ in (3.3), we obtain

$$\begin{aligned}
\mathbf{r_P}^T &= (r_{1,1}, r_{1,2}^*, r_{1,3}^*, r_{1,4}) \\
&= (s_1, s_2, s_3, s_4) \begin{pmatrix} \alpha_{1,1} & \alpha_{1,2}^* & \alpha_{1,3}^* & \alpha_{1,4} \\ \alpha_{1,2} & -\alpha_{1,1}^* & \alpha_{1,4}^* & -\alpha_{1,3} \\ \alpha_{1,3} & \alpha_{1,4}^* & -\alpha_{1,1}^* & -\alpha_{1,2} \\ \alpha_{1,4} & -\alpha_{1,3}^* & -\alpha_{1,2}^* & \alpha_{1,1} \end{pmatrix} + (n_{1,1}, n_{1,2}^*, n_{1,3}^*, n_{1,4}) \\
&= \mathbf{s}^T\mathbf{H} + \mathbf{n_P}^T
\end{aligned} \tag{3.5}$$

where

$$\mathbf{H} = \begin{pmatrix} \alpha_{1,1} & \alpha_{1,2}^* & \alpha_{1,3}^* & \alpha_{1,4} \\ \alpha_{1,2} & -\alpha_{1,1}^* & \alpha_{1,4}^* & -\alpha_{1,3} \\ \alpha_{1,3} & \alpha_{1,4}^* & -\alpha_{1,1}^* & -\alpha_{1,2} \\ \alpha_{1,4} & -\alpha_{1,3}^* & -\alpha_{1,2}^* & \alpha_{1,1} \end{pmatrix} \tag{3.6}$$

It is shown in Appendix A.1 that

$$||\mathbf{r_P}^T - \tilde{\mathbf{s}}^T\mathbf{H}||^2 = ||\mathbf{r}^T - \mathbf{a}^T\tilde{\mathbf{C}}||^2 \tag{3.7}$$

and therefore an equivalent ML algorithm to select the codeword matrix $\tilde{\mathbf{C}}$ that minimizes (3.4)

is to select the vector $\tilde{\mathbf{s}}$ made up of $\tilde{s_1}$, $\tilde{s_2}$, $\tilde{s_3}$ and $\tilde{s_4}$ that minimizes

$$||\mathbf{r_P}^T - \tilde{\mathbf{s}}^T\mathbf{H}||^2 \tag{3.8}$$

The representation (3.5) leads to symbol pair joint decoding shown later. From (3.6), we have

$$\mathbf{H}\mathbf{H}^H = \begin{pmatrix} A & 0 & 0 & B \\ 0 & A & -B & 0 \\ 0 & -B & A & 0 \\ B & 0 & 0 & A \end{pmatrix} \tag{3.9}$$

where

$$A = \sum_{i=1}^{4} |\alpha_{1,i}|^2 = (\alpha_{1,1}, \alpha_{1,2}, \alpha_{1,3}, \alpha_{1,4}) \begin{pmatrix} 1 & 0 & 0 & 0 \\ 0 & 1 & 0 & 0 \\ 0 & 0 & 1 & 0 \\ 0 & 0 & 0 & 1 \end{pmatrix} \begin{pmatrix} \alpha_{1,1}^* \\ \alpha_{1,2}^* \\ \alpha_{1,3}^* \\ \alpha_{1,4}^* \end{pmatrix} \tag{3.10}$$

and

$$B = 2\mathrm{Re}(\alpha_{1,1}\alpha_{1,4}^* - \alpha_{1,2}\alpha_{1,3}^*) = (\alpha_{1,1}, \alpha_{1,2}, \alpha_{1,3}, \alpha_{1,4}) \begin{pmatrix} 0 & 0 & 0 & 1 \\ 0 & 0 & -1 & 0 \\ 0 & -1 & 0 & 0 \\ 1 & 0 & 0 & 0 \end{pmatrix} \begin{pmatrix} \alpha_{1,1}* \\ \alpha_{1,2}* \\ \alpha_{1,3}* \\ \alpha_{1,4}* \end{pmatrix} \tag{3.11}$$

The determinant of $\mathbf{H}\mathbf{H}^H$ is

$$\begin{aligned}
& (A-B)^2(A+B)^2 \\
= \; & [(\mathrm{Re}(\alpha_{1,1})+\mathrm{Re}(\alpha_{1,4}))^2+(\mathrm{Im}(\alpha_{1,1})+\mathrm{Im}(\alpha_{1,4}))^2 \\
+ \; & (\mathrm{Re}(\alpha_{1,2})-\mathrm{Re}(\alpha_{1,3}))^2+(\mathrm{Im}(\alpha_{1,2})-\mathrm{Im}(\alpha_{1,3}))^2]^2 \\
+ \; & [(\mathrm{Re}(\alpha_{1,1})-\mathrm{Re}(\alpha_{1,4}))^2+(\mathrm{Im}(\alpha_{1,1})-\mathrm{Im}(\alpha_{1,4}))^2 \\
+ \; & (\mathrm{Re}(\alpha_{1,2})+\mathrm{Re}(\alpha_{1,3}))^2+(\mathrm{Im}(\alpha_{1,2})+\mathrm{Im}(\alpha_{1,3}))^2]^2
\end{aligned} \tag{3.12}$$

From (3.12), the determinant of $\mathbf{H}\mathbf{H}^H$ is equal to zero iff

$$\begin{aligned}
& [(\mathrm{Re}(\alpha_{1,1})+\mathrm{Re}(\alpha_{1,4}))^2+(\mathrm{Im}(\alpha_{1,1})+\mathrm{Im}(\alpha_{1,4}))^2 \\
+ \; & (\mathrm{Re}(\alpha_{1,2})-\mathrm{Re}(\alpha_{1,3}))^2+(\mathrm{Im}(\alpha_{1,2})-\mathrm{Im}(\alpha_{1,3}))^2]^2=0
\end{aligned} \tag{3.13}$$

and

$$\begin{aligned}
& [(\mathrm{Re}(\alpha_{1,1})-\mathrm{Re}(\alpha_{1,4}))^2+(\mathrm{Im}(\alpha_{1,1})-\mathrm{Im}(\alpha_{1,4}))^2 \\
+ \; & (\mathrm{Re}(\alpha_{1,2})+\mathrm{Re}(\alpha_{1,3}))^2+(\mathrm{Im}(\alpha_{1,2})+\mathrm{Im}(\alpha_{1,3}))^2]^2=0
\end{aligned} \tag{3.14}$$

(3.13) and (3.14) can be satisfied iff

$$\mathrm{Re}(\alpha_{1,1})+\mathrm{Re}(\alpha_{1,4})=\mathrm{Re}(\alpha_{1,1})-\mathrm{Re}(\alpha_{1,4})=0 \Rightarrow \mathrm{Re}(\alpha_{1,1})=\mathrm{Re}(\alpha_{1,4})=0 \tag{3.15}$$

$$\mathrm{Im}(\alpha_{1,1})+\mathrm{Im}(\alpha_{1,4})=\mathrm{Im}(\alpha_{1,1})-\mathrm{Im}(\alpha_{1,4})=0 \Rightarrow \mathrm{Im}(\alpha_{1,1})=\mathrm{Im}(\alpha_{1,4})=0 \tag{3.16}$$

$$\mathrm{Re}(\alpha_{1,2})+\mathrm{Re}(\alpha_{1,3})=\mathrm{Re}(\alpha_{1,2})-\mathrm{Re}(\alpha_{1,3})=0 \Rightarrow \mathrm{Re}(\alpha_{1,2})=\mathrm{Re}(\alpha_{1,3})=0 \tag{3.17}$$

and

$$\mathrm{Im}(\alpha_{1,2}) + \mathrm{Im}(\alpha_{1,3}) = \mathrm{Im}(\alpha_{1,2}) - \mathrm{Im}(\alpha_{1,3}) = 0 \Rightarrow \mathrm{Im}(\alpha_{1,2}) = \mathrm{Im}(\alpha_{1,3}) = 0 \tag{3.18}$$

or we can say that the determinant of $\mathbf{H}\mathbf{H}^H$ is equal to zero iff all the channel coefficients $\alpha_{1,i}$'s $(i = 1, 2, 3, 4)$ are equal to zero. From the transmission model, we know that the real parts and the imaginary parts of the channel coefficients are continuous Gaussian random variables. The probability that at least one of these random variables is non-zero is 1. Therefore, $\mathbf{H}\mathbf{H}^H$ is a non-singular matrix with probability 1. By multiplying both sides of (3.5) by $\mathbf{H}^H$ we get

$$\begin{aligned} \mathbf{r_H}^T &= (r_{H\,1,1}, r_{H\,2,1}, r_{H\,3,1}, r_{H\,4,1}) = \mathbf{r_P}^T\mathbf{H}^H = \mathbf{s}^T\mathbf{H}\mathbf{H}^H + \mathbf{n_P}^T\mathbf{H}^H = \mathbf{s}^T\mathbf{H}\mathbf{H}^H + \mathbf{n_H}^T \\ &= (s_1, s_2, s_3, s_4) \begin{pmatrix} A & 0 & 0 & B \\ 0 & A & -B & 0 \\ 0 & -B & A & 0 \\ B & 0 & 0 & A \end{pmatrix} + (n_{H\,1,1}, n_{H\,2,1}, n_{H\,3,1}, n_{H\,4,1}) \end{aligned} \tag{3.19}$$

We can naturally decouple (3.19) into

$$\begin{pmatrix} r_{H\,1,1} \\ r_{H\,4,1} \end{pmatrix} = \begin{pmatrix} A & B \\ B & A \end{pmatrix} \begin{pmatrix} s_1 \\ s_4 \end{pmatrix} + \begin{pmatrix} n_{H\,1,1} \\ n_{H\,4,1} \end{pmatrix} \tag{3.20}$$

and

$$\begin{pmatrix} r_{H\,2,1} \\ r_{H\,3,1} \end{pmatrix} = \begin{pmatrix} A & -B \\ -B & A \end{pmatrix} \begin{pmatrix} s_2 \\ s_3 \end{pmatrix} + \begin{pmatrix} n_{H\,2,1} \\ n_{H\,3,1} \end{pmatrix} \tag{3.21}$$

From (3.20) and (3.21), we see that the decoding of s_1 and s_4 is independent from the decoding of s_2 and s_3. The joint decoding of symbols s_1, s_2, s_3 and s_4 is equivalent to pairwise joint decoding of s_1, s_4 and s_2, s_3. The pairwise decoding scheme in each group is described as follows. From (3.19), the covariance matrix of $\mathbf{n_H}$ is

$$\mathbf{C}_0 = E\{\mathbf{n_H} \mathbf{n_H}^H\} = 2\sigma^2 \mathbf{H}\mathbf{H}^\mathbf{H} \tag{3.22}$$

Correspondingly, the correlation matrix of $n_{H\,1,1}$ and $n_{H\,4,1}$ is

$$\mathbf{C}_1 = 2\sigma^2 \begin{pmatrix} A & B \\ B & A \end{pmatrix} \tag{3.23}$$

and the correlation matrix of $n_{H\,2,1}$ and $n_{H\,3,1}$ is

$$\mathbf{C}_2 = 2\sigma^2 \begin{pmatrix} A & -B \\ -B & A \end{pmatrix} \tag{3.24}$$

where $2\sigma^2$ is the variance of the complex Gaussian noise samples $n_{1,i}$; $(i = 1, 2, 3, 4)$ in (3.3). In order to de-correlate the noise in (3.20) and (3.21), we make the following operations. We denote

the Hermitian root of matrix $\mathbf{C}_i$ as $\mathbf{C}_i^{\frac{1}{2}}$, which is defined by

$$\mathbf{C}_i = \mathbf{C}_i^{\frac{1}{2}} \mathbf{C}_i^{\frac{1}{2}} \tag{3.25}$$

From (3.25), we re-write (3.20) and (3.21) as

$$\begin{pmatrix} r_{H\,1,1} \\ r_{H\,4,1} \end{pmatrix} = \begin{pmatrix} A & B \\ B & A \end{pmatrix} \begin{pmatrix} s_1 \\ s_4 \end{pmatrix} + \mathbf{C}_1^{\frac{1}{2}} \begin{pmatrix} n_{D\,1,1} \\ n_{D\,4,1} \end{pmatrix} \tag{3.26}$$

and

$$\begin{pmatrix} r_{H\,2,1} \\ r_{H\,3,1} \end{pmatrix} = \begin{pmatrix} A & -B \\ -B & A \end{pmatrix} \begin{pmatrix} s_1 \\ s_4 \end{pmatrix} + \mathbf{C}_2^{\frac{1}{2}} \begin{pmatrix} n_{D\,2,1} \\ n_{D\,3,1} \end{pmatrix} \tag{3.27}$$

where $n_{D\,1,1}, n_{D\,4,1}, n_{D\,2,1}, n_{D\,3,1}$ are i.i.d circularly symmetric complex Gaussian with zero mean and unit variance. By multiplying both sides of (3.20) and (3.21) with $\mathbf{C}_1^{-\frac{1}{2}}$ and $\mathbf{C}_2^{-\frac{1}{2}}$ respectively, we de-correlated the noise in (3.20) and (3.21). The results of the operation are expressed as

$$\mathbf{C}_1^{-\frac{1}{2}} \begin{pmatrix} r_{H\,1,1} \\ r_{H\,4,1} \end{pmatrix} = \mathbf{C}_1^{-\frac{1}{2}} \begin{pmatrix} A & B \\ B & A \end{pmatrix} \begin{pmatrix} s_1 \\ s_4 \end{pmatrix} + \begin{pmatrix} n_{D\,1,1} \\ n_{D\,4,1} \end{pmatrix} \tag{3.28}$$

and

$$\mathbf{C}_2^{-\frac{1}{2}} \begin{pmatrix} r_{H\,2,1} \\ r_{H\,3,1} \end{pmatrix} = \mathbf{C}_2^{-\frac{1}{2}} \begin{pmatrix} A & -B \\ -B & A \end{pmatrix} \begin{pmatrix} s_1 \\ s_4 \end{pmatrix} + \begin{pmatrix} n_{D\,2,1} \\ n_{D\,3,1} \end{pmatrix} \tag{3.29}$$

With ML decoding for s_1 and s_4, the decoder chooses the values for $\tilde{s_1}$ and $\tilde{s_4}$ that minimize

$$\left[\begin{pmatrix} r_{H\,1,1} \\ r_{H\,4,1} \end{pmatrix} - \begin{pmatrix} A & B \\ B & A \end{pmatrix} \begin{pmatrix} \tilde{s_1} \\ \tilde{s_4} \end{pmatrix} \right]^H \mathbf{C}_1^{-1} \left[\begin{pmatrix} r_{H\,1,1} \\ r_{H\,4,1} \end{pmatrix} - \begin{pmatrix} A & B \\ B & A \end{pmatrix} \begin{pmatrix} \tilde{s_1} \\ \tilde{s_4} \end{pmatrix} \right] \tag{3.30}$$

Also, when it decodes s_2 and s_3, the decoder chooses the values for $\tilde{s_2}$ and $\tilde{s_3}$ that minimize

$$\left[\begin{pmatrix} r_{H\,2,1} \\ r_{H\,3,1} \end{pmatrix} - \begin{pmatrix} A & -B \\ -B & A \end{pmatrix} \begin{pmatrix} \tilde{s_2} \\ \tilde{s_3} \end{pmatrix} \right]^H \mathbf{C}_2^{-1} \left[\begin{pmatrix} r_{H\,2,1} \\ r_{H\,3,1} \end{pmatrix} - \begin{pmatrix} A & -B \\ -B & A \end{pmatrix} \begin{pmatrix} \tilde{s_2} \\ \tilde{s_3} \end{pmatrix} \right] \tag{3.31}$$

Theorem: For Quasi-Orthogonal Code Family, the Symbol Pair Joint Decoding is Optimal

Proof: An optimal decoder based on (3.19) selects the value for $\tilde{\mathbf{s}}$ that minimizes

$$(\mathbf{r_H}^T - \tilde{\mathbf{s}}^T \mathbf{H}\mathbf{H}^H)\mathbf{C}_0^{-1}(\mathbf{r_H}^T - \tilde{\mathbf{s}}^T \mathbf{H}\mathbf{H}^{\mathbf{H}})^H \tag{3.32}$$

According to (3.7) and (3.22),

$$(\mathbf{r_H}^T - \tilde{\mathbf{s}}^T \mathbf{H}\mathbf{H}^H)\mathbf{C}_0^{-1}(\mathbf{r_H}^T - \tilde{\mathbf{s}}^T \mathbf{H}\mathbf{H}^{\mathbf{H}})^H$$

$$
\begin{aligned}
&= \frac{1}{2\sigma^2}(\mathbf{r_H}^T - \tilde{\mathbf{s}}^T\mathbf{H}\mathbf{H}^H)(\mathbf{H}\mathbf{H}^H)^{-1}(\mathbf{r_H}^T - \tilde{\mathbf{s}}^T\mathbf{H}\mathbf{H}^H)^H \\
&= \frac{1}{2\sigma^2}(\mathbf{r_P}^T - \tilde{\mathbf{s}}^T\mathbf{H})\mathbf{H}^H(\mathbf{H}\mathbf{H}^H)^{-1}\mathbf{H}(\mathbf{r_P}^T - \tilde{\mathbf{s}}^T\mathbf{H}^H)^{\mathbf{H}} = \frac{1}{2\sigma^2}(\mathbf{r_P}^T - \tilde{\mathbf{s}}^T\mathbf{H})(\mathbf{r_P}^T - \tilde{\mathbf{s}}^T\mathbf{H}^H)^{\mathbf{H}} \\
&= \frac{1}{2\sigma^2}||\mathbf{r_P}^T - \tilde{\mathbf{s}}^T\mathbf{H}||^2 = \frac{1}{2\sigma^2}||\mathbf{r}^T - \mathbf{a}^T\tilde{\mathbf{C}}||^2 \qquad (3.33)
\end{aligned}
$$

where $\mathbf{r_P}$ and $\mathbf{r_H}$ are defined in (3.5) and (3.19), respectively.

We see that minimizing (3.32) is equivalent to minimizing (3.4). So the decoding result that minimizes (3.32) is optimal. In (3.32)

$$
\mathbf{C}_0^{-1} = \frac{1}{2\sigma^2(A^2 - B^2)} \begin{pmatrix} A & 0 & 0 & -B \\ 0 & A & B & 0 \\ 0 & B & A & 0 \\ -B & 0 & 0 & A \end{pmatrix} \qquad (3.34)
$$

We define

$$
\mathbf{d}^T = (d_{1,1},\ d_{2,1},\ d_{3,1},\ d_{4,1}) = \mathbf{r_H}^T - \tilde{\mathbf{s}}^T\mathbf{H}\mathbf{H}^H \qquad (3.35)
$$

then by combining (3.34) and (3.35), (3.32) is re-written as

$$
\begin{aligned}
&(\mathbf{r_H}^T - \tilde{\mathbf{s}}^T\mathbf{H}\mathbf{H}^H)\mathbf{C}_0^{-1}(\mathbf{r_H}^T - \tilde{\mathbf{s}}^T\mathbf{H}\mathbf{H}^{\mathbf{H}})^H \\
&= \frac{1}{2\sigma^2(A^2 - B^2)}\mathbf{d}^T \begin{pmatrix} A & 0 & 0 & -B \\ 0 & A & B & 0 \\ 0 & B & A & 0 \\ -B & 0 & 0 & A \end{pmatrix} \mathbf{d}^*
\end{aligned}
$$

$$
\begin{aligned}
&= \frac{1}{2\sigma^2(A^2-B^2)}(d_{1,1}^*,\ d_{4,1}^*)\begin{pmatrix} A & -B \\ -B & A \end{pmatrix}\begin{pmatrix} d_{1,1} \\ d_{4,1} \end{pmatrix} \\
&\quad + \frac{1}{2\sigma^2(A^2-B^2)}(d_{2,1}^*,\ d_{3,1}^*)\begin{pmatrix} A & B \\ B & A \end{pmatrix}\begin{pmatrix} d_{2,1} \\ d_{3,1} \end{pmatrix} \\
&= \left[\begin{pmatrix} r_{H\,1,1} \\ r_{H\,4,1} \end{pmatrix} - \begin{pmatrix} A & B \\ B & A \end{pmatrix}\begin{pmatrix} \tilde{s_1} \\ \tilde{s_4} \end{pmatrix}\right]^H \mathbf{C}_1^{-1}\left[\begin{pmatrix} r_{H\,1,1} \\ r_{H\,4,1} \end{pmatrix} - \begin{pmatrix} A & B \\ B & A \end{pmatrix}\begin{pmatrix} \tilde{s_1} \\ \tilde{s_4} \end{pmatrix}\right] \\
&\quad + \left[\begin{pmatrix} r_{H\,2,1} \\ r_{H\,3,1} \end{pmatrix} - \begin{pmatrix} A & -B \\ -B & A \end{pmatrix}\begin{pmatrix} \tilde{s_2} \\ \tilde{s_3} \end{pmatrix}\right]^H \mathbf{C}_2^{-1}\left[\begin{pmatrix} r_{H\,2,1} \\ r_{H\,3,1} \end{pmatrix} - \begin{pmatrix} A & -B \\ -B & A \end{pmatrix}\begin{pmatrix} \tilde{s_2} \\ \tilde{s_3} \end{pmatrix}\right]
\end{aligned}
\tag{3.36}
$$

According to (3.36), we see that the optimal decoding of s_1, s_2, s_3, s_4 can be decoupled into the pair-wise decoding of the group made up of s_1, s_4 and the group made up of s_2, s_3. Q.E.D

Assuming that symbol pair joint decoding algorithm described in section 3.2.1 and MPSK modulation are employed, in the decoding of the symbol pair s_1 and s_4, the decoder chooses the pair of values over M^2 pairs of values that minimize the metric (3.30). Also, in the decoding of the symbol pair s_2 and s_3, the decoder chooses the pair of values over M^2 pair of values that minimize the metric (3.31). In decoding a codeword, the decoder makes $2M^2$ comparisons totally, which increases quadratically with M. Compared to the decoding algorithm which makes joint decision of s_1, s_2, s_3 and s_4 and makes comparisons among M^4 possible values, the complexity of the symbol pair joint decoding is much lower. When compared to the complexity of symbol-by-symbol decoding, which increases linearly with M, there is still the need to reduce the decoding

complexity. In order to reduce the decoding complexity further, we propose a symbol-by-symbol with decision feedback decoding as described in the following. In decoding each pair of symbols, one of the two is decoded by using ML algorithm first and the decoding result is carried back to the detection of the second symbol. Then the second symbol is decoded by using ML algorithm. This decoding technique requires the QR decomposition [32].

3.2.2 Step Two: QR-Decomposition

QR-decomposition: A square matrix $\mathbf{A}$ can be factorized in the form [32]

$$\mathbf{A} = \mathbf{WT} = \begin{pmatrix} w_{1,1} & w_{1,2} \\ w_{2,1} & w_{2,2} \end{pmatrix} \begin{pmatrix} t_{1,1} & t_{1,2} \\ 0 & t_{2,2} \end{pmatrix} \tag{3.37}$$

where $\mathbf{W}$ is a unitary matrix and $\mathbf{T}$ is an upper triangular matrix.

We write (3.28) and (3.29) in the form

$$\mathbf{r_x} = \mathbf{H_x s} + \mathbf{n_x} \tag{3.38}$$

In order to realize symbol-by-symbol with decision feedback decoding we need to put (3.38) into the form

$$\mathbf{r_y} = \mathbf{H_y s} + \mathbf{n_y} \tag{3.39}$$

where $\mathbf{H_y}$ is an upper-triangular matrix and the elements of the noise vector $\mathbf{n_y}$ are independent complex Gaussian. In order to get the upper-triangular matrix, we employ QR decomposition. From (3.37), after making a QR decomposition of $\mathbf{H_x}$. we have

$$\mathbf{r_x} = \mathbf{W}^{'}\mathbf{H_y s} + \mathbf{n_x} \tag{3.40}$$

where $\mathbf{W}'$ is unitary and $\mathbf{H_y}$ is the upper-triangular matrix from (3.39). By comparing (3.40) with (3.39), we find the difference between (3.40) and (3.39) is the existence of $\mathbf{W}'$. In order to remove $\mathbf{W}'$, we multiply both sides of (3.40) by $\mathbf{W}'^{-1}$ and resulting in

$$\mathbf{W}'^{-1}\mathbf{r_x} = \mathbf{H_y s} + \mathbf{W}'^{-1}\mathbf{n_x} \tag{3.41}$$

Let

$$\mathbf{r_y} = \mathbf{W}'^{-1}\mathbf{r_x} \tag{3.42}$$

and

$$\mathbf{n_y} = \mathbf{W}'^{-1}\mathbf{n_x} \tag{3.43}$$

then (3.41) has the same form as (3.39). We know that $\mathbf{W}'$ is a unitary matrix and multiplying both sides of (3.40) with $\mathbf{W}'^{-1}$ will not change the distribution of the noise. So, the elements of $\mathbf{n_y}$ in (3.43) are independent. Based on previous description, the requirements of the symbol-by-symbol with decision feedback decoding are satisfied.

For applying symbol-by-symbol with decision feedback decoding for the Quasi-Orthogonal code family, we re-write (3.28) and (3.29) in the form of (3.38) as

$$\mathbf{r_D}' = \mathbf{H_1 s}' + \mathbf{n_D}' \tag{3.44}$$

and

$$\mathbf{r_D}'' = \mathbf{H_2 s}'' + \mathbf{n_D}'' \tag{3.45}$$

respectively, where

$$\mathbf{H}_1 = \mathbf{C}_1^{-\frac{1}{2}} \begin{pmatrix} A & B \\ B & A \end{pmatrix} = \frac{1}{\sqrt{2\sigma^2}} \begin{pmatrix} A & B \\ B & A \end{pmatrix}^{\frac{1}{2}}$$

$$= \frac{1}{2\sqrt{2\sigma^2}} \begin{pmatrix} \sqrt{A+B}+\sqrt{A-B} & \sqrt{A+B}-\sqrt{A-B} \\ \sqrt{A+B}-\sqrt{A-B} & \sqrt{A+B}+\sqrt{A-B} \end{pmatrix} = \begin{pmatrix} h_{1\,1,1} & h_{1\,1,2} \\ h_{1\,1,2} & h_{1\,1,1} \end{pmatrix} \tag{3.46}$$

$$\mathbf{H}_2 = \mathbf{C}_2^{-\frac{1}{2}} \begin{pmatrix} A & -B \\ -B & A \end{pmatrix} = \frac{1}{\sqrt{2\sigma^2}} \begin{pmatrix} A & -B \\ -B & A \end{pmatrix}^{\frac{1}{2}}$$

$$= \frac{1}{2\sqrt{2\sigma^2}} \begin{pmatrix} \sqrt{A+B}+\sqrt{A-B} & \sqrt{A-B}-\sqrt{A+B} \\ \sqrt{A-B}-\sqrt{A+B} & \sqrt{A+B}+\sqrt{A-B} \end{pmatrix} = \begin{pmatrix} h_{2\,1,1} & h_{2\,1,2} \\ h_{2\,1,2} & h_{2\,1,1} \end{pmatrix} \tag{3.47}$$

Applying the QR decomposition on $\mathbf{H}_1$ and $\mathbf{H}_2$, we get

$$\mathbf{H}_1 = \mathbf{W}_1\mathbf{T}_1 = \begin{pmatrix} \mathbf{w}_1 & \mathbf{w}_4 \end{pmatrix} \begin{pmatrix} \grave{a} & \grave{b} \\ 0 & \grave{c} \end{pmatrix} \tag{3.48}$$

and

$$\mathbf{H}_2 = \mathbf{W}_2\mathbf{T}_2 = \begin{pmatrix} \mathbf{w}_2 & \mathbf{w}_3 \end{pmatrix} \begin{pmatrix} \grave{d} & \grave{e} \\ 0 & \grave{f} \end{pmatrix} \tag{3.49}$$

where $\mathbf{W}_1$ and $\mathbf{W}_2$ are unitary matrices and

$$\grave{a} = \sqrt{h_{1\,1,1}^2 + h_{1\,1,2}^2} \tag{3.50}$$

$$\grave{b} = \frac{2h_{1\,1,1}\ h_{1\,1,2}}{\grave{a}} \tag{3.51}$$

$$\grave{c} = \sqrt{\left(h_{1\,1,2} - \frac{\grave{b}}{\grave{a}}h_{1\,1,1}\right)^2 + \left(h_{1\,1,1} - \frac{\grave{b}}{\grave{a}}h_{1\,1,2}\right)^2} \tag{3.52}$$

$$\grave{d} = \sqrt{h_{2\,1,1}^2 + h_{2\,1,2}^2} \tag{3.53}$$

$$\grave{e} = \frac{2h_{2\,1,1}\ h_{2\,1,2}}{\grave{d}} \tag{3.54}$$

$$\grave{f} = \sqrt{\left(h_{2\,1,2} - \frac{\grave{e}}{\grave{d}}h_{2\,1,1}\right)^2 + \left(h_{2\,1,1} - \frac{\grave{e}}{\grave{d}}h_{2\,1,2}\right)^2} \tag{3.55}$$

Since $\mathbf{W}_1$ and $\mathbf{W}_2$ are unitary matrices, multiplying both sides of (3.28) and (3.29) with $\mathbf{W}_1^{-1}$ and $\mathbf{W}_2^{-1}$ will not change the distribution of the noise. We multiply both sides of (3.28) by $\mathbf{W}_1^{-1}$ and both sides of (3.29) by $\mathbf{W}_2^{-1}$, which are the same operations as shown in (3.41), and get

$$\mathbf{W}_1^{-1}\mathbf{C}_1^{-\frac{1}{2}} \begin{pmatrix} r_{H\,1,1} \\ r_{H\,4,1} \end{pmatrix} = \begin{pmatrix} r_{U\,1,1} \\ r_{U\,4,1} \end{pmatrix} = \begin{pmatrix} \grave{a} & \grave{b} \\ 0 & \grave{c} \end{pmatrix} \begin{pmatrix} s_1 \\ s_4 \end{pmatrix} + \begin{pmatrix} n_{U\,1,1} \\ n_{U\,4,1} \end{pmatrix} \tag{3.56}$$

and

$$\mathbf{W}_2^{-1}\mathbf{C}_2^{-\frac{1}{2}}\begin{pmatrix} r_{H\,2,1} \\ r_{H\,3,1} \end{pmatrix} = \begin{pmatrix} r_{U\,2,1} \\ r_{U\,3,1} \end{pmatrix} = \begin{pmatrix} \grave{d} & \grave{e} \\ 0 & \grave{f} \end{pmatrix}\begin{pmatrix} s_2 \\ s_3 \end{pmatrix} + \begin{pmatrix} n_{U\,2,1} \\ n_{U\,3,1} \end{pmatrix} \tag{3.57}$$

Then $n_{U\,1,1}$, $n_{U\,2,1}$, $n_{U\,3,1}$, $n_{U\,4,1}$ are i.i.d complex Gaussian with zero mean and unit variance.

3.2.3 Step Three: Joint Decoding vs Symbol-by-Symbol with Decision Feedback Decoding

After the QR-decomposition, we have two options for decoding, either joint decoding or symbol-by-symbol with decision feedback decoding.

Joint Decoding Scheme: From (3.56) and (3.57), in decoding s_1 and s_4, the receiver chooses values for $\tilde{s_1}$ and $\tilde{s_4}$ that minimize

$$\left[\begin{pmatrix} r_{U\,1,1} \\ r_{U\,4,1} \end{pmatrix} - \begin{pmatrix} \grave{a} & \grave{b} \\ 0 & \grave{c} \end{pmatrix}\begin{pmatrix} \tilde{s_1} \\ \tilde{s_4} \end{pmatrix}\right]^H \left[\begin{pmatrix} r_{U\,1,1} \\ r_{U\,4,1} \end{pmatrix} - \begin{pmatrix} \grave{a} & \grave{b} \\ 0 & \grave{c} \end{pmatrix}\begin{pmatrix} \tilde{s_1} \\ \tilde{s_4} \end{pmatrix}\right] \tag{3.58}$$

In decoding s_2 and s_3, the receiver chooses values for $\tilde{s_2}$ and $\tilde{s_3}$ that minimize

$$\left[\begin{pmatrix} r_{U\,2,1} \\ r_{U\,3,1} \end{pmatrix} - \begin{pmatrix} \grave{d} & \grave{e} \\ 0 & \grave{f} \end{pmatrix}\begin{pmatrix} \tilde{s_2} \\ \tilde{s_3} \end{pmatrix}\right]^H \left[\begin{pmatrix} r_{U\,2,1} \\ r_{U\,3,1} \end{pmatrix} - \begin{pmatrix} \grave{d} & \grave{e} \\ 0 & \grave{f} \end{pmatrix}\begin{pmatrix} \tilde{s_2} \\ \tilde{s_3} \end{pmatrix}\right] \tag{3.59}$$

Assuming MPSK modulation, from (3.58) and (3.59), in decoding each pair of symbols, the decoder makes comparisons among M^2 pairs of possible values. Totally, the decoder makes $2M^2$ comparisons. So, the joint decoding algorithm after QR decompositions has the same complexity as that of pair-wise decoding algorithm and its decoding results are optimal.

Theorem: Decoding Results Obtained from QR Decomposition with Joint Decoding are Optimal

We take the decoding for s_1 and s_4 as an example. The analysis of the decoding for s_2 and s_3 is similar. We re-write (3.28) as

$$\mathbf{r_V}' = \mathbf{C_1}^{-\frac{1}{2}} \begin{pmatrix} r_{H\,1,1} \\ r_{H\,4,1} \end{pmatrix} = \mathbf{H_1} \begin{pmatrix} s_1 \\ s_4 \end{pmatrix} + \begin{pmatrix} n_{D\,1,1} \\ n_{D\,4,1} \end{pmatrix} = \mathbf{H_1 s}' + \mathbf{n_D}' \tag{3.60}$$

where the elements in $\mathbf{n_D}'$ are i.i.d complex Gaussian with zero mean and unit variance. By using ML algorithm, the receiver chooses values for $\tilde{s_1}$ and $\tilde{s_4}$, which are elements of $\tilde{\mathbf{s}}'$, that minimize

$$||\mathbf{r_V}' - \mathbf{H_1}\tilde{\mathbf{s}}'||^2 \tag{3.61}$$

After making a QR-decomposition, we get

$$\mathbf{H_1} = \mathbf{Q_1 R_1} \tag{3.62}$$

where $\mathbf{Q_1}$ is unitary and $\mathbf{R_1}$ is an upper triangular matrix, correspondingly, (3.60) changes to

$$\mathbf{r_V}' = \mathbf{Q_1 R_1 s}' + \mathbf{n_D}' \tag{3.63}$$

We multiply both sides of (3.63) with $\mathbf{Q_1}^{-1}$ and get

$$\mathbf{r_Q}' = \mathbf{Q_1}^{-1}\mathbf{r_V}' = \mathbf{R_1 s}' + \mathbf{n_Q}' \tag{3.64}$$

Because $\mathbf{Q_1}$ is unitary, multiplying $\mathbf{n_D}'$ with $\mathbf{Q_1}^{-1}$ does not change the distribution of the elements in $\mathbf{n_D}'$. If we choose QR decomposition with joint decision decoding algorithm, by ML

algorithm, the decoder chooses value for $\tilde{\mathbf{s}}'$ that minimizes

$$||\mathbf{r_Q}' - \mathbf{R}_1\tilde{\mathbf{s}}'||^2 \tag{3.65}$$

Because

$$\begin{aligned} & ||\mathbf{r_Q}' - \mathbf{R}_1\tilde{\mathbf{s}}'||^2 = \left[(\mathbf{Q}_1^{-1}\mathbf{r_V}')^H - \tilde{\mathbf{s}}'^H\mathbf{R}_1^H\right]\left[\mathbf{Q}_1^{-1}\mathbf{r_v}' - \mathbf{R}_1\tilde{\mathbf{s}}'\right] \\ = & \left[\mathbf{r_V}'^H\mathbf{Q}_1 - \tilde{\mathbf{s}}'^H\mathbf{R}_1^H\right]\left[\mathbf{Q}_1^H\mathbf{r_V}' - \mathbf{R}_1\tilde{\mathbf{s}}'\right] \\ = & \mathbf{r_V}'^H\mathbf{r_V}' - \tilde{\mathbf{s}}'(\mathbf{Q}_1\mathbf{R}_1)^H\mathbf{r_V}' - \mathbf{r_V}'^H\mathbf{Q}_1\mathbf{R}_1\tilde{\mathbf{s}}' + \tilde{\mathbf{s}}'^H(\mathbf{Q}_1\mathbf{R}_1)^H(\mathbf{Q}_1\mathbf{R}_1)\tilde{\mathbf{s}}' \\ = & \mathbf{r_V}'^H\mathbf{r_V}' - \tilde{\mathbf{s}}'\mathbf{H}_1^H\mathbf{r_V}' - \mathbf{r_V}'^H\mathbf{H}_1\tilde{\mathbf{s}}' + \tilde{\mathbf{s}}'^H\mathbf{H}_1^H\mathbf{H}_1\tilde{\mathbf{s}}' = ||\mathbf{r_V}' - \mathbf{H}_1\tilde{\mathbf{s}}'||^2 \end{aligned} \tag{3.66}$$

which is equivalent to (3.61). According to the analysis, the decoding result obtained from the QR decomposition and joint decision is optimal.

Symbol-by-Symbol with Decision Feedback Decoding Scheme: As we have mentioned, the complexity of symbol-by-symbol with decision feedback decoding increases linearly with respect to the size of modulation constellation. The corresponding decoding algorithm is described in the followings. Based on (3.56) and (3.57), in decoding s_4 and s_3, the decoder first chooses values for $\tilde{s_4}$ and $\tilde{s_3}$ that minimize

$$|r_{U\,4,1} - \grave{c}\tilde{s_4}|^2 \tag{3.67}$$

and

$$|r_{U\,3,1} - \grave{f}\tilde{s_3}|^2 \tag{3.68}$$

Then the decoder carries the decoding results $\hat{s_4}$ and $\hat{s_3}$ back to the decoding of s_1 and s_2. It chooses the values for $\tilde{s_1}$ and $\tilde{s_2}$ that minimize

$$|r_{U\,1,1} - \grave{b}\hat{s_4} - \grave{a}\tilde{s_1}|^2 \tag{3.69}$$

and

$$|r_{U\,2,1} - \grave{e}\hat{s}_3 - \grave{d}\tilde{s}_2|^2 \tag{3.70}$$

Before compare the error performance of symbol pair joint decoding scheme and symbol-by-symbol with decision feedback decoding scheme by computer simulations, we present the general simulation settings.

General Computer Simulation Settings: In the computer simulations of different decoding schemes, we have the general simulation setting as the following unless specified. The signal to noise ratio (SNR) is defined as

$$SNR = \frac{E_b}{N_0} \tag{3.71}$$

where E_b stands for signal energy per bit and N_0 stands for the variance of the independent samples of additive complex Gaussian noise. We assume the received symbol energy to be one and QPSK modulation is employed, then

$$E_b = \frac{1}{2} \tag{3.72}$$

By choosing different values for the variance of the additive complex Gaussian noise, which is denoted as $2\sigma^2 = N_0$, we get the different SNR/bit. The relation between σ^2 and SNR/bit (in dB) is expressed as

$$\sigma^2 = \frac{10^{-\frac{\text{SNR/bit}}{10}}}{4} \tag{3.73}$$

which is also shown in Appendix B.1.3.

As presented in Appendix B.1.1, information is produced by a binary integer random generator. By using Gray mapping shown in Fig.3.2, the information bits are mapped to transmitted symbols. Then the information-carried symbols are transmitted through a four transmit and one receive antenna quasi-static channel simulated by four independent zero-mean and unit variance complex Gaussian random generators described in Appendix B.1.2. The additive noise at the

receiver is produced by a complex Gaussian random generator with zero-mean and variance $2\sigma^2$, where σ^2 is calculated by (3.73). The error performance is measured in terms of bit error rate (BER), symbol error rate (SER) or frame error rate (FER) as required. When FER is evaluated, each frame contains 256 information bits. The error performances of the symbol pair joint de-

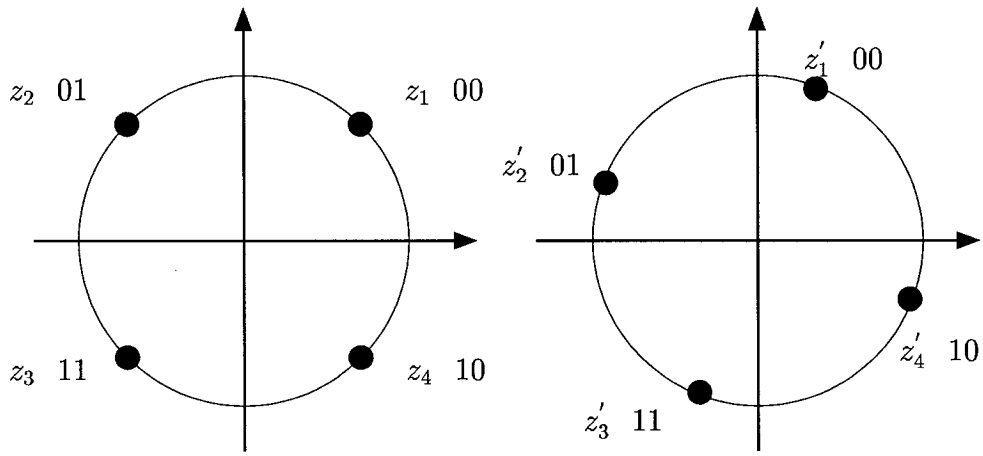

Fig. 3.2 Gray Mapping for QPSK and Rotated QPSK Constellations

coding scheme and symbol-by-symbol with decision feedback decoding scheme are shown in Fig.3.3 and Fig.3.4. The error performance curves are plotted based on the computer simulations over 2.24×10^9 information bits, i.e. 8.75×10^6 frames. As illustrated in Fig.3.3 and Fig.3.4, the error performance curves of two decoding schemes are parallel with when SNR is sufficiently large. The parallelism between the curves indicates that the diversity orders provided by the two decoding schemes are exactly the same. Besides this, there is a 1 dB degradation of the symbol-by-symbol with decision feedback decoding scheme related to the symbol pair joint decoding scheme. In the following section, we are going to evaluate the performance analytically.

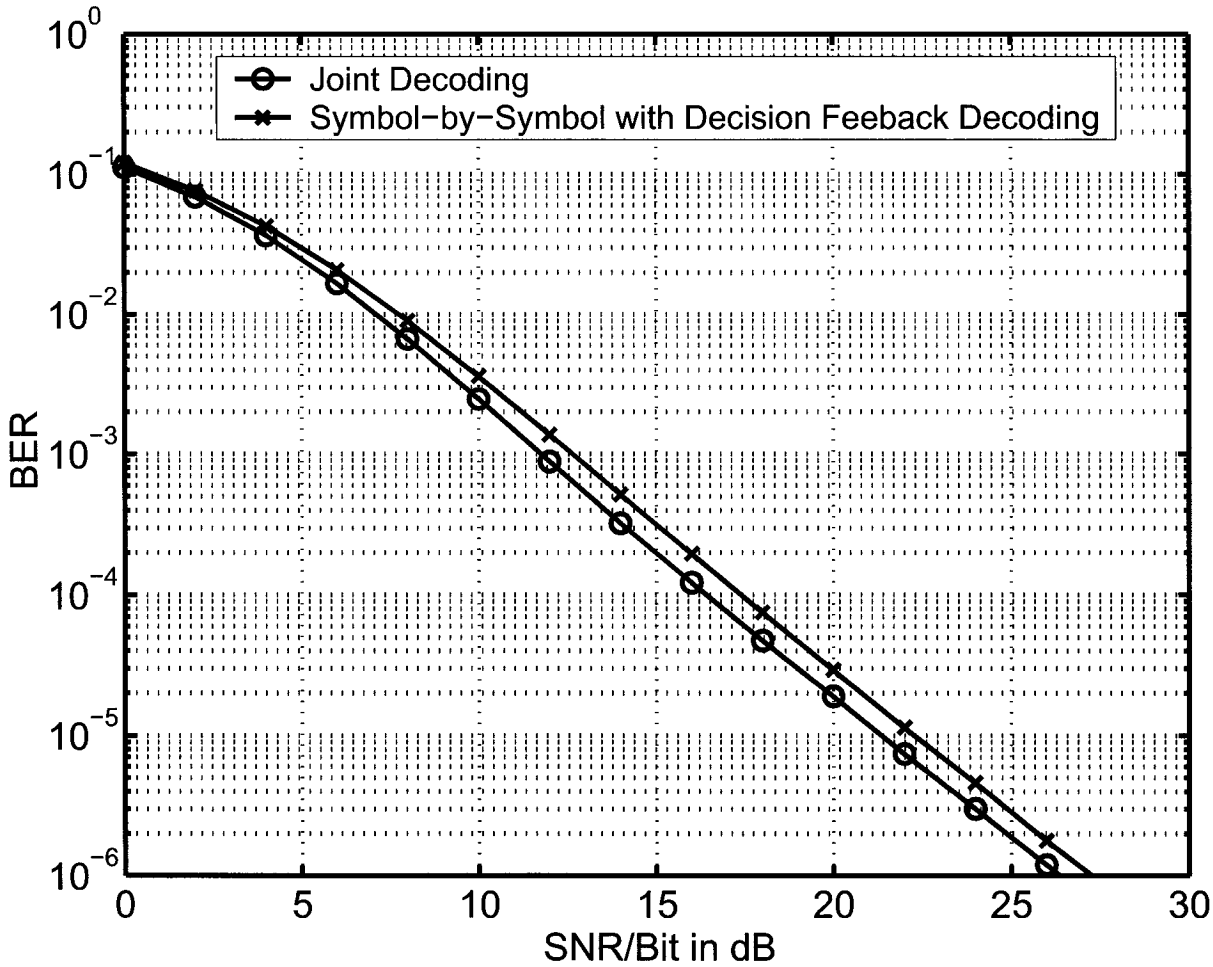

Fig. 3.3 Different Decoding Algorithms for the Quasi-Orthogonal code: Bit Error Rate

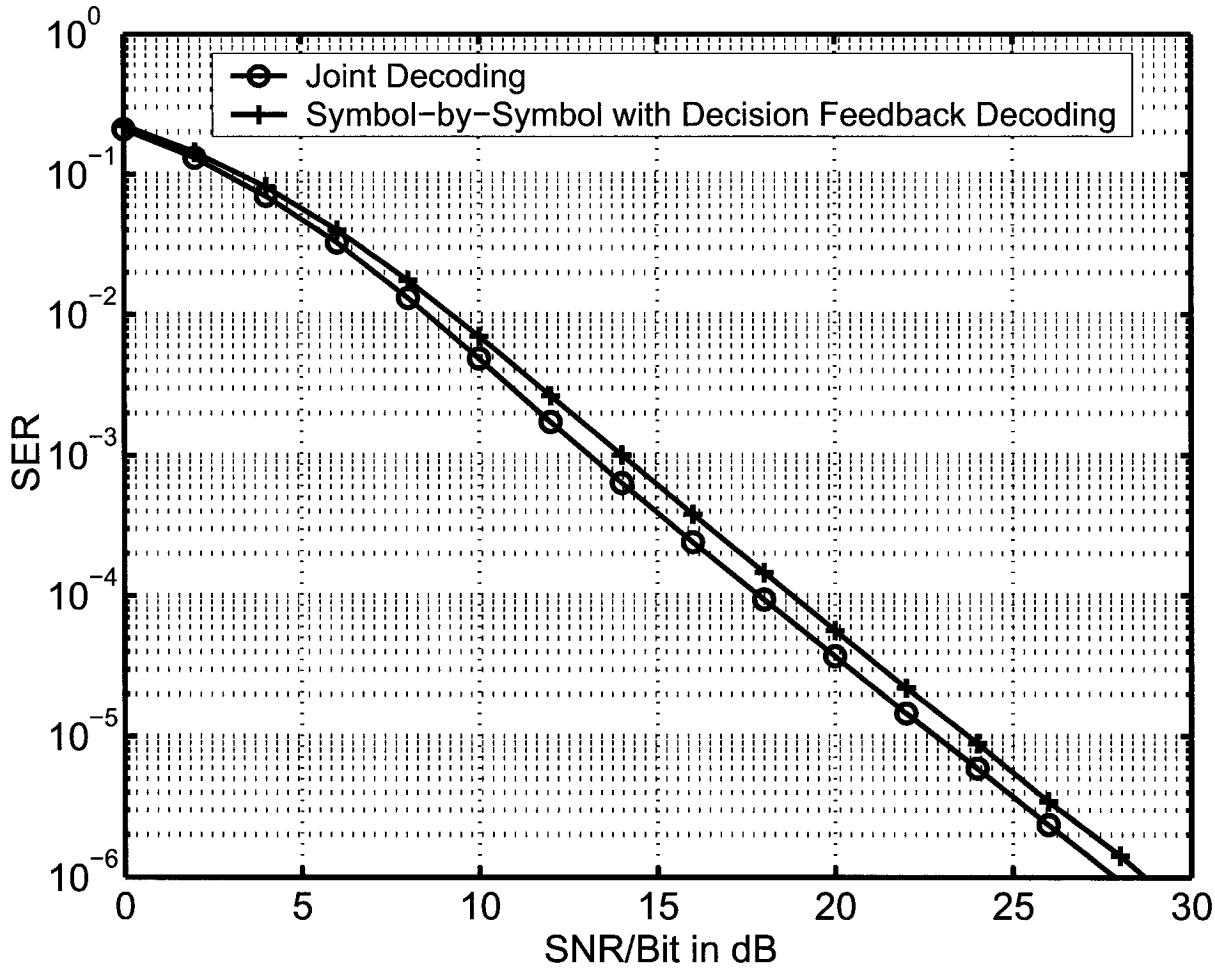

Fig. 3.4 Different Decoding Algorithms for the Quasi-Orthogonal code: Symbol Error Rate

3.3 Performance Evaluations of the Quasi-Orthogonal Code Family with Different Decoding Schemes

In the performance evaluation of the decoding of Quasi-Orthogonal code family, we will take the decoding of s_1 and s_4 as an example. The analysis for the decoding of s_2 and s_3 is similar. In order to keep the summation of the received symbol energy to be one in the four transmit antennas system, we set the symbol energy from each transmit antenna to $\frac{1}{4}$. Also, we assume the constellations shown in Fig.3.1 are employed, then the value of s_1 is chosen from $\pm\frac{1}{\sqrt{8}} \pm j\frac{1}{\sqrt{8}}$ and the value of s_4 is chosen from $(\pm\frac{1}{\sqrt{8}} \pm j\frac{1}{\sqrt{8}})e^{j\beta}$, where β is the relative rotation angle as indicated in Fig.3.1. For Quasi-Orthogonal code, β is equal to zero.

3.3.1 Mathematical Preliminaries

Craig's Formula[40]: The Gaussian probability function $Q(x)$, which is defined as

$$Q(x) = \frac{1}{\sqrt{2\pi}} \int_x^{+\infty} \exp\left(-\frac{x^2}{2}\right) dx \tag{3.74}$$

can be calculated also by

$$Q(x) = \frac{1}{\pi} \int_0^{\frac{\pi}{2}} \exp\left(-\frac{x^2}{2\sin^2\theta}\right) d\theta \tag{3.75}$$

when $x > 0$.

Joint Moment Generating Function of Random Variables in Quadratic Forms

Lemma [34]: Let x be an N-tuple random vector and

$$\bar{\mathbf{x}} = E(\mathbf{x}) \tag{3.76}$$

the covariance matrix

$$\mathbf{L} = E\{(\mathbf{x} - \bar{\mathbf{x}})(\mathbf{x} - \bar{\mathbf{x}})^H\} \tag{3.77}$$

Then the joint moment generating function of the quadratic forms

$$v_i = \mathbf{x}^H \mathbf{Q}_i \mathbf{x} \quad i = 1, ..., M \tag{3.78}$$

where $\mathbf{Q}_i$'s are Hermitian, is

$$\begin{aligned} & M_{v_1,...,v_M}(t_1, ..., t_M) \\ = & \left|\mathbf{I} - \sum_{i=1}^{M} t_i \mathbf{L}\mathbf{Q}_i\right|^{-1} \exp\left\{ - \bar{\mathbf{x}}^H \mathbf{L}^{-1} \left[\mathbf{I} - \left(\mathbf{I} - \sum_{i=1}^{M} t_i \mathbf{L}\mathbf{Q}_i\right)^{-1}\right] \bar{\mathbf{x}} \right\} \end{aligned} \tag{3.79}$$

Average Error Probability for Symbol Detection with MPSK Modulation

When MPSK modulation is employed, from [37] (pp.198), the average symbol error probability is

$$P(\hat{s} \neq s) = \frac{1}{\pi} \int_0^{\frac{(M-1)\pi}{M}} \exp\left(- \frac{E_s}{N_0} \frac{g_{\text{PSK}}}{\sin^2 \theta} \right) d\theta \tag{3.80}$$

where

$$g_{\text{PSK}} = \sin^2 \frac{\pi}{M} \tag{3.81}$$

For QPSK modulation, the average symbol error rate is evaluated by

$$P(\hat{s} \neq s) = \frac{1}{\pi} \int_0^{\frac{3\pi}{4}} \exp\left(- \frac{E_s}{N_0} \frac{1}{2 \sin^2 \theta} \right) d\theta \tag{3.82}$$

or by [37] (pp.197)

$$\begin{aligned} P(\hat{s} \neq s) &= 2Q\left(\sqrt{\frac{E_s}{N_0}}\right) - Q^2\left(\sqrt{\frac{E_s}{N_0}}\right) \\ &= \frac{2}{\pi} \int_0^{\frac{\pi}{2}} \exp\left(- \frac{E_s}{2N_0 \sin^2 \theta} \right) d\theta - \frac{1}{\pi} \int_0^{\frac{\pi}{4}} \exp\left(- \frac{E_s}{2N_0 \sin^2 \theta} \right) d\theta \end{aligned} \tag{3.83}$$

Evaluation of Definite Integrals of the Form

$$\frac{1}{\pi}\int_0^{\phi}\left(\frac{\sin^2\theta}{\sin^2\theta+c}\right)^m d\theta \tag{3.84}$$

From the derivation included in Appendix 5A of [37] (pp.129-131), we can evaluate the definite integrals (3.84) in close form as

$$\begin{aligned}&\frac{\phi}{\pi}-\frac{T}{\pi}\sqrt{\frac{c}{1+c}}\sum_{k=0}^{m-1}\binom{2k}{k}\frac{1}{[4(1+c)]^k}\\&-\frac{2}{\pi}\sqrt{\frac{c}{1+c}}\sum_{k=0}^{m-1}\sum_{j=0}^{k-1}\binom{2k}{j}\frac{(-1)^{j+k}}{[4(1+c)]^k}\frac{\sin[(2k-2j)T]}{2k-2j}\\&0\le\phi\le\pi\end{aligned} \tag{3.85}$$

where

$$T=\frac{1}{2}\tan^{-1}\frac{N}{D}+\frac{\pi}{2}\left[1-\left(\frac{1+\mathrm{sgn}D}{2}\right)\mathrm{sgn}N\right] \tag{3.86}$$

with

$$N=2\sqrt{c(1+c)}\sin 2\phi\,;\qquad D=(1+2c)\cos 2\phi-1 \tag{3.87}$$

Lebesgue's Dominated Convergence Theorem [38]

Suppose that $\{f_n\}$ is a sequence of measurable functions, that $f_n \to f$, as $n \to \infty$, and that $|f_n| \le g$ for all n, where g is integrable. Then f is integrable, and

$$\lim_{n\to\infty}\int f_n\,d\mu=\int f\,d\mu \tag{3.88}$$

3.3.2 Error Performance of Optimal Decoding for the Quasi-Orthogonal Code Family

From (3.46) and (3.60), we have

$$\begin{pmatrix} r_{V\,1,1} \\ r_{V\,4,1} \end{pmatrix} = \mathbf{H}_1 \begin{pmatrix} s_1 \\ s_4 \end{pmatrix} + \begin{pmatrix} n_{D\,1,1} \\ n_{D\,4,1} \end{pmatrix}$$

$$= \frac{\sqrt{2}}{4\sigma} \begin{pmatrix} \sqrt{A+B}+\sqrt{A-B} & \sqrt{A+B}-\sqrt{A-B} \\ \sqrt{A+B}-\sqrt{A-B} & \sqrt{A+B}+\sqrt{A-B} \end{pmatrix} \begin{pmatrix} s_1 \\ s_4 \end{pmatrix} + \begin{pmatrix} n_{D\,1,1} \\ n_{D\,4,1} \end{pmatrix} \tag{3.89}$$

where $n_{D\,1,1}$ and $n_{D\,4,1}$ are i.i.d complex Gaussian with zero mean and variance 0.5 in each complex dimension. From(3.60), when the channel coefficients are known, the receiver decodes the transmitted symbol vector $\mathbf{s}_i'$ erroneously as $\hat{\mathbf{s}}_j'$ if and only if the Euclidian distance between $\mathbf{r_V}'$ and $\mathbf{H}_1\hat{\mathbf{s}}_j'$ is less than the Euclidian distance between $\mathbf{r_V}'$ and $\mathbf{H}_1\hat{\mathbf{s}}_i'$, where $\hat{\mathbf{s}}_i' = \mathbf{s}_i'$. So the pair-wise error probability of optimal decoding is

$$\begin{aligned} & P\big(\hat{\mathbf{s}}_i' \rightarrow \hat{\mathbf{s}}_j';\ i \neq j \ \big|\ \alpha_{1,n}\ \ n = 1,2,3,4\big) \\ = \ & P\big(\,||\mathbf{r_V}' - \mathbf{H}_1\hat{\mathbf{s}}_j'||^2 < ||\mathbf{r_V}' - \mathbf{H}_1\hat{\mathbf{s}}_i'||^2\,\big) \\ = \ & P\big(\,||\mathbf{H}_1(\hat{\mathbf{s}}_i' - \hat{\mathbf{s}}_j') + \mathbf{n_D}'||^2 - ||\mathbf{n_D}'||^2) < 0\,\big) \end{aligned} \tag{3.90}$$

We denote the difference between $\hat{\mathbf{s}}_i'$ and $\hat{\mathbf{s}}_j'$ as

$$\mathbf{e_s} = \begin{pmatrix} e_1 \\ e_4 \end{pmatrix} = \hat{\mathbf{s}}_i' - \hat{\mathbf{s}}_j' = \begin{pmatrix} \hat{s_{i1}} - \hat{s_{j1}} \\ \hat{s_{i4}} - \hat{s_{j4}} \end{pmatrix} \tag{3.91}$$

then (3.90) changes to

$$P\big(\,||\mathbf{H}_1\mathbf{e}_s + \mathbf{n_D}'||^2 - ||\mathbf{n_D}'||^2 < 0\,\big) \;=\; P\big(\,||\mathbf{H}_1\mathbf{e}_s||^2 + 2\mathrm{Re}(\mathbf{e}_s{}^H\mathbf{H}_1^H\mathbf{n_D}')<0\,\big) \quad (3.92)$$

We denote by

$$n_Z = 2\mathrm{Re}(\mathbf{e}_s{}^H\mathbf{H}_1^H\mathbf{n_D}') \quad (3.93)$$

which is shown in Appendix A.2 to be a Gaussian random variable with zero mean and variance $2||\mathbf{H}_1\mathbf{e}_s||^2$. Therefore:

$$\begin{aligned} &P(\,\hat{\mathbf{s}}_i' \to \hat{\mathbf{s}}_j'; i\neq j\,) = E\{\,P(\,\hat{\mathbf{s}}_i' \to \hat{\mathbf{s}}_j'; i\neq j \;|\; \alpha_{1,n}\;\; n=1,2,3,4\,)\,\} \\ =\;& E\{\,P(\,n_Z < -||\mathbf{H}_1\mathbf{e}_s||^2\,)\,\} = E\Big\{Q\big(\frac{||\mathbf{H}_1\mathbf{e}_s||}{\sqrt{2}}\big)\Big\} \end{aligned} \quad (3.94)$$

where E denotes expectation with respect to channel coefficients $\{\alpha_{1,n};\; n=1,2,3,4\}$.

By using Craig's formula, (3.94) changes to

$$\frac{1}{\pi}\int_0^{\frac{\pi}{2}} E\Big\{\exp\Big(-\frac{||\mathbf{H}_1\mathbf{e}_s||^2}{4\sin^2\theta}\Big)\Big\}d\theta \quad (3.95)$$

Let $\Omega = ||\mathbf{H}_1\mathbf{e}_s||^2 = \mathbf{e}_s{}^H\mathbf{H}_1^H\mathbf{H}_1\mathbf{e}_s$, where

$$\mathbf{H}_1^H\mathbf{H}_1 = \frac{1}{2\sigma^2}\begin{pmatrix} A & B \\ B & A \end{pmatrix} \quad (3.96)$$

then

$$\Omega = \mathbf{e_s}^H \mathbf{H}_1^H \mathbf{H}_1 \mathbf{e_s} = \frac{1}{2\sigma^2}(\, e_1^*, e_4^*\,) \begin{pmatrix} A & B \\ B & A \end{pmatrix} \begin{pmatrix} e_1 \\ e_4 \end{pmatrix}$$
$$= \frac{1}{2\sigma^2}\Big[A(||e_1||^2 + ||e_4||^2) + B\big\{2\mathrm{Re}(e_1 e_4^*)\big\}\Big] \tag{3.97}$$

Let

$$\boldsymbol{\alpha} = [\alpha_{1,1}, \alpha_{1,2}, \alpha_{1,3}, \alpha_{1,4}]^T \tag{3.98}$$

then

$$\bar{\boldsymbol{\alpha}} = E(\boldsymbol{\alpha}) = [0, 0, 0, 0]^T \tag{3.99}$$

and the covariance matrix

$$\mathbf{L} = E(\boldsymbol{\alpha}\boldsymbol{\alpha}^H) = \mathbf{I} \tag{3.100}$$

By substituting for A and B from (3.10) and (3.11) we re-write Ω in quadratic form as

$$\Omega = \boldsymbol{\alpha}^T \frac{1}{2\sigma^2} \begin{pmatrix} ||e_1||^2 + ||e_4||^2 & 0 & 0 & 2\mathrm{Re}(e_1 e_4^*) \\ 0 & ||e_1||^2 + ||e_4||^2 & -2\mathrm{Re}(e_1 e_4^*) & 0 \\ 0 & -2\mathrm{Re}(e_1 e_4^*) & ||e_1||^2 + ||e_4||^2 & 0 \\ 2\mathrm{Re}(e_1 e_4^*) & 0 & 0 & ||e_1||^2 + ||e_4||^2 \end{pmatrix} \boldsymbol{\alpha}^* = \boldsymbol{\alpha}^H \boldsymbol{\Lambda} \boldsymbol{\alpha} \tag{3.101}$$

where

$$\mathbf{\Lambda} = \frac{1}{2\sigma^2}\begin{pmatrix} ||e_1||^2 + ||e_4||^2 & 0 & 0 & 2\mathrm{Re}(e_1 e_4^*) \\ 0 & ||e_1||^2 + ||e_4||^2 & -2\mathrm{Re}(e_1 e_4^*) & 0 \\ 0 & -2\mathrm{Re}(e_1 e_4^*) & ||e_1||^2 + ||e_4||^2 & 0 \\ 2\mathrm{Re}(e_1 e_4^*) & 0 & 0 & ||e_1||^2 + ||e_4||^2 \end{pmatrix} \tag{3.102}$$

As derived in Appendix A.3, the eigenvalues of $\mathbf{\Lambda}$ are

$$\lambda_1^{\mathbf{\Lambda}} = \lambda_2^{\mathbf{\Lambda}} = \frac{1}{2\sigma^2}|e_1 + e_4|^2 \tag{3.103}$$

$$\lambda_3^{\mathbf{\Lambda}} = \lambda_4^{\mathbf{\Lambda}} = \frac{1}{2\sigma^2}|e_1 - e_4|^2 \tag{3.104}$$

From (3.79), the moment generating function of Ω is

$$\Phi_\Omega(s) = \prod_{i=1}^{4}(1 - s\lambda_i^{\mathbf{\Lambda}})^{-1} \tag{3.105}$$

From (3.95) and (3.105)

$$P(\hat{\mathbf{s}}_i' \to \hat{\mathbf{s}}_j'; i \neq j) = \frac{1}{\pi}\int_0^{\frac{\pi}{2}} E\Big\{\exp\Big(-\frac{||\mathbf{H}_1\mathbf{e}_\mathbf{s}||^2}{4\sin^2\theta}\Big)\Big\}d\theta = \frac{1}{\pi}\int_0^{\frac{\pi}{2}} \Phi_\Omega(s)\Big|_{s=-\frac{1}{4\sin^2\theta}} d\theta$$

$$= \frac{1}{\pi}\int_0^{\frac{\pi}{2}} \prod_{i=1}^{4}(1 - s\lambda_i^{\mathbf{\Lambda}})^{-1}\Big|_{s=-\frac{1}{4\sin^2\theta}} d\theta = \frac{1}{\pi}\int_0^{\frac{\pi}{2}} \Big(\frac{\sin^2\theta}{\sin^2\theta + \frac{\lambda_1^{\mathbf{\Lambda}}}{4}}\Big)^2\Big(\frac{\sin^2\theta}{\sin^2\theta + \frac{\lambda_3^{\mathbf{\Lambda}}}{4}}\Big)^2 d\theta \tag{3.106}$$

3.3.3 Diversity Order Provided by Optimal Decoding for the Quasi-Orthogonal Code Family: Asymptotical Approach

For the Quasi-Orthogonal code, both s_1 and s_4 are taken from the QPSK constellation shown in Fig.3.1. For any distinct pair of $\hat{\mathbf{s}}_i'$ and $\hat{\mathbf{s}}_j'$, either e_1 or e_4 in (3.91) could be zero, but they could

not be zeros simultaneously. From (3.103), λ_1^{Λ} and λ_3^{Λ} are zeros if and only if $e_1 = e_4 = 0$. So, we conclude that either λ_1^{Λ} or λ_3^{Λ} could be zero, but they could not be both zeros. Assuming $\lambda_3^{\Lambda} = 0$ and $\lambda_1^{\Lambda} \neq 0$, as the SNR approaches infinity, i.e., σ^2 approaches zero, (3.106) changes to

$$\lim_{\sigma^2 \to 0} P(\, \hat{\mathbf{s}}_i' \to \hat{\mathbf{s}}_j'; i \neq j,\ \lambda_3^{\Lambda} = 0\,) = \lim_{\sigma^2 \to 0} \frac{1}{\pi} \int_0^{\frac{\pi}{2}} \Big(\frac{\sin^2\theta}{\sin^2\theta + \frac{|e_1+e_4|^2}{8\sigma^2}} \Big)^2 d\theta \quad (3.107)$$

In the calculations of (3.107) and some of the following equations, by using Lebesgue's Dominated Convergence Theorem presented in section 3.3.1, we switch the sequence of integral and limitation. In (3.107), we know that

$$\lim_{\sigma^2 \to 0} \Big(\frac{\sin^2\theta}{\sin^2\theta + \frac{|e_1+e_4|^2}{8\sigma^2}} \Big)^2 = \Big(\frac{8\sigma^2}{|e_1+e_4|^2} \Big)^2 \sin^4\theta \quad (3.108)$$

and

$$\Big| \Big(\frac{\sin^2\theta}{\sin^2\theta + \frac{|e_1+e_4|^2}{8\sigma^2}} \Big)^2 \Big| \leq 1 \quad (3.109)$$

which is integrable. Therefore using the Lebesgue's Dominated Convergence Theorem,

$$\begin{aligned} &\lim_{\sigma^2 \to 0} P(\, \hat{\mathbf{s}}_i' \to \hat{\mathbf{s}}_j'; i \neq j,\ \lambda_3^{\Lambda} = 0\,) \\ &= \frac{1}{\pi} \int_0^{\frac{\pi}{2}} \lim_{\sigma^2 \to 0} \Big(\frac{\sin^2\theta}{\sin^2\theta + \frac{|e_1+e_4|^2}{8\sigma^2}} \Big)^2 d\theta = \Big(\frac{8\sigma^2}{|e_1+e_4|^2} \Big)^2 \frac{1}{\pi} \int_0^{\frac{\pi}{2}} \sin^4\theta \, d\theta \end{aligned} \quad (3.110)$$

By taking logarithm on both sides of (3.110), when $\sigma^2 \to 0$,

$$\log P(\, \hat{\mathbf{s}}_i' \to \hat{\mathbf{s}}_j'; i \neq j,\ \lambda_3^{\Lambda} = 0\,) = -2\log\frac{1}{\sigma^2} + \log\Big\{ \Big(\frac{8}{|e_1+e_4|^2} \Big)^2 \frac{1}{\pi} \int_0^{\frac{\pi}{2}} \sin^4\theta \, d\theta \Big\} \quad (3.111)$$

According to (3.111), if we plot the error probability curve in logarithm scale versus SNR (in dB), the slope of the curve is -2. From section 2.1.3, we know that the slope of error performance

curve in the high SNR range indicates the diversity order, thus the diversity order provided by optimal decoding of Quasi-Orthogonal code is 2. We know from (3.103) and (3.104) that λ_1^{Λ} and λ_2^{Λ} are zeros if and only if $e_1 = -e_4$. Also, λ_3^{Λ} and λ_4^{Λ} are zeros if and only if $e_1 = e_4$.

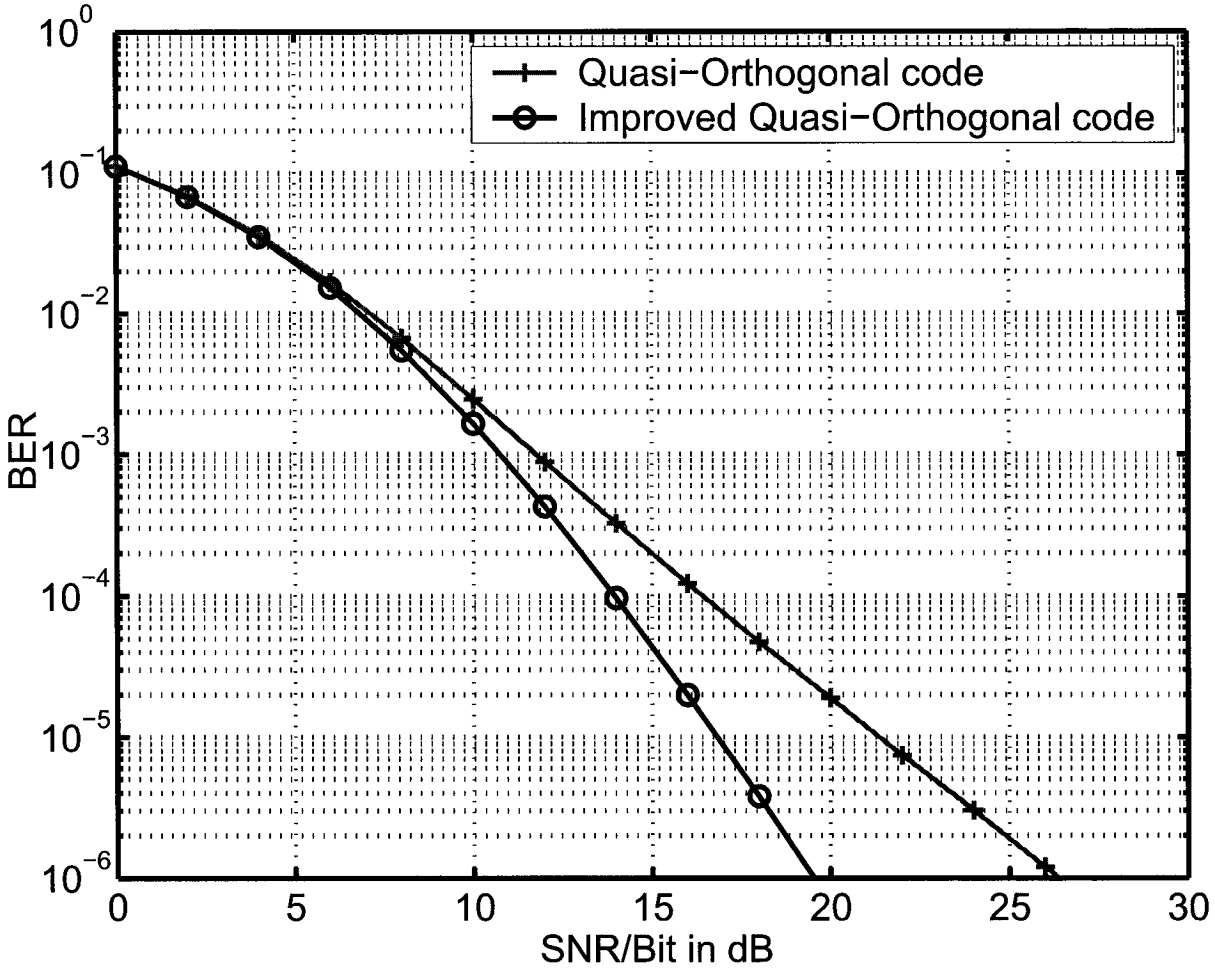

Fig. 3.5 Optimal Decoding for Quasi-Orthogonal code Family: Bit Error Rate

For Improved Quasi-Orthogonal code, s_4 is taken from the rotated QPSK constellation and s_1 is taken from QPSK constellation as given in Fig.3.1. For any distinct pair of $\hat{\mathbf{s}}_i'$ and $\hat{\mathbf{s}}_j'$, $e_1 \neq \pm e_4$ because of the relative rotation of signal constellations. So, none of the eigenvalues λ_i^{Λ}'s could be zero. As SNR approaches infinity, i.e., σ^2 approaches zero, by using Lebesgue's Dominated

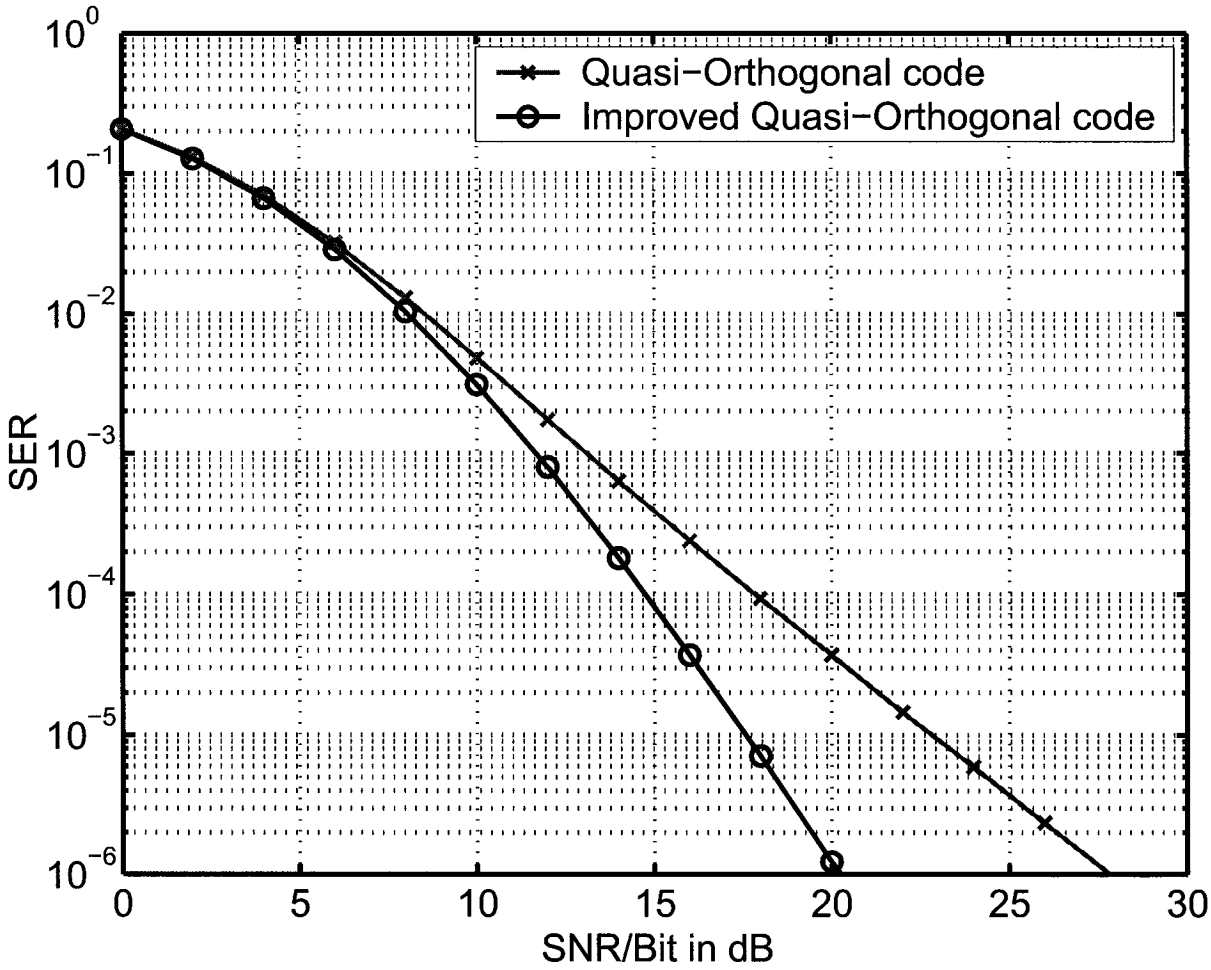

Fig. 3.6 Optimal Decoding for Quasi-Orthogonal code Family: Symbol Error Rate

Convergence Theorem, (3.106) changes to

$$\begin{aligned}
&\lim_{\sigma^2\to 0} P(\hat{\mathbf{s}}_i' \to \hat{\mathbf{s}}_j'; i \neq j,) = \lim_{\sigma^2\to 0} \frac{1}{\pi}\int_0^{\frac{\pi}{2}} \Big(\frac{\sin^2\theta}{\sin^2\theta + \frac{|e_1+e_4|^2}{8\sigma^2}}\Big)^2 \Big(\frac{\sin^2\theta}{\sin^2\theta + \frac{|e_1-e_4|^2}{8\sigma^2}}\Big)^2 d\theta \\
&= \frac{1}{\pi}\int_0^{\frac{\pi}{2}} \lim_{\sigma^2\to 0} \Big(\frac{\sin^2\theta}{\sin^2\theta + \frac{|e_1+e_4|^2}{8\sigma^2}}\Big)^2 \Big(\frac{\sin^2\theta}{\sin^2\theta + \frac{|e_1-e_4|^2}{8\sigma^2}}\Big)^2 d\theta \\
&= \Big(\frac{8\sigma^2}{|e_1+e_4|^2}\Big)^2 \Big(\frac{8\sigma^2}{|e_1-e_4|^2}\Big)^2 \frac{1}{\pi}\int_0^{\frac{\pi}{2}} \sin^8\theta\, d\theta
\end{aligned} \tag{3.112}$$

By taking logarithm on both sides of (3.112), when $\sigma^2 \to 0$,

$$\log P(\hat{\mathbf{s}}_i' \to \hat{\mathbf{s}}_j'; i \neq j,) = -4\log\frac{1}{\sigma^2} + \log\Big\{\Big(\frac{64}{|e_1+e_4|^2|e_1-e_4|^2}\Big)^2 \frac{1}{\pi}\int_0^{\frac{\pi}{2}} \sin^8\theta\, d\theta\Big\} \tag{3.113}$$

According to (3.113), if we plot the error probability curve in logarithm scale versus SNR (in dB), the slope of the curve is -4. From section 2.1.3, we know that that the slope of error performance curve in the high SNR range indicates the associated diversity order, thus the diversity order provided by optimal decoding of Improved Quasi-Orthogonal code is 4.

Computer simulations of optimal decoding of the Quasi-Orthogonal code and the Improved Quasi-Orthogonal code are illustrated in Fig.3.5 and Fig.3.6. The settings of the simulations have been presented in section 3.2.3 and the error performance curves are plotted based the computer simulations over 2.24×10^9 information bits. As we know, the slopes of the performance curves in the high SNR range indicate the diversity orders provided by the corresponding coding-decoding schemes. From Fig.3.5 and Fig.3.6, we see that the diversity orders provided by optimal decoding of Improved Quasi-Orthogonal code and Quasi-Orthogonal are 4 and 2 respectively, which have been proven by the analysis previously.

3.3.4 Error Performance for Simplified Decoding of the Quasi-Orthogonal Code Family

Error Performance of Decoding s_4

For decoding s_4, we have from (3.56),

$$r_{U\,4,1} = \grave{c}s_4 + n_{U\,4,1} \tag{3.114}$$

From (3.82) and (3.114), when the channel coefficients are known and with QPSK modulation, the symbol error probability (SEP) in decoding s_4 is

$$P(\hat{s_4} \neq s_4 \,\Big|\, \alpha_{1,n}; n = 1,2,3,4) = \frac{1}{\pi}\int_0^{\frac{3\pi}{4}} \exp\Big(-\frac{\grave{c}^2}{8\sin^2\theta}\Big)\, d\theta \tag{3.115}$$

By taking expectation with respect to $\grave{c}$, the symbol error probability in decoding s_4 is

$$P(\hat{s_4} \neq s_4) = E\{\, P(\hat{s_4} \neq s_4 \,\Big|\, \alpha_{1,n};\ ; n = 1,2,3,4)\,\} = \frac{1}{\pi}\int_0^{\frac{3\pi}{4}} E\Big\{\, \exp\big(-\frac{\grave{c}^2}{8\sin^2\theta}\big)\Big\}\, d\theta \tag{3.116}$$

From (3.46) and (3.52), we have

$$\grave{c} = \sqrt{\frac{A}{2\sigma^2} - \frac{B^2}{2A\sigma^2}} \tag{3.117}$$

where A and B are defined in (3.10) and (3.11). We substitute (3.117) into (3.116) and get

$$P(\hat{s_4} \neq s_4) = \frac{1}{\pi}\int_0^{\frac{3\pi}{4}} E\Big\{\exp\Big(-\frac{1}{8\sin^2\theta\sigma^2}\Big[\frac{1}{2}\Big(A - \frac{B^2}{A}\Big)\Big]\Big)\Big\} d\theta \tag{3.118}$$

where E denotes the expectation with respect to A and B.

Joint PDF of Random Variables A and B

From (3.10), (3.11) and (3.98), we re-write A and B as quadratic forms

$$A = \boldsymbol{\alpha}^H \boldsymbol{\Theta}_1 \boldsymbol{\alpha} = \boldsymbol{\alpha}^H \begin{pmatrix} 1 & 0 & 0 & 0 \\ 0 & 1 & 0 & 0 \\ 0 & 0 & 1 & 0 \\ 0 & 0 & 0 & 1 \end{pmatrix} \boldsymbol{\alpha} \tag{3.119}$$

and

$$B = \boldsymbol{\alpha}^H \boldsymbol{\Theta}_2 \boldsymbol{\alpha} = \boldsymbol{\alpha}^H \begin{pmatrix} 0 & 0 & 0 & 1 \\ 0 & 0 & -1 & 0 \\ 0 & -1 & 0 & 0 \\ 1 & 0 & 0 & 0 \end{pmatrix} \boldsymbol{\alpha} \tag{3.120}$$

From (3.79), we get the joint characteristic function of A and B as

$$\begin{aligned} \Phi_{A,B}(\omega_1, \omega_2) &= M_{A,B}(t_1, t_2)\big|_{t_1 = j\omega_1, t_2 = j\omega_2} \\ &= [1 - j(\omega_1 - \omega_2)]^{-2}[1 - j(\omega_1 + \omega_2)]^{-2} \end{aligned} \tag{3.121}$$

We take the inverse Fourier transform of $\Phi_{A,B}(\omega_1, \omega_2)$ as shown in Appendix A.4 to get the joint probability density function (pdf) of A and B as

$$\begin{aligned} f_{A,B}(a,b) &= \mathcal{F}^{-1}\big(\, \Phi_{A,B}(\omega_1, \omega_2) \,\big) \\ &= \begin{cases} \frac{1}{8}(a+b)(a-b)e^{-\frac{a+b}{2}} e^{-\frac{a-b}{2}}; & a+b>0 \text{ and } a-b>0 \\ 0 & \text{otherwise} \end{cases} \end{aligned} \tag{3.122}$$

Upper and Lower Bounds for Error Performance of Decoding s_4

In practice, it is hard to evaluate (3.118), and as an alternative, we calculate upper and lower bounds. Let

$$\begin{cases} U = A + B \\ V = A - B \end{cases} \Rightarrow \begin{cases} A = \frac{U+V}{2} \\ B = \frac{U-V}{2} \end{cases} \tag{3.123}$$

then

$$\frac{1}{2}\left(A - \frac{B^2}{A}\right) = \frac{(A+B)(A-B)}{2A} = \frac{UV}{U+V} \tag{3.124}$$

From the joint pdf of A and B given in (3.122), we have the joint pdf of U and V as derived in Appendix A.5, which is expressed as

$$f_{U,V}(u,v) = \begin{cases} \frac{1}{16}uve^{-\frac{u}{2}}e^{-\frac{v}{2}}; & u > 0 \text{ and } v > 0 \\ 0; & \text{otherwise.} \end{cases} \tag{3.125}$$

and the probability distribution functions of U and V are

$$f_U(u) = \int_0^\infty f_{U,V}(u,v)dv = \begin{cases} \frac{1}{4}ue^{-\frac{u}{2}}; & u > 0, \\ 0; & \text{otherwise} \end{cases} \tag{3.126}$$

and

$$f_V(v) = \int_0^\infty f_{U,V}(u,v)du = \begin{cases} \frac{1}{4}ve^{-\frac{v}{2}}; & v > 0 \\ 0; & \text{otherwise} \end{cases} \tag{3.127}$$

respectively. Since U and V are non-negative, we have

$$\begin{cases} \frac{UV}{U+V} < \frac{UV}{U} = V \\ \frac{UV}{U+V} < \frac{UV}{V} = U \end{cases} \Rightarrow \frac{UV}{U+V} < \min(U,V) \tag{3.128}$$

We also have

$$\begin{cases} \frac{UV}{U+V} > \frac{UV}{V+V} & \text{if } U < V \\ \frac{UV}{U+V} > \frac{UV}{U+U} & \text{if } U > V \end{cases} \Rightarrow \begin{cases} \frac{UV}{U+V} > \frac{U}{2} & \text{if } U < V \\ \frac{UV}{U+V} > \frac{V}{2} & \text{if } U > V \end{cases} \Rightarrow \frac{UV}{U+V} > \frac{1}{2}\min(U,V) \tag{3.129}$$

By combining (3.128) and (3.129), we get

$$\frac{1}{2}\min(U,V) < \frac{UV}{U+V} < \min(U,V) \tag{3.130}$$

Let $W = \min(U,V)$. From Appendix A.6, we have

$$f_W(w) = \frac{1}{2}we^{-w} + \frac{1}{4}w^2e^{-w}; \quad w > 0 \tag{3.131}$$

So the moment generating functions of W, which is calculated in Appendix A.7, is

$$\Phi_W(s) = \frac{1}{2}(1-s)^{-2} + \frac{1}{2}(1-s)^{-3} \tag{3.132}$$

By using (3.118), (3.124) and (3.130), we get

$$\frac{1}{\pi}\int_0^{\frac{3\pi}{4}} E\Big\{\exp\Big(-\frac{W}{8\sin^2\theta\sigma^2}\Big)\Big\}d\theta < P(\hat{s_4} \neq s_4) < \frac{1}{\pi}\int_0^{\frac{3\pi}{4}} E\Big\{\exp\Big(-\frac{W}{16\sin^2\theta\sigma^2}\Big)\Big\}d\theta \tag{3.133}$$

that can be put in the form

$$\frac{1}{\pi}\int_0^{\frac{3\pi}{4}} \Phi_W(s)\Big|_{s=-\frac{1}{8\sin^2\theta\sigma^2}} d\theta < P(\hat{s_4} \neq s_4) < \frac{1}{\pi}\int_0^{\frac{3\pi}{4}} \Phi_W(s)\Big|_{s=-\frac{1}{16\sin^2\theta\sigma^2}} d\theta \ . \quad (3.134)$$

From (3.132) and (3.134), the lower bound of the symbol error rate in decoding s_4 is given by

$$\begin{aligned} P_L(\hat{s_4} \neq s_4) &= \frac{1}{\pi}\int_0^{\frac{3\pi}{4}} \Phi_W(s)\Big|_{s=-\frac{1}{8\sin^2\theta\sigma^2}} d\theta \\ &= \frac{1}{2\pi}\int_0^{\frac{3\pi}{4}} \left(\frac{\sin^2\theta}{\sin^2\theta+\frac{1}{8\sigma^2}}\right)^2 d\theta + \frac{1}{2\pi}\int_0^{\frac{3\pi}{4}} \left(\frac{\sin^2\theta}{\sin^2\theta+\frac{1}{8\sigma^2}}\right)^3 d\theta \end{aligned} \quad (3.135)$$

and the upper bound of the symbol error rate in decoding s_4 is given by

$$\begin{aligned} P_U(\hat{s_4} \neq s_4) &= \frac{1}{\pi}\int_0^{\frac{3\pi}{4}} \Phi_W(s)\Big|_{s=-\frac{1}{16\sin^2\theta\sigma^2}} d\theta \\ &= \frac{1}{2\pi}\int_0^{\frac{3\pi}{4}} \left(\frac{\sin^2\theta}{\sin^2\theta+\frac{1}{16\sigma^2}}\right)^2 d\theta + \frac{1}{2\pi}\int_0^{\frac{3\pi}{4}} \left(\frac{\sin^2\theta}{\sin^2\theta+\frac{1}{16\sigma^2}}\right)^3 d\theta \end{aligned} \quad (3.136)$$

Numerical Evaluations for the Lower and Upper Bounds of Symbol Error Probability of Decoding s_4

Each of the two integrals in (3.135) and (3.136) has the form shown by (3.84) multiplied by scalar $\frac{1}{2}$. The difference between evaluations of upper and lower bounds is the value of c in (3.84), which is $\frac{1}{8\sigma^2}$ for the lower bound and $\frac{1}{16\sigma^2}$ for the upper bound. The relation between σ^2 and SNR/bit (in dB) is given by (3.73). With the aid of (3.85)-(3.87), we plot in Fig.3.7 the upper and lower bounds for SEP of decoding s_4 by using the Matlab routine in Program C.1.1 in Appendix C.1.

From Fig.3.7, we can see the upper bound is parallel to the lower bound and there is a 3 dB gap between two bounds. Both lower bound and upper bound show a diversity order of 2. The simulation result and the lower bound converge at high SNR, and the simulation result and upper bound converge at lower SNR. The simulation result of decoding s_4 in Fig.3.7 is obtained from computer simulations over 2.24×10^9 information bits.

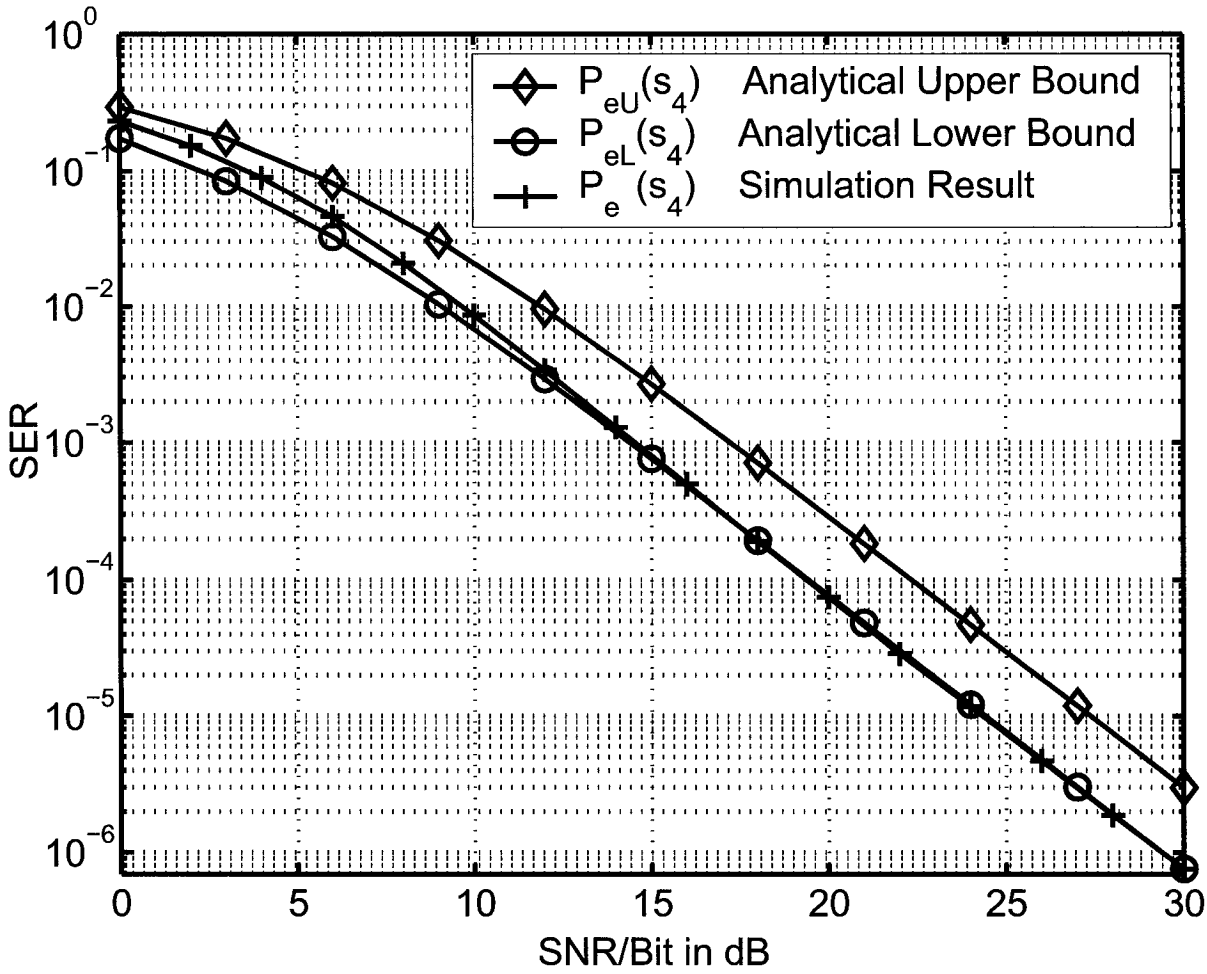

Fig. 3.7 Error Performance of Decoding s_4

Error Performance of Decoding s_1 Assuming s_4 Has Been Decoded Correctly

We consider the decoding of s_1 assuming s_4 has been decoded correctly. From (3.56), we have

$$r_{U\,1,1} = \grave{a}s_1 + \grave{b}s_4 + n_{U\,1,1} \tag{3.137}$$

Assuming s_4 has been decoded correctly, which means $\hat{s_4} = s_4$, then

$$r'_{U\,1,1} = r_{U\,1,1} - \grave{b}\hat{s_4} = r_{U\,1,1} - \grave{b}s_4 = \grave{a}s_1 + n_{U\,1,1} \tag{3.138}$$

where $n_{U\,1,1}$ is a zero-mean and unit-variance complex Gaussian. From (3.80), the symbol error rate of decoding s_1 assuming s_4 has been decoded correctly and the channel coefficients are known is

$$P(\hat{s_1} \neq s_1 \,\Big|\, \hat{s_4} = s_4;\ \alpha_{1,n}, n = 1,2,3,4) = \frac{1}{\pi}\int_0^{\frac{3\pi}{4}} \exp\Big(-\frac{\grave{a}^2}{8\sin^2\theta}\Big)\,d\theta \tag{3.139}$$

By taking expectation with respect to $\grave{a}$, the SEP in decoding s_1 assuming s_4 is known is

$$\begin{aligned} P(\hat{s_1} \neq s_1 \,\Big|\, \hat{s_4} = s_4) &= E\{\, P(\hat{s_1} \neq s_1 \,\Big|\, \hat{s_4} = s_4;\ \alpha_{1,n}, n = 1,2,3,4)\,\} \\ &= \frac{1}{\pi}\int_0^{\frac{3\pi}{4}} E\Big\{\, \exp\big(-\frac{\grave{a}^2}{8\sin^2\theta}\big)\Big\}\,d\theta \end{aligned} \tag{3.140}$$

From (3.46) and (3.50), we have

$$\grave{a} = \sqrt{\frac{A}{2\sigma^2}} \tag{3.141}$$

where A is defined by (3.10). Substituting (3.141) into (3.140), we get

$$P(\hat{s_1} \neq s_1 \,\Big|\, \hat{s_4} = s_4) = \frac{1}{\pi}\int_0^{\frac{3\pi}{4}} E\Big(\exp\Big\{-\frac{A}{16\sigma^2\sin^2\theta}\Big\}\Big)d\theta \tag{3.142}$$

where the expectation is with respect to A. We write A in quadratic form as given by (3.119). According to (3.79), the moment generating function of the random variable A is

$$\Phi_A(s) = (1-s)^{-4} \tag{3.143}$$

Accordingly, the symbol error rate in decoding s_1 assuming s_4 has been decoded correctly is

$$P(\hat{s_1} \neq s_1 \mid \hat{s_4} = s_4) = \frac{1}{\pi}\int_0^{\frac{3\pi}{4}} \Phi_A(s)\Big|_{s=-\frac{1}{16\sin^2\theta\sigma^2}} d\theta = \frac{1}{\pi}\int_0^{\frac{3\pi}{4}} \Big(\frac{\sin^2\theta}{\sin^2\theta + \frac{1}{16\sigma^2}}\Big)^4 d\theta \tag{3.144}$$

Numerical Evaluations for the Lower and Upper Bounds of Symbol Error Probability of Decoding s_4

(3.144) and (3.136) has the form shown by (3.84) with ϕ, m and c are replaced by $\frac{3\pi}{4}$, 4 and $\frac{1}{16\sigma^2}$ respectively. The relation between σ^2 and SNR/bit (in dB) is given by (3.73). With the aid of (3.85)-(3.87), we plot in Fig.3.8 the exact SEP of decoding s_1 assuming s_4 has been decoded correctly by using the Matlab routine in Program C.2.1 in Appendix C.2. The associated computer simulation over 2.24×10^9 information bits is also included in Fig 3.8. From Fig.3.8, we see that the simulation result matches the analytical result exactly and the diversity order provided by decoding s_1 assuming has been decoded correctly is 4.

As the SNR approaches infinity, i.e., σ^2 approaches 0, by using Lebesgue's Dominated Convergence Theorem, (3.135) changes to

$$\begin{aligned}
\lim_{\sigma^2\to 0} P_L(\hat{s_4} \neq s_4) &= \lim_{\sigma^2\to 0}\frac{1}{2\pi}\int_0^{\frac{3\pi}{4}} \Big(\frac{\sin^2\theta}{\sin^2\theta+\frac{1}{8\sigma^2}}\Big)^2 d\theta + \lim_{\sigma^2\to 0}\frac{1}{2\pi}\int_0^{\frac{3\pi}{4}} \Big(\frac{\sin^2\theta}{\sin^2\theta+\frac{1}{8\sigma^2}}\Big)^3 d\theta \\
&= \frac{1}{2\pi}\int_0^{\frac{3\pi}{4}} \lim_{\sigma^2\to 0}\Big(\frac{\sin^2\theta}{\sin^2\theta+\frac{1}{8\sigma^2}}\Big)^2 d\theta + \frac{1}{2\pi}\int_0^{\frac{3\pi}{4}} \lim_{\sigma^2\to 0}\Big(\frac{\sin^2\theta}{\sin^2\theta+\frac{1}{8\sigma^2}}\Big)^3 d\theta \\
&= \frac{1}{2\pi}(8\sigma^2)^2\int_0^{\frac{3\pi}{4}} \sin^4\theta\, d\theta + \frac{1}{2\pi}(8\sigma^2)^3\int_0^{\frac{3\pi}{4}} \sin^6\theta\, d\theta
\end{aligned} \tag{3.145}$$

and (3.136) changes to

$$\begin{aligned}\lim_{\sigma^2\to 0} P_U(\hat{s_4} \neq s_4) &= \lim_{\sigma^2\to 0} \frac{1}{2\pi}\int_0^{\frac{3\pi}{4}} \left(\frac{\sin^2\theta}{\sin^2\theta+\frac{1}{16\sigma^2}}\right)^2 d\theta + \lim_{\sigma^2\to 0} \frac{1}{2\pi}\int_0^{\frac{3\pi}{4}} \left(\frac{\sin^2\theta}{\sin^2\theta+\frac{1}{16\sigma^2}}\right)^3 d\theta \\ &= \frac{1}{2\pi}\int_0^{\frac{3\pi}{4}} \lim_{\sigma^2\to 0}\left(\frac{\sin^2\theta}{\sin^2\theta+\frac{1}{16\sigma^2}}\right)^2 d\theta + \frac{1}{2\pi}\int_0^{\frac{3\pi}{4}} \lim_{\sigma^2\to 0}\left(\frac{\sin^2\theta}{\sin^2\theta+\frac{1}{16\sigma^2}}\right)^3 d\theta \\ &= \frac{1}{2\pi}(16\sigma^2)^2\int_0^{\frac{3\pi}{4}} \sin^4\theta\, d\theta + \frac{1}{2\pi}(16\sigma^2)^3\int_0^{\frac{3\pi}{4}} \sin^6\theta\, d\theta \end{aligned} \tag{3.146}$$

Also (3.144) changes to

$$P(\hat{s_1} \neq s_1 \,\Big|\, \hat{s_4} = s_4) = \frac{1}{\pi}(16\sigma^2)^4\int_0^{\frac{3\pi}{4}} \sin^8\theta\, d\theta \propto \sigma^8 \tag{3.147}$$

Because as σ^2 approaches 0, the values of (3.145) and (3.146) are dominated by the first items, which are proportional to σ^4. If we plot the upper and lower bounds in logarithm scale to SNR (in dB). The slopes of the curves are -2. According to section 2.1.3, the diversity orders provided by the upper and lower bounds of simplified decoding of Quasi Orthogonal code family are 2. So the diversity order provided by the simplified decoding of Quasi Orthogonal code family is 2. For the same reason, from (3.147), we see that the diversity order of decoding s_1 assuming s_4 has been decoded correctly is 4. This matches the simulation result indicated in Fig. 3.8.

Error Performance of Decoding s_1 When $\hat{s_4}$ is Obtained From Decision Feedback

Now, we consider the performance of decoding s_1 when $\hat{s_4}$ is obtained from decision feedback. We assume the transmitted symbol for s_4 is z_1' illustrated in Fig.3.2. When we take the symmetrical property of the constellations in Fig.3.2 into account, the error probability of decoding s_1 is

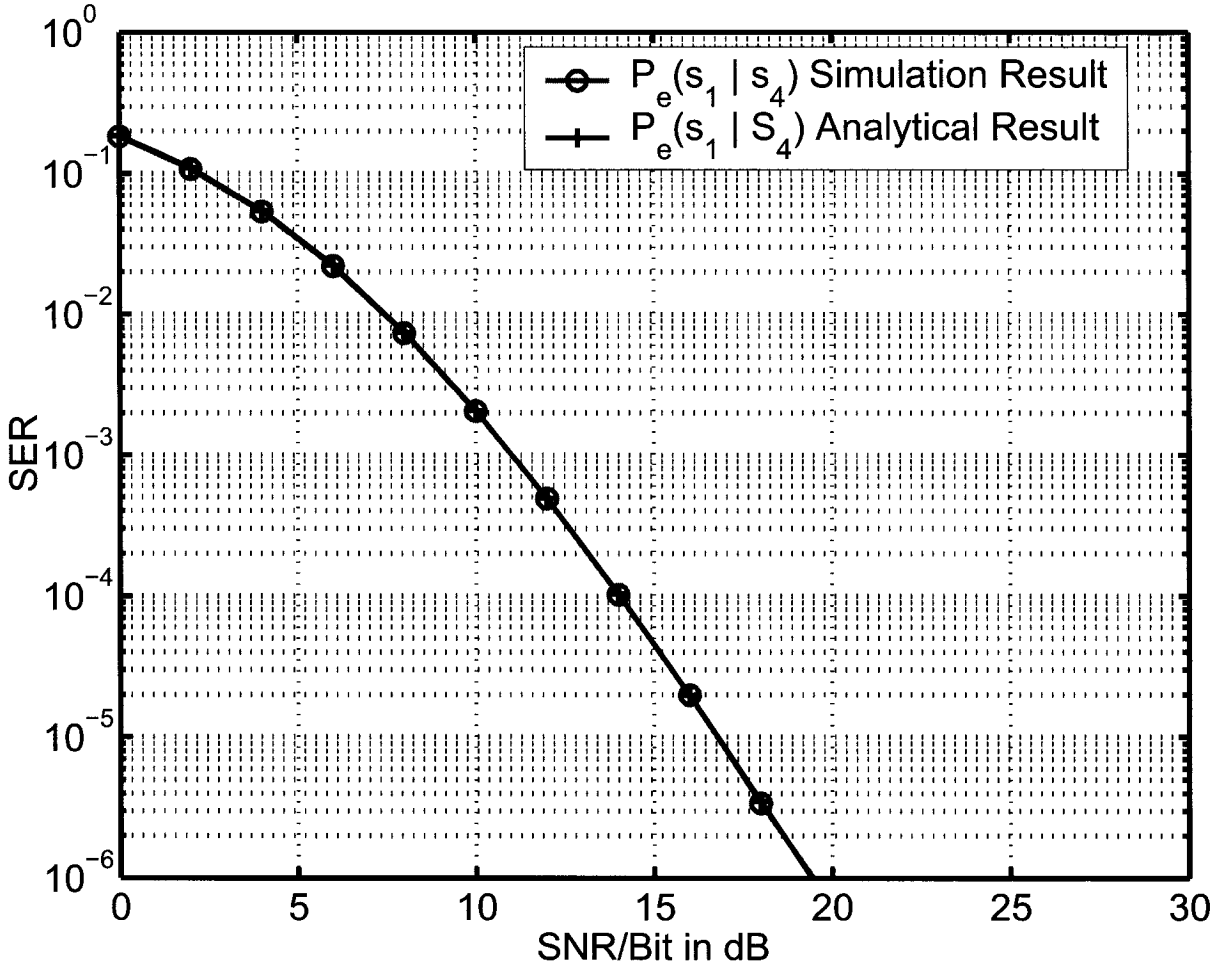

Fig. 3.8 Error Performance of Decoding s_1 Assuming s_4 Has Been Decoded Correctly

given as

$$\begin{aligned} & P(\hat{s_1} \neq s_1) = P(\hat{s_1} \neq s_1 \mid s_4 = z_1^{'}) \\ = \; & P(\hat{s_1} \neq s_1 \mid \hat{s_4} = z_1^{'}; s_4 = z_1^{'}) P(\hat{s_4} = z_1^{'} \mid s_4 = z_1^{'}) \\ & + P(\hat{s_1} \neq s_1 \mid \hat{s_4} = z_2^{'}; s_4 = z_1^{'}) P(\hat{s_4} = z_2^{'} \mid s_4 = z_1^{'}) \\ & + P(\hat{s_1} \neq s_1 \mid \hat{s_4} = z_3^{'}; s_4 = z_1^{'}) P(\hat{s_4} = z_3^{'} \mid s_4 = z_1^{'}) \\ & + P(\hat{s_1} \neq s_1 \mid \hat{s_4} = z_4^{'}; s_4 = z_1^{'}) P(\hat{s_4} = z_4^{'} \mid s_4 = z_1^{'}) \end{aligned} \tag{3.148}$$

where z_i's and $z_i^{'}$'s $(i = 1, 2, 3, 4)$ are indicated in Fig.3.2.

Next we investigate the diversity order of decoding s_1 when $\hat{s_4}$ is obtained from decision feedback as SNR approaches infinity, i.e., σ^2 approaches 0. Based on the calculations included in Appendix A.8, as SNR approaches infinity, (3.148) changes to

$$\begin{aligned} & P(\hat{s_1} \neq s_1 \mid \hat{s_4} = z_1^{'}; s_4 = z_1^{'}) \\ = \; & P(\hat{s_1} \neq s_1 \mid \hat{s_4} = z_1^{'}; s_4 = z_1^{'}) + P(\grave{a} + \sqrt{3}\grave{b} < 0) P(\hat{s_4} = z_2^{'} \mid s_4 = z_1^{'}) \\ + \; & \{1 - P^2[\grave{a} + (1 + \sqrt{3})\grave{b} > 0]\} P(\hat{s_4} = z_3^{'} \mid s_4 = z_1^{'}) + P(\grave{a} + \sqrt{3}\grave{b} < 0) P(\hat{s_4} = z_4^{'} \mid s_4 = z_1^{'}) \end{aligned} \tag{3.149}$$

Because

$$0 \leq 1 - P^2[\grave{a} + (1 + \sqrt{3})\grave{b} > 0] \leq 1 \quad \text{and} \quad 0 \leq P(\grave{a} + \sqrt{3}\grave{b} < 0) \leq 1 \tag{3.150}$$

we can form lower and upper bounds to (3.149) as

$$P(\hat{s_1} \neq s_1 \mid \hat{s_4} = z_1^{'}; s_4 = z_1^{'})$$

$$
\begin{aligned}
&+\min\{1-P^2[\grave{a}+(1+\sqrt{3})\grave{b}>0]\,;\,P(\grave{a}+\sqrt{3}\grave{b}<0)\}P(\hat{s_4}=z_2^{'}\mid s_4=z_1^{'})\\
&+\min\{1-P^2[\grave{a}+(1+\sqrt{3})\grave{b}>0]\,;\,P(\grave{a}+\sqrt{3}\grave{b}<0)\}P(\hat{s_4}=z_3^{'}\mid s_4=z_1^{'})\\
&+\min\{1-P^2[\grave{a}+(1+\sqrt{3})\grave{b}>0]\,;\,P(\grave{a}+\sqrt{3}\grave{b}<0)\}P(\hat{s_4}=z_4^{'}\mid s_4=z_1)^{'}\\
\leq\;& P(\hat{s_1}\neq s_1\mid s_4=z_1^{'})\\
\leq\;& P(\hat{s_1}\neq s_1\mid \hat{s_4}=z_1^{'};s_4=z_1^{'})+P(\hat{s_4}=z_2^{'}\mid s_4=z_1^{'})\\
&+P(\hat{s_4}=z_3^{'}\mid s_4=z_1^{'})+P(\hat{s_4}=z_4^{'}\mid s_4=z_1^{'})
\end{aligned}
\tag{3.151}
$$

or in the form

$$
\begin{aligned}
&P(\hat{s_1}\neq s_1\mid \hat{s_4}=s_4)\\
&+\min\{1-P^2[\grave{a}+(1+\sqrt{3})\grave{b}>0]\,;\,P(\grave{a}+\sqrt{3}\grave{b}<0)\}P(\hat{s_4}\neq s_4)\\
\leq\;& P(\hat{s_1}\neq s_1\mid s_4=z_1^{'})\\
\leq\;& P(\hat{s_1}\neq s_1\mid \hat{s_4}=s_4)+P(\hat{s_4}\neq s_4)
\end{aligned}
\tag{3.152}
$$

From the evaluation in Appendix A.9, we have that $\min\{1-P^2[\grave{a}+(1+\sqrt{3})\grave{b}>0];\,P(\grave{a}+\sqrt{3}\grave{b}<0)\}=0.1151$. We have already derived the analytical upper and lower bounds for decoding s_4, which is denoted as $P(\hat{s_4}\neq s_4)$ in (3.152). We also have derived the analytical result for decoding s_1 assuming s_4 has been decoded correctly, which is denoted as $P(\hat{s_1}\neq s_1\mid \hat{s_4}=s_4)$ in (3.152). According to (3.152), we plot the analytical lower bound expressed as

$$
P(\hat{s_1}\neq s_1\mid \hat{s_4}=s_4)+0.1151P_L(\hat{s_4}\neq s_4) \tag{3.153}
$$

and the analytical upper bound expressed as

$$
P(\hat{s_1}\neq s_1\mid \hat{s_4}=s_4)+P_U(\hat{s_4}\neq s_4) \tag{3.154}
$$

in Fig.3.9, as well as the analytical approximation expressed as

$$P(\hat{s_1} \neq s_1 \mid \hat{s_4} = s_4) + P_L(\hat{s_4} \neq s_4) \tag{3.155}$$

and the result from computer simulations over 2.24×10^9 information bits in Fig.3.9. From the

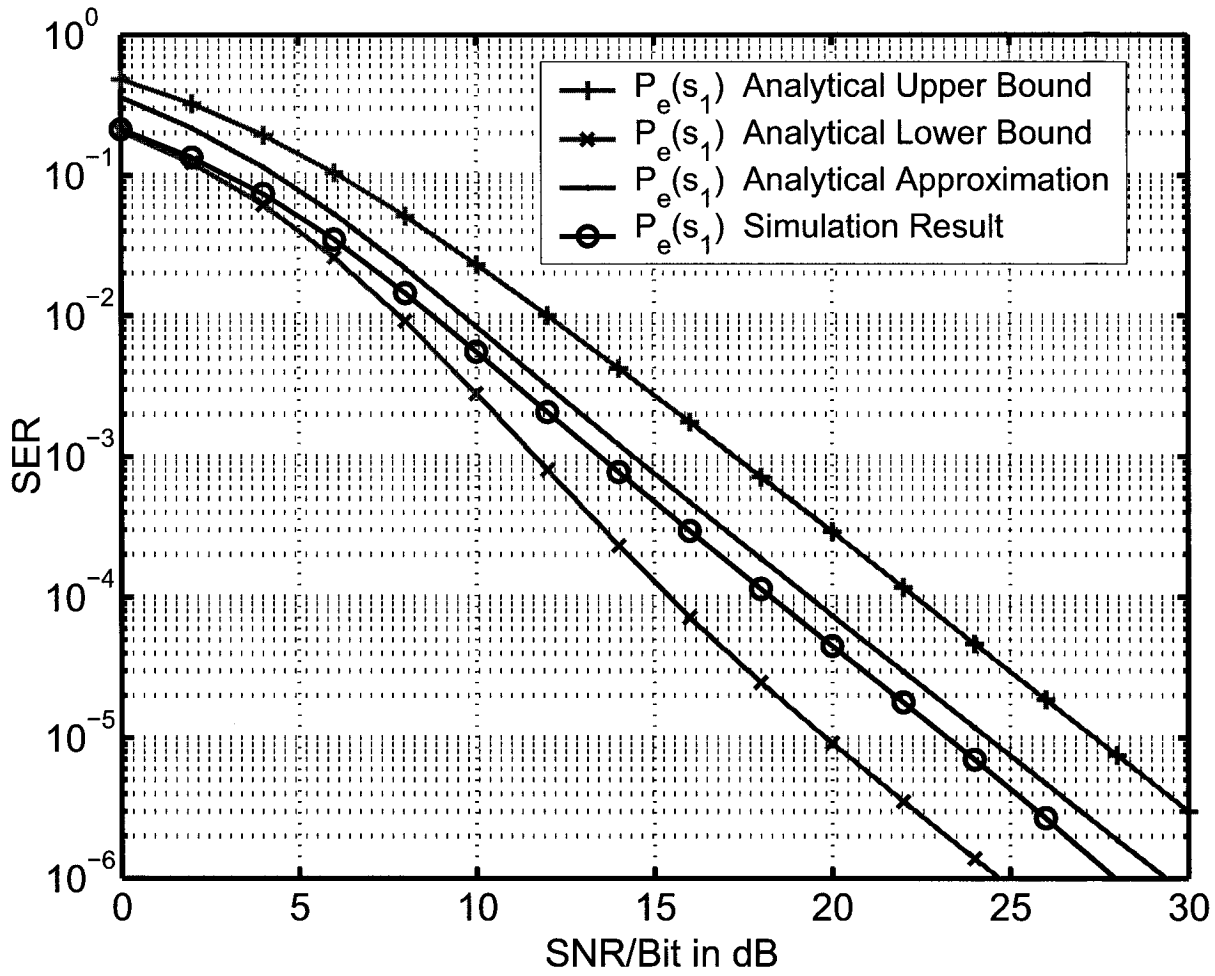

Fig. 3.9 Error Performance of Decoding s_1 When $\hat{s_4}$ is From Decision Feedback

previous analysis in this section we know that the diversity order provided by decoding s_4 is 2 and the diversity order provided by decoding s_1 assuming s_4 has been decoded correctly is 4. From the expression of (3.152), we conclude that if $\min\{1-P^2[\grave{a}+(1+\sqrt{3})\grave{b} < 0]; P(\grave{a}+\sqrt{3}\grave{b} > 0)\} \neq 0$,

which has been proven to be true in Appendix A.9, the diversity order of decoding s_1 assuming s_4 is from the decision feedback is decided by the diversity order provided by decoding s_4, which is 2 (3.135) (3.136). From Fig.3.9, we find that the simulation result and upper and lower bounds are parallel with slope -2 when SNR is sufficiently large, which implies the diversity order of decoding s_1 when s_4 is from decision feedback is 2. This confirms the conclusion that the diversity order of decoding s_1 when s_4 is from decision feedback is 2 based on (3.152).

3.3.5 Analysis of Diversity Loss in the Simplified Decoding for the Improved Quasi Orthogonal code

From (3.112), the diversity order provided by the optimal decoding of Improved Quasi-Orthogonal code is 4. However, from section 3.3.4 and the simulation results based on the evaluation over 2.24×10^9 information bits illustrated in Fig.3.10 and Fig.3.11, we see that when the simplified decoding is employed, the diversity order provided by Improved Quasi-Orthogonal code is 2. In the following, we analyze this diversity order loss. Assuming MPSK modulation, from (3.80) and (3.118), the average symbol error rate in decoding s_4 is

$$\begin{aligned} P(\hat{s_4} \neq s_4) &= \frac{1}{\pi}\int_0^{\frac{(M-1)\pi}{M}} E\Big\{ \exp\big(-\frac{\sin^2\frac{\pi}{M}}{8\sigma^2\sin^2\theta}[A-\frac{B^2}{A}]\big)\Big\}d\theta \\ &= \frac{1}{\pi}\int_0^{\frac{(M-1)\pi}{M}} E\Big\{ \exp\big(-\frac{\sin^2\frac{\pi}{M}}{4\sigma^2\sin^2\theta}[\frac{(A+B)(A-B)}{(A+B)+(A-B)}]\big)\Big\}d\theta \\ &= \frac{1}{\pi}\int_0^{\frac{(M-1)\pi}{M}} M_{\frac{(A+B)(A-B)}{(A+B)+(A-B)}}(t)\Big|_{t=-\frac{\sin^2\frac{\pi}{M}}{4\sigma^2\sin^2\theta}} d\,\theta \end{aligned} \tag{3.156}$$

where $M_{\frac{(A+B)(A-B)}{(A+B)+(A-B)}}(t)$ denotes the moment generating function of random variable $\frac{(A+B)(A-B)}{(A+B)+(A-B)}$.

From the previous derivation given by (3.126) and (3.127), we know that $U = A + B$ and $V = A - B$ are non-negative. So

$$\frac{1}{2}\min(A-B, A+B) < \frac{(A+B)(A-B)}{(A+B)+(A-B)} < \min(A-B, A+B) \tag{3.157}$$

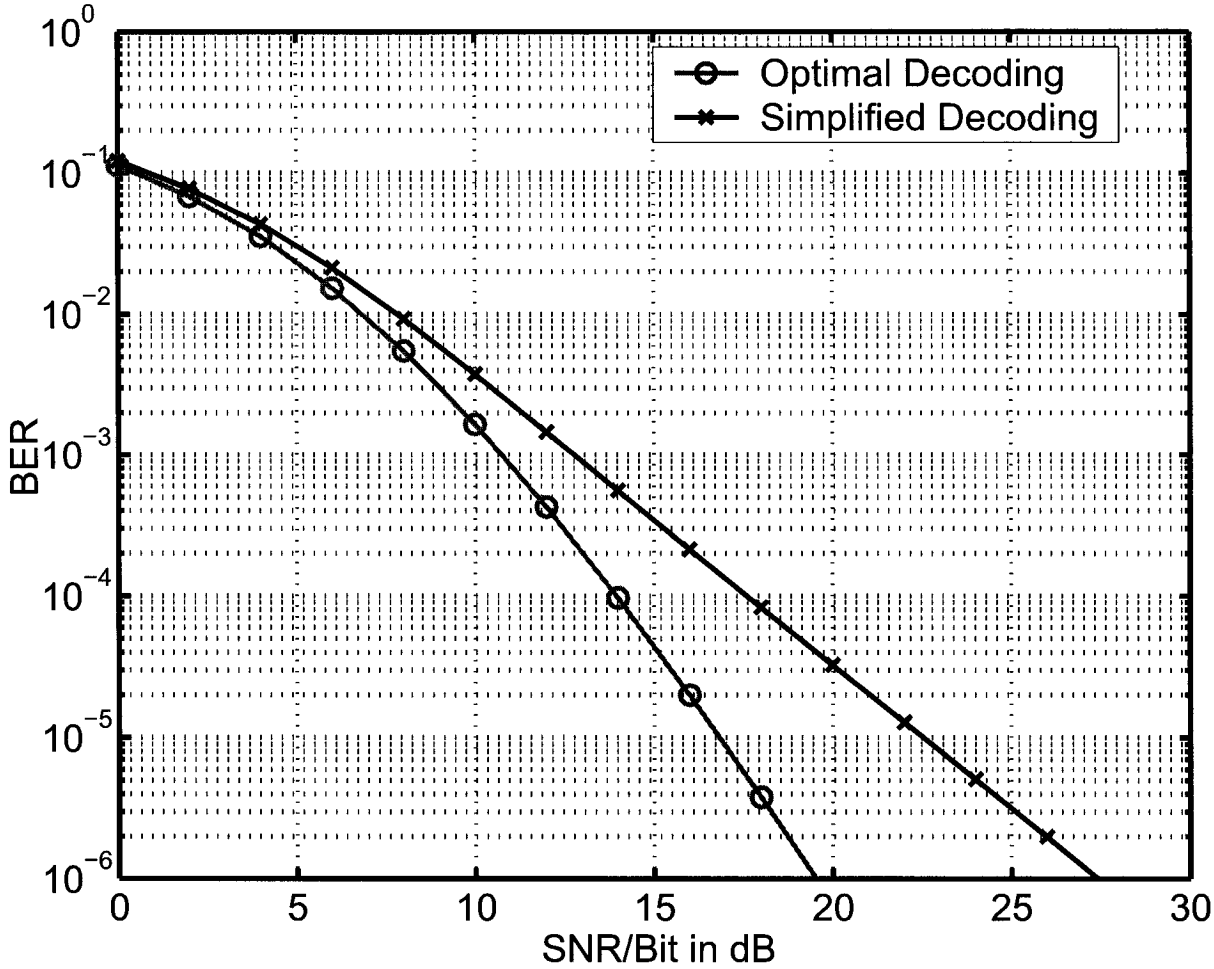

Fig. 3.10 Different Decoding Algorithms for the Improved Quasi-Orthogonal code: Bit Error Rate

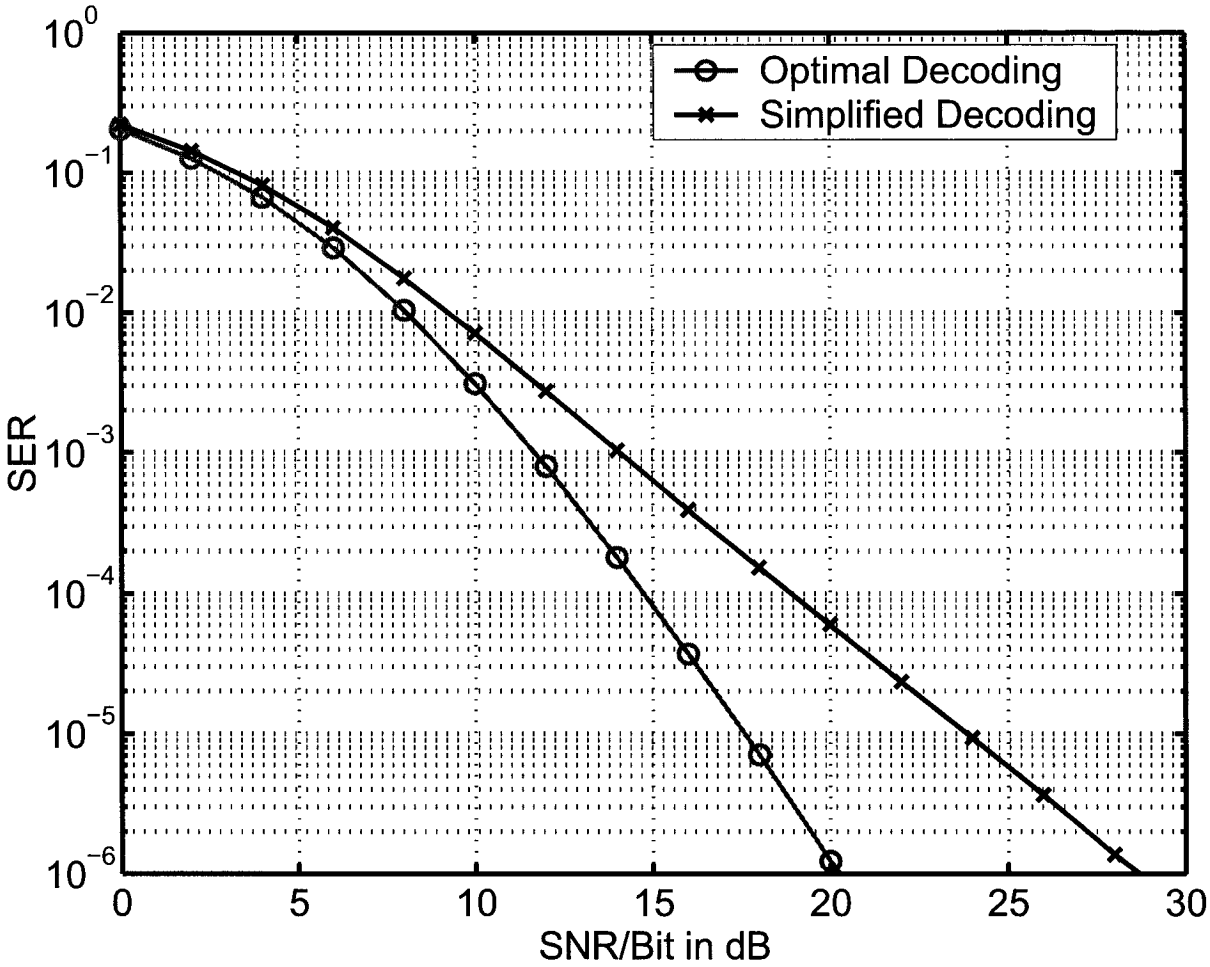

Fig. 3.11 Different Decoding Algorithms for the Improved Quasi-Orthogonal code: Symbol Error Rate

We combine (3.156) and (3.157) and have the lower bound of error probability in decoding s_4 as

$$P_{\mathcal{L}}(\hat{s_4} \neq s_4) = \frac{1}{\pi}\int_0^{\frac{(M-1)\pi}{M}} M_{\min(A-B,A+B)}(t)\Big|_{t=-\frac{\sin^2\frac{\pi}{M}}{4\sigma^2\sin^2\theta}} d\,\theta \tag{3.158}$$

We write A, B in the generalized Hermitian quadratic form as

$$A = \boldsymbol{\alpha}^H \begin{pmatrix} a_1 & & & \\ & a_2 & & \\ & & a_3 & \\ & & & a_4 \end{pmatrix} \boldsymbol{\alpha} = \boldsymbol{\alpha}^H \boldsymbol{\Theta_3} \boldsymbol{\alpha} \tag{3.159}$$

$$B = \boldsymbol{\alpha}^H \begin{pmatrix} & & & b_1 \\ & & b_2 & \\ & b_3 & & \\ b_4 & & & \end{pmatrix} \boldsymbol{\alpha} = \boldsymbol{\alpha}^H \boldsymbol{\Theta_4} \boldsymbol{\alpha} \tag{3.160}$$

where $\boldsymbol{\alpha}$ is defined by (3.98) and

$$a_1 = a_2 = a_3 = a_4 = b_1 = b_4 = 1; \quad b_2 = b_3 = -1 \tag{3.161}$$

According to (3.79), the joint moment generating function of A and B is

$$\begin{aligned} M_{A,B}(t_1, t_2) &= \frac{1}{\left|\mathbf{I} - t_1\boldsymbol{\Theta_3} - t_2\boldsymbol{\Theta_4}\right|} \\ &= \frac{1}{\left[(1-a_1t_1)(1-a_4t_1) - b_1b_4t_2^2\right]\left[(1-a_2t_1)(1-a_3t_1) - b_2b_3t_2^2\right]} \end{aligned} \tag{3.162}$$

Because

$$M_{A+B}(t) = M_{A,B}(t_1, t_2)\Big|_{t_2=t_1=t} \tag{3.163}$$

and

$$M_{A-B}(t) = M_{A,B}(t_1, t_2)\Big|_{t_1=t,t_2=-t} \tag{3.164}$$

By combining (3.162), (3.163) and (3.164), we have

$$\begin{aligned} M_{A+B}(t) &= M_{A-B}(t) \\ &= \frac{1}{\left[(1-a_1t)(1-a_4t) - b_1b_4t^2\right]\left[(1-a_2t)(1-a_3t) - b_2b_3t^2\right]} \end{aligned} \tag{3.165}$$

If we take $a_1 = a_4$, $b_1 = b_4$, $a_2 = a_3$ and $b_2 = b_3$ as indicated in (3.161), then (3.165) changes to

$$M_{A+B}(t) = M_{A-B}(t) = \frac{1}{\left[1-(a_1-b_1)t\right]\left[1-(a_1+b_1)t\right]\left[1-(a_2-b_2)t\right]\left[1-(a_2+b_2)t\right]} \tag{3.166}$$

From (3.158) and (3.166), when SNR approaches infinity,

$$\begin{aligned} &\lim_{\sigma^2\to 0} P_{\mathcal{L}}(\hat{s_4} \neq s_4) = \lim_{\sigma^2\to 0} \frac{1}{\pi}\int_0^{\frac{(M-1)\pi}{M}} M_{\min(A-B,A+B)}(t)\Big|_{t=-\frac{\sin^2\frac{\pi}{M}}{4\sigma^2\sin^2\theta}} d\theta \\ &= \frac{1}{\pi}\int_0^{\frac{(M-1)\pi}{M}} \lim_{\sigma^2\to 0} \frac{1}{\left[1-(a_1-b_1)t\right]\left[1-(a_1+b_1)t\right]\left[1-(a_2-b_2)t\right]\left[1-(a_2+b_2)t\right]}\Big|_{t=-\frac{\sin^2\frac{\pi}{M}}{4\sigma^2\sin^2\theta}} d\theta \\ &= \frac{1}{\pi}\int_0^{\frac{(M-1)\pi}{M}} \frac{(4\sigma^2\sin^2\theta)^4}{(a_1+b_1)(a_1-b_1)(a_2+b_2)(a_2-b_2)\sin^8\frac{\pi}{M}} d\theta \propto \sigma^8 \end{aligned} \tag{3.167}$$

From (3.167), if we plot $P_{\mathcal{L}}(\hat{s_4} \neq s_4)$ in logarithm scale versus SNR (in dB), the slope of the curve is -4. From section 2.1.3, we know that the lower bound of error probability in decoding s_4 is 4. However, for Improved Quasi-Orthogonal code, we should take $a_1 - b_1 = 0$ and $a_2 + b_2 = 0$ as indicated in (3.161) into consideration as well. So, when SNR approaches infinity, we evaluate

the lower bound of error probability in decoding s_4 differently as

$$\begin{aligned}
&\lim_{\sigma^2\to 0} P_{\mathcal{L}}(\hat{s_4} \neq s_4) = \lim_{\sigma^2\to 0} \frac{1}{\pi} \int_0^{\frac{(M-1)\pi}{M}} M_{\min(A-B,A+B)}(t)\Big|_{t=-\frac{\sin^2\frac{\pi}{M}}{4\sigma^2\sin^2\theta}} \, d\,\theta \\
= &\frac{1}{\pi} \int_0^{\frac{(M-1)\pi}{M}} \lim_{\sigma^2\to 0} \frac{1}{\left[1-(a_1-b_1)t\right]\left[1-(a_1+b_1)t\right]\left[1-(a_2-b_2)t\right]\left[1-(a_2+b_2)t\right]}\Big|_{t=-\frac{\sin^2\frac{\pi}{M}}{4\sigma^2\sin^2\theta}} d\theta \\
= &\frac{1}{\pi} \int_0^{\frac{(M-1)\pi}{M}} \lim_{\sigma^2\to 0} \frac{1}{\left[1-(a_1+b_1)t\right]\left[1-(a_2-b_2)t\right]}\Big|_{t=-\frac{\sin^2\frac{\pi}{M}}{4\sigma^2\sin^2\theta}} d\theta \\
= &\frac{1}{\pi} \int_0^{\frac{(M-1)\pi}{M}} \frac{(4\sigma^2\sin^2\theta)^2}{(a_1+b_1)(a_2-b_2)\sin^4\frac{\pi}{M}} d\theta \propto \sigma^4
\end{aligned} \tag{3.168}$$

From (3.168), if we plot $P_{\mathcal{L}}(\hat{s_4} \neq s_4)$ in logarithm scale versus SNR (in dB), the slope of the curve is -2. From section 2.1.3, we know that the actual lower bound of error probability in decoding s_4 is 2. So, the error probability in decoding s_4 is 2 at most. By comparing (3.167) and (3.168), we know that because of $a_1 - b_1 = 0$ and $a_2 + b_2 = 0$, the diversity order provided by Improved Quasi-Orthogonal code in decoding s_4 is reduced from 4 to 2 as shown in Fig.3.10 and Fig.3.11.

Chapter 4

Performance over Spatially Correlated Rayleigh Fading Channels

Up to this point, we have only considered the transmissions over independent Rayleigh fading channels described in section 2.1.1. However, in real propagation environments, the fading coefficients from different channels are not necessarily independent. For example, in order to realize independent fading channels for downlinks, a separation of a few wavelengths is required between two adjacent antennas. In the implementation, this requirement can not be satisfied all the time. Insufficient spacing between the transmit antennas results in spatially correlated fading channels. It is interesting to investigate the performances of the decoding schemes described in chapter 3 over correlated Rayleigh fading channels. In this chapter, we consider the performances of decoding schemes over correlated Rayleigh fading channels by using the "one-ring" model [41] [42].

4.1 One Ring Model

The one-ring model, which was first mentioned in [41] and extended in [42], is employed to determine the correlation coefficients between different fading channels. One-ring model is an

appropriate abstract model of the communication system when transmit antennas are elevated and unobstructed by local scatters. In the one-ring model, the receive antenna is assumed to be surrounded by local scatters. We denote

- λ as the wavelength;
- D as the distance between base station and mobile station;
- R as the radius of scatters around mobile station;
- d as the distance between two transmit antennas;

as indicated in the Fig.4.1.

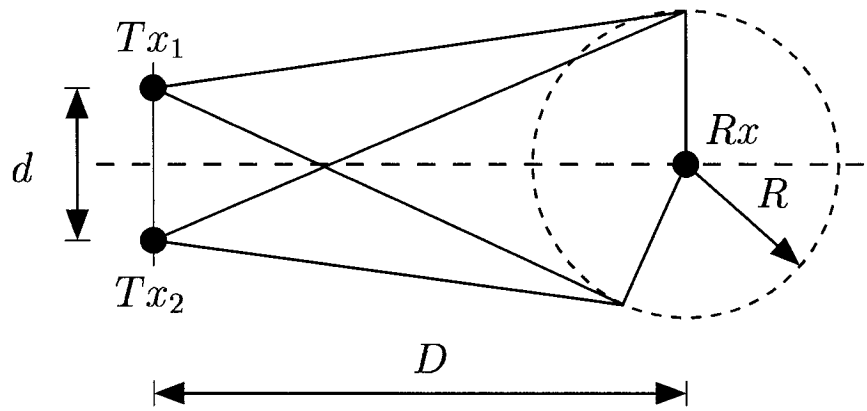

Fig. 4.1 One-ring Model

From [42], the correlation coefficient between the fading processes associated with the two transmit antennas is given by

$$\gamma = J_0\Big(\arcsin\big(\frac{R}{D}\big)\frac{2\pi}{\lambda}d\Big) \tag{4.1}$$

In (4.1), J_0 stands for the first kind Bessel function of the zeroth order. From (4.1), we find that the value of the correlation coefficient depends on two factors: d/λ and R/D. The factor d/λ is

determined by the carrier frequency and the antenna array topology of a wireless communication system. Once the system is set up, seldom does the ratio d/λ change. The factor of R/D reflects the working environment close to the mobile, which can change with the movement of the mobile. Typical values of the distance between base station and mobile station are listed in Table 4.1 and the typical value of the radius of the scatters ranges from 100λ to 200λ.

	Suburban Macro Cell	Urban Macro Cell	Urban Micro Cell
D	1500m	1500m	500m

Table 4.1 Typical Values of the Distance Between BS and MS

From (4.1), we calculate the correlation coefficients based on different combinations of the ratio d/λ and the ratio R/D. The results are listed in Table 4.2. From Table4.2, we have the

d/λ R/D	0.5	2	5	10	20
$D = 1500m$					
0.0111	0.9997	0.9951	0.9698	0.8818	0.5689
0.0139	0.9995	0.9924	0.9530	0.8185	0.3717
0.0167	0.9993	0.9891	0.9326	0.7440	0.1697
0.0194	0.9991	0.9851	0.9089	0.6602	−0.0200
0.0222	0.9988	0.9806	0.8818	0.5688	−0.1821
$D = 500m$					
0.0333	0.9973	0.9566	0.7440	0.1696	−0.3780
0.0417	0.9957	0.9326	0.6152	−0.1056	−0.0974
0.0500	0.9938	0.9036	0.4716	−0.3046	0.2208
0.0583	0.9916	0.8700	0.3204	−0.3972	0.2852
0.0667	0.9890	0.8319	0.1689	−0.3777	0.0735

Table 4.2 Correlation Coefficients Between the Adjacent Antennas f = 1.8GHz $R = 100\lambda \sim 200\lambda$

following observations.

1. Considering any row we see that the correlation coefficient decreases as d/λ increases. In the implementation, when the carrier frequency is fixed, we can decrease the correlation between

channels by increasing the distance between transmit antennas.

2. When d/λ and R are fixed, the correlation coefficient decreases as the distance between base station (BS) and mobile station (MS) decreases. In the implementation, when carrier frequency and the distance between antennas are fixed, we can decrease the correlation between channels by decreasing the distance between BS and MS.

4.2 Realization of Spatially Correlated Rayleigh Fading Channels in Computer Simulations

In the following sections, we investigate the influence of spatially correlation on the performances of the optimal and the simplified decoding schemes discussed in chapter 3 by the use of computer simulations.

The general settings of simulations are exactly the same as those described in section 3.2.3 except the realization of spatially correlated Rayleigh fading channels. The method employed to implement the spatially correlated Rayleigh fading channels is presented in the following. The correlations among different transmission paths of a four transmit antennas to one receive antenna wireless communication system can be described by a 4×4 symmetric matrix $\mathbf{C_s}$. The $(i,j)^{\text{th}}$ and the $(j,i)^{\text{th}}$ $(1 \leq i,j \leq 4)$ elements of $\mathbf{C_s}$ denote the correlation coefficient between the channel from the i^{th} transmit antenna and the channel from the j^{th} transmit antenna. Assuming that the transmit antennas form an equally-spaced linear array. From (4.1), the $(i,j)^{\text{th}}$ and $(j,i)^{\text{th}}$ element of $\mathbf{C_s}$ are calculated by

$$\mathbf{C_s}(i,j) = \mathbf{C_s}(j,i) = J_0\big(\arcsin\big(\frac{R}{D}\big)\frac{2\pi}{\lambda}|i-j|d'\big) \tag{4.2}$$

where d' denotes the distance between the adjacent antennas. We denote by $\mathbf{C_R}$ the Hermitian

root of $\mathbf{C_s}$, which means

$$\mathbf{C_s} = \mathbf{C_R} \cdot \mathbf{C_R} \tag{4.3}$$

We also denote

$$\mathbf{a} = (a_{1,1} \ a_{1,2} \ a_{1,3} \ a_{1,4})^T \tag{4.4}$$

as the independent channel fading coefficients, where $a_{1,j}$ $(1 \leq j \leq 4)$ denotes the channel fading coefficient from the j^{th} transmit antenna to the receive antenna. The coefficients $a_{1,j}$'s are modeled as i.i.d complex Gaussian distributed with zero-mean and variance 0.5 in each complex dimension. In order to generate the channel coefficients with correlation matrix $\mathbf{C_s}$, which is denoted as $\mathbf{a}'$, we left-multiply $\mathbf{a}$ with $\mathbf{C_R}$,

$$\mathbf{a}' = (a'_{1,1} \ a'_{1,2} \ a'_{1,3} \ a'_{1,4})^T = \mathbf{C_R a} \tag{4.5}$$

We have

$$E\{\mathbf{a}'\mathbf{a}'^H\} = \mathbf{C_R} E\{\mathbf{a}\mathbf{a}^H\} \mathbf{C_R}^H = \mathbf{C_s} \tag{4.6}$$

From (4.2), we know that the diagonal elements of $\mathbf{C_s}$ are equal to 1. So, we can conclude that generating the channel coefficients by using (4.5) does not change the SNR of the system model.

4.3 Performance over Spatially Correlated Channels

We choose several typical values of correlation coefficients from Table 4.2 corresponding to different level of correlation for the computer simulations. The settings of the computation simulations have been presented in section 3.2.3 and section 4.2. The performances of the optimal de-

coding and the simplified decoding of the Improve Quasi-Orthogonal code over correlated channels based on the experiments of 2.24×10^9 information bits are shown in Fig.4.2 and Fig.4.3. The performances of the optimal decoding and the simplified decoding of the Improve Quasi-Orthogonal code over independent channels are also included as the baseline of comparisons.

As we discussed previously, the slopes of the error performance curves in the high SNR range indicate the diversity orders provided by corresponding coding-decoding schemes. For example, as shown in Fig.4.2 and Fig.4.3, the diversity orders provided by the optimal and the simplified decoding schemes of the Improved Quasi-Orthogonal code over independent channels ($\gamma = 0$) are 4 and 2, respectively. These are also backed up by the mathematical analysis included in chapter 3. As indicated in Fig.4.2 and Fig.4.3, the slopes of the performance curves decrease as the correlation coefficient, which is denoted as γ, increases. When $\gamma = 0.9993$, the slopes of the curves decrease to the values close to 1. In other words, the diversity gains brought by STBC schemes are reduced because of the correlations among the channels.

The other phenomenon we are interested in is the change of the performance gaps between the optimal and the simplified decoding schemes of the Improved Quasi-Orthogonal code. We take the measurements in terms of bit error rate shown in Fig.4.2 as example. For the BER at 10^{-4} level, the performance gap between the optimal and the simplified decoding schemes over independent channels is about 3.5 dB. When $\gamma = 0.7440$, the gap decreases to 2.5 dB. As γ increases to 0.9993, which is corresponding to highly correlated channels, the gap is less than 0.5 dB. Therefore, the performance gaps between the optimal and the simplified decoding schemes of the Improved Quasi-Orthogonal code decrease as the correlations among the channels increase.

4.4 Conclusion

In designing a wireless communication system, we seek a technique that achieves better performance and lower complexity. When the requirements of performance and complexity can not be

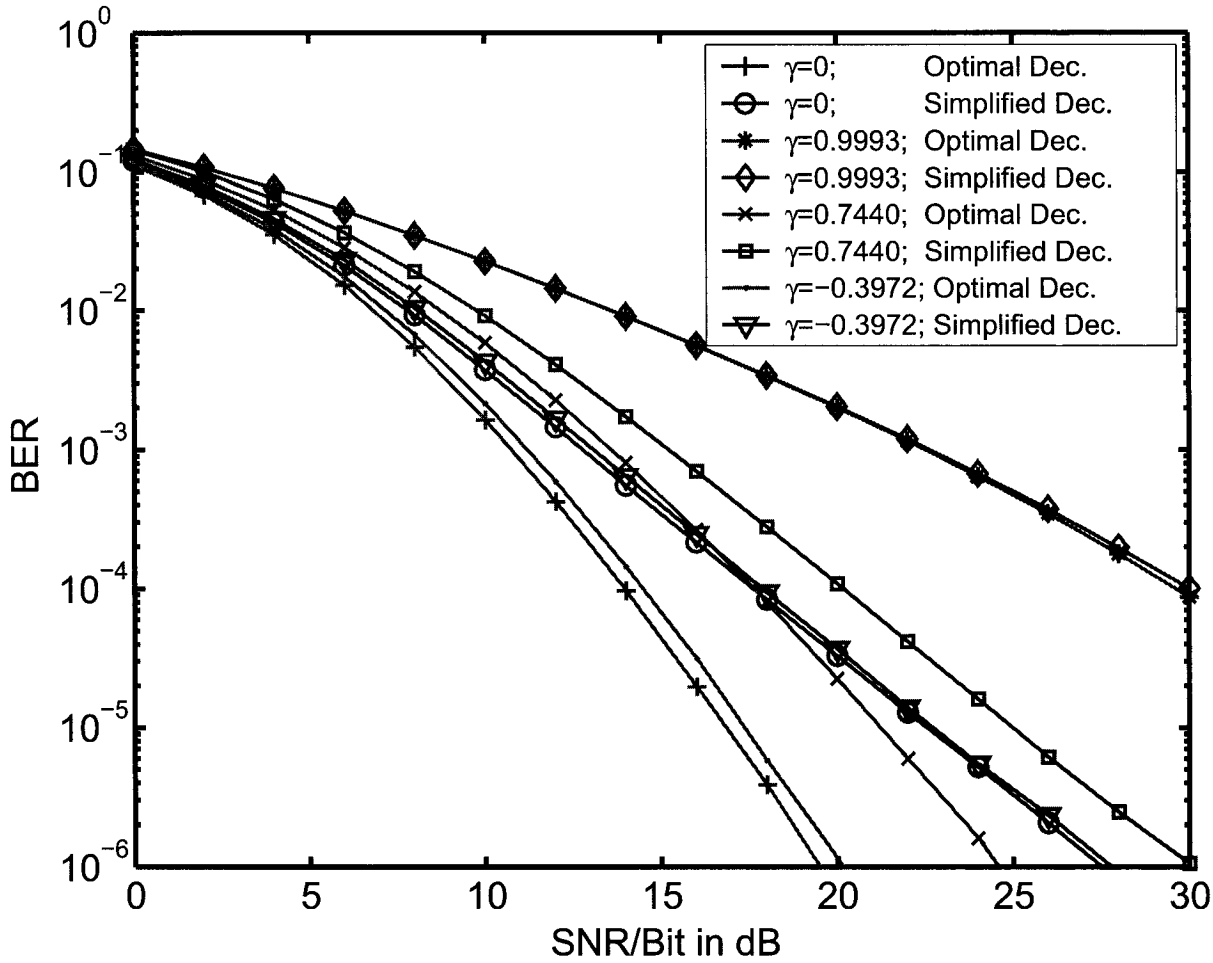

Fig. 4.2 Different Decoding Algorithms for the Improved Quasi-Orthogonal code Over Independent and Spatially Correlated Channels: Bit Error Rate

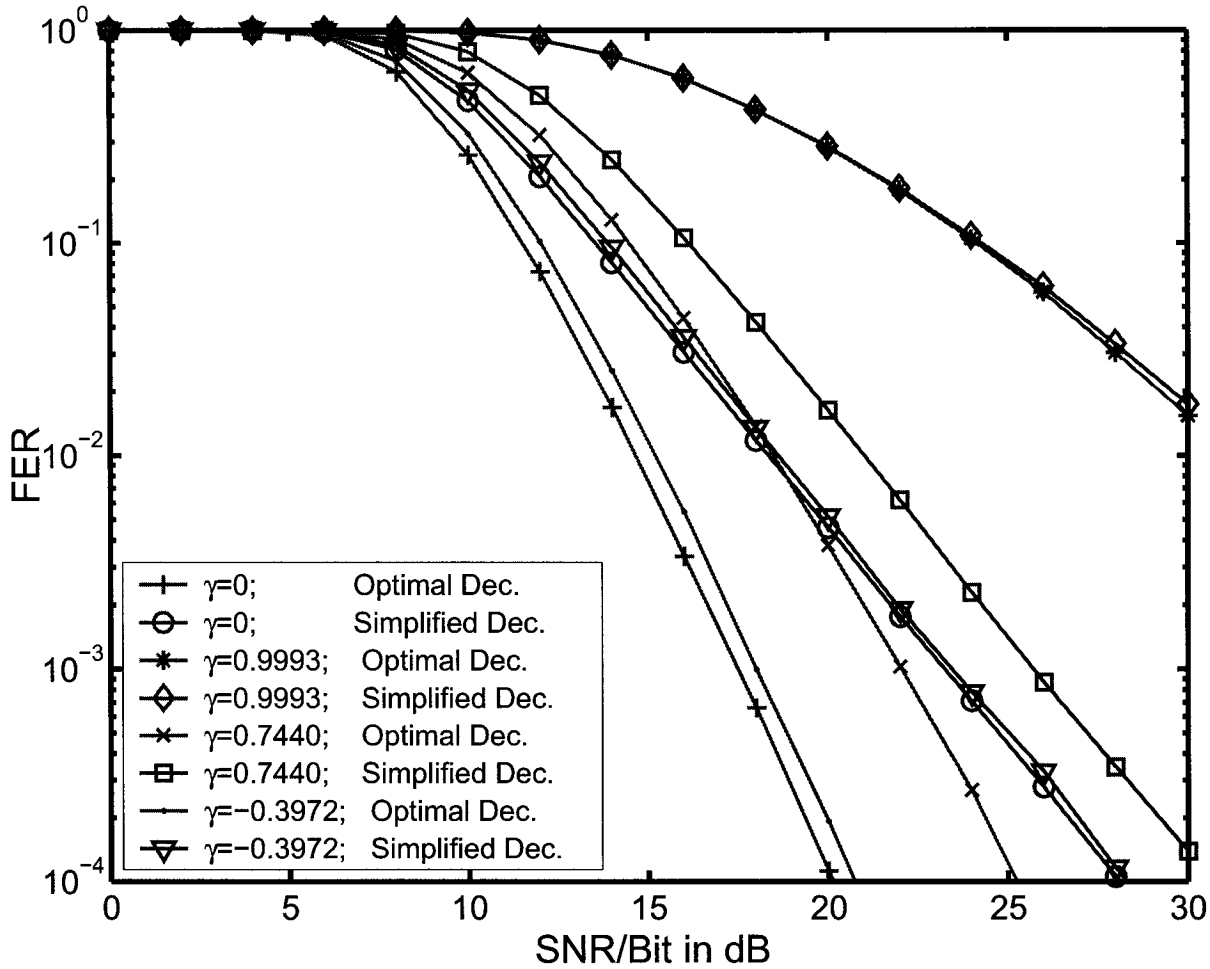

Fig. 4.3 Different Decoding Algorithms for the Improved Quasi-Orthogonal code Over Independent and Spatially Correlated Channels: Frame Error Rate; Frame-length=256 Information Bits

satisfied at the same time, we are going to satisfy either performance or complexity with respect to different transmission models.

As we discussed in chapter 3, the diversity orders provided by the optimal and the simplified decoding schemes of the Improved Quasi-Orthogonal code over independent channels are 4 and 2, respectively. The performance gap between two decoding schemes increases significantly as SNR increases. So, over space uncorrelated channels, the simplified decoding scheme is not desirable though it provides lower decoding complexity.

The situation in space correlated channels is different. As we discussed in section 4.3, the performance gaps between the optimal and the simplified decoding schemes of the Improved Quasi-Orthogonal code decrease as the correlations among the channel increase. When the gaps are smaller than a certain amount, the simplified decoding scheme is suitable because of its relative lower decoding complexity and tolerable performance loss.

Chapter 5

Conclusion

In this thesis, we considered simplified and optimal decoding algorithms for the Quasi-Orthogonal STBC family that comprises the Quasi-Orthogonal code [28] and the Improved Quasi-Orthogonal code [29] over Rayleigh fading channels. A symbol-by-symbol decision feedback decoding algorithm was proposed. The associated performances were evaluated by mathematical analysis and were verified through computer simulations.

A complex orthogonal STBC exists iff the order of the code matrix is 2 [7], which is Alamouti's scheme [18]. For the complex STBCs other than Alamouti's scheme, full rate and full orthogonality (which results in full diversity and symbol-by-symbol ML decoding) can not be satisfied at the same time. The Quasi-Orthogonal code family [28] [29] is made up of two types of full code rate non-orthogonal STBCs. Because the loss of orthogonality, the ML decoding of Quasi-Orthogonal code family can not be as simple as symbol-by-symbol decoding. This thesis introduced a simplified decoding algorithm for such codes. This simplified decoding decouples four information bearing symbols into two groups. In decoding each pair of symbols, by using QR decomposition, one of the symbols is decoded first, then the decoding result is carried back to the decoding of the second symbol. The decoding complexity, which is measured in terms of number of comparisons over all possible linear combinations of transmitted symbols, increases

linearly with the size of modulation constellation size, and it is much lower than the decoding complexity of optimal decoding, which increases quadratically with the size of modulation constellation. Compared to sphere decoding, there is no need for the simplified decoding algorithm to find a initial sphere radius, which contributes to the complexity of the sphere decoding algorithm.

In addressing the performances of different decoding schemes for the Quasi-Orthogonal code family, we provided a mathematical analysis as well as computer simulation results. Through mathematical analysis, we showed that

1. The diversity orders provided by optimal decodings of the Improved Quasi-Orthogonal code and the Quasi-Orthogonal code are 4 and 2, respectively.

2. For the simplified decoding of the Improved Quasi-Orthogonal code, the diversity order provided by the decoding of the first symbol in each symbol pair is 2. The diversity order provided by the decoding of the second symbol in the same symbol pair assuming the first symbol has been decoded correctly is 4. However, due to the decoding errors of the first symbol, the actual diversity order provided by the decoding of the second symbol in the same symbol pair is employed is 2. Therefore the simplified decoding of the Improved Quasi-Orthogonal code yields diversity order of 2.

Finally, we presented the performances of the simplified decoding and optimal decoding over correlated Rayleigh fading channels by using the "one-ring" channel model [42]. Through computer simulations, we showed that relative performance loss of the simplified decoding to optimal decoding decreases as channel correlation increases. Therefore, the simplified decoding scheme is suitable for highly spatially correlated Rayleigh fading channels.

Appendix A

Proofs and Calculations

A.1 Proof of Equation (3.7)

From (3.3) and (3.5), we have

$$||\mathbf{r}^T - \mathbf{a}^T\tilde{\mathbf{C}}||^2 = ||\mathbf{a}^T(\mathbf{C}-\tilde{\mathbf{C}}) + \mathbf{n}^T||^2 = [\mathbf{a}^T(\mathbf{C}-\tilde{\mathbf{C}}) + \mathbf{n}^T][(\mathbf{C}-\tilde{\mathbf{C}})^H\mathbf{a}^* + \mathbf{n}^*]$$

$$= \mathbf{a}^T(\mathbf{C}-\tilde{\mathbf{C}})(\mathbf{C}-\tilde{\mathbf{C}})^H\mathbf{a}^* + 2\mathrm{Re}[\mathbf{n}^T(\mathbf{C}-\tilde{\mathbf{C}})^H\mathbf{a}^*] + \mathbf{n}^T\mathbf{n}^* \quad \text{(A.1)}$$

and

$$||\mathbf{r_P}^T - \tilde{\mathbf{s}}^T\mathbf{H}||^2 = ||(\mathbf{s}-\tilde{\mathbf{s}})^T\mathbf{H} + \mathbf{n_P}^T||^2 = [(\mathbf{s}-\tilde{\mathbf{s}})^T\mathbf{H} + \mathbf{n_P}^T][\mathbf{H}^H(\mathbf{s}-\tilde{\mathbf{s}})^* + \mathbf{n_P}^*]$$

$$= (\mathbf{s}-\tilde{\mathbf{s}})^T\mathbf{H}\mathbf{H}^H(\mathbf{s}-\tilde{\mathbf{s}})^* + 2\mathrm{Re}[\mathbf{n_P}^T\mathbf{H}^H(\mathbf{s}-\tilde{\mathbf{s}})^*] + \mathbf{n_P}^T\mathbf{n_P}^* \quad \text{(A.2)}$$

According to (3.3) and (3.5), we have

$$\mathbf{a}^T(\mathbf{C}-\tilde{\mathbf{C}})(\mathbf{C}-\tilde{\mathbf{C}})^H\mathbf{a}^* = (\mathbf{s}-\tilde{\mathbf{s}})^T\mathbf{H}\mathbf{H}^H(\mathbf{s}-\tilde{\mathbf{s}})^*$$

$$= A\sum_{i=1}^{4}||s_i - \tilde{s_i}||^2 + 2B\big(\mathrm{Re}[(s_1-\tilde{s_1})(s_4-\tilde{s_4})^*] - \mathrm{Re}[(s_2-\tilde{s_2})(s_3-\tilde{s_3})^*]\big) \quad \text{(A.3)}$$

and

$$\mathbf{n}^T\mathbf{n}^* = \mathbf{n_P}^T\mathbf{n_P}^* = \sum_{i=1}^{4} ||n_{1,i}||^2 \tag{A.4}$$

and

$$\begin{aligned}
& \mathrm{Re}[\mathbf{n}^T(\mathbf{C}-\tilde{\mathbf{C}})^H\mathbf{a}^*] = \mathrm{Re}[\mathbf{n_P}^T\mathbf{H}^H(\mathbf{s}-\tilde{\mathbf{s}})^*] \\
= \; & \alpha_{1,1}^* n_{1,1}(s_1-\tilde{s_1})^* + \alpha_{1,2}^* n_{1,1}(s_2-\tilde{s_2})^* + \alpha_{1,3}^* n_{1,1}(s_3-\tilde{s_3})^* + \alpha_{1,4}^* n_{1,1}(s_4-\tilde{s_4})^* \\
+ \; & \alpha_{1,1} n_{1,1}^*(s_1-\tilde{s_1}) + \alpha_{1,2} n_{1,1}^*(s_2-\tilde{s_2}) + \alpha_{1,3} n_{1,1}^*(s_3-\tilde{s_3}) + \alpha_{1,4} n_{1,1}^*(s_4-\tilde{s_4}) \\
- \; & \alpha_{1,1} n_{1,2}^*(s_2-\tilde{s_2})^* + \alpha_{1,2} n_{1,2}^*(s_1-\tilde{s_1})^* - \alpha_{1,3} n_{1,2}^*(s_4-\tilde{s_4})^* + \alpha_{1,4} n_{1,2}^*(s_3-\tilde{s_3})^* \\
- \; & \alpha_{1,1}^* n_{1,2}(s_2-\tilde{s_2}) + \alpha_{1,2}^* n_{1,2}(s_1-\tilde{s_1}) - \alpha_{1,3}^* n_{1,2}(s_4-\tilde{s_4}) + \alpha_{1,4}^* n_{1,2}(s_3-\tilde{s_3}) \\
- \; & \alpha_{1,1} n_{1,3}^*(s_3-\tilde{s_3})^* - \alpha_{1,2} n_{1,3}^*(s_4-\tilde{s_4})^* + \alpha_{1,3} n_{1,3}^*(s_1-\tilde{s_1})^* + \alpha_{1,4} n_{1,3}^*(s_2-\tilde{s_2})^* \\
- \; & \alpha_{1,1}^* n_{1,3}(s_3-\tilde{s_3}) - \alpha_{1,2}^* n_{1,3}(s_4-\tilde{s_4}) + \alpha_{1,3}^* n_{1,3}(s_1-\tilde{s_1}) + \alpha_{1,4}^* n_{1,3}(s_2-\tilde{s_2}) \\
+ \; & \alpha_{1,1} n_{1,4}(s_4-\tilde{s_4})^* - \alpha_{1,2}^* n_{1,4}(s_3-\tilde{s_3})^* - \alpha_{1,3}^* n_{1,4}(s_2-\tilde{s_2})^* + \alpha_{1,4}^* n_{1,4}(s_1-\tilde{s_1})^* \\
+ \; & \alpha_{1,1}^* n_{1,4}^*(s_4-\tilde{s_4}) - \alpha_{1,2} n_{1,4}^*(s_3-\tilde{s_3}) - \alpha_{1,3} n_{1,4}^*(s_2-\tilde{s_2}) + \alpha_{1,4} n_{1,4}^*(s_1-\tilde{s_1})
\end{aligned} \tag{A.5}$$

in (A.3), A and B are defined by (3.10) and (3.11), respectively. By combing (A.1)-(A.5), we have

$$||\mathbf{r_P}^T - \tilde{\mathbf{s}}^T\mathbf{H}||^2 = ||\mathbf{r}^T - \mathbf{a}^T\tilde{\mathbf{C}}||^2 \tag{A.6}$$

Q.E.D

A.2 Variance of n_Z in (3.93)

We denote

$$\mathbf{e_h} = \mathbf{H_l}\mathbf{e_s} = \mathbf{e_{hR}} + j\mathbf{e_{hI}} \tag{A.7}$$

where $\mathbf{e_{hR}}$ and $\mathbf{e_{hI}}$ denotes the real and imaginary part of $\mathbf{e_h}$, respectively. We also denote

$$\mathbf{n_D}' = \mathbf{n_{DR}}' + j\mathbf{n_{DI}}' \tag{A.8}$$

where $\mathbf{n_{DR}}'$ and $\mathbf{n_{DI}}'$ denotes the real part and imaginary part of $\mathbf{n_D}'$. So

$$\begin{aligned} \mathbf{e_s}^H\mathbf{H_1}^H\mathbf{n_D}' &= \mathbf{e_h}^H\mathbf{n_D}' = (\mathbf{e_{hR}}^T - j\mathbf{e_{hI}}^T)(\mathbf{n_{DR}}' + j\mathbf{n_{DI}}') \\ &= \mathbf{e_{hR}}^T\mathbf{n_{DR}}' + \mathbf{e_{hI}}^T\mathbf{n_{DI}}' + j(\mathbf{e_{hR}}\mathbf{n_{DI}}' - \mathbf{e_{hI}}\mathbf{n_{DR}}') \end{aligned} \tag{A.9}$$

From the definition of n_Z in (3.93), we know that

$$n_Z = 2\mathrm{Re}(\mathbf{e_s}^H\mathbf{H_1}^H\mathbf{n_D}') = 2(\mathbf{e_{hR}}^T\mathbf{n_{DR}}' + \mathbf{e_{hI}}^T\mathbf{n_{DI}}') \tag{A.10}$$

Accordingly, the mean of n_Z is

$$E(n_Z) = E\{2(\mathbf{e_{hR}}^T\mathbf{n_{DR}}' + \mathbf{e_{hI}}^T\mathbf{n_{DI}}')\} \tag{A.11}$$

and the variance of n_Z is

$$\mathrm{Var}(n_Z) = E\{(n_Z - \bar{n_Z})^2\} = 4E\{(\mathbf{e_{hR}}^T\mathbf{n_{DR}}' + \mathbf{e_{hI}}^T\mathbf{n_{DI}}' - \bar{n_Z})^2\} \tag{A.12}$$

where $\bar{n_Z}$ denotes the mean of n_Z. From (A.10) and section 3.3.2, we know that n_Z is a linear combination of i.i.d Gaussian random variables with zero mean. So

$$E(n_Z) = 0 \tag{A.13}$$

and

$$\begin{aligned}\mathrm{Var}(n_Z) &= 4E\{(\mathbf{e_{hR}}^T\mathbf{n_{DR}}' + \mathbf{e_{hI}}^T\mathbf{n_{DI}}')^2\} \\ &= 4\{\mathbf{e_{hR}}^T E(\mathbf{n_{DR}}'\mathbf{n_{DR}}'^T)\mathbf{e_{hR}} + \mathbf{e_{hR}}^T E(\mathbf{n_{DR}}'\mathbf{n_{DI}}'^T)\mathbf{e_{hI}} \\ &\quad + \mathbf{e_{hI}}^T E(\mathbf{n_{DI}}'\mathbf{n_{DR}}'^T)\mathbf{e_{hR}} + \mathbf{e_{hI}}^T E(\mathbf{n_{DI}}'\mathbf{n_{DI}}'^T)\mathbf{e_{hI}}\} \\ &= 2(\mathbf{e_{hR}}^T\mathbf{e_{hR}} + \mathbf{e_{hI}}^T\mathbf{e_{hI}}) = 2||\mathbf{e_h}||^2 = 2||\mathbf{H_1 e_s}||^2 \end{aligned} \tag{A.14}$$

A.3 Eigenvalues of $\mathbf{\Lambda}$

We denote by $\lambda_i^{\mathbf{\Lambda}}$'s as the eigenvalues of $\mathbf{\Lambda}$. From [32], all $\lambda_i^{\mathbf{\Lambda}}$'s satisfy $\det(\lambda_i^{\mathbf{\Lambda}}\mathbf{I} - \mathbf{\Lambda}) = 0$, i.e.,

$$\det\begin{pmatrix} \lambda_i^{\mathbf{\Lambda}} - \frac{||e_1||^2+||e_4||^2}{2\sigma^2} & 0 & 0 & -\frac{\mathrm{Re}(e_1e_4^*)}{\sigma^2} \\ 0 & \lambda_i^{\mathbf{\Lambda}} - \frac{||e_1||^2+||e_4||^2}{2\sigma^2} & \frac{\mathrm{Re}(e_1e_4^*)}{\sigma^2} & 0 \\ 0 & \frac{\mathrm{Re}(e_1e_4^*)}{\sigma^2} & \lambda_i^{\mathbf{\Lambda}} - \frac{||e_1||^2+||e_4||^2}{2\sigma^2} & 0 \\ -\frac{\mathrm{Re}(e_1e_4^*)}{\sigma^2} & 0 & 0 & \lambda_i^{\mathbf{\Lambda}} - \frac{||e_1||^2+||e_4||^2}{2\sigma^2} \end{pmatrix}$$

$$= \left(\lambda_i^{\mathbf{\Lambda}} - \frac{||e_1||^2 + ||e_4||^2}{2\sigma^2}\right)\det\begin{pmatrix} \lambda_i^{\mathbf{\Lambda}} - \frac{||e_1||^2+||e_4||^2}{2\sigma^2} & \frac{\mathrm{Re}(e_1e_4^*)}{\sigma^2} & 0 \\ \frac{\mathrm{Re}(e_1e_4^*)}{\sigma^2} & \lambda_i^{\mathbf{\Lambda}} - \frac{||e_1||^2+||e_4||^2}{2\sigma^2} & 0 \\ 0 & 0 & \lambda_i^{\mathbf{\Lambda}} - \frac{||e_1||^2+||e_4||^2}{2\sigma^2} \end{pmatrix}$$

$$+\left(\frac{\mathrm{Re}(e_1e_4^*)}{\sigma^2}\right)\det\begin{pmatrix} 0 & 0 & -\frac{\mathrm{Re}(e_1e_4^*)}{\sigma^2} \\ \lambda_i^{\mathbf{\Lambda}} - \frac{||e_1||^2+||e_4||^2}{2\sigma^2} & \frac{\mathrm{Re}(e_1e_4^*)}{\sigma^2} & 0 \\ \frac{\mathrm{Re}(e_1e_4^*)}{\sigma^2} & \lambda_i^{\mathbf{\Lambda}} - \frac{||e_1||^2+||e_4||^2}{2\sigma^2} & 0 \end{pmatrix}$$

$$
\begin{aligned}
&= \left(\lambda_i^{\mathbf{\Lambda}} - \frac{||e_1||^2 + ||e_4||^2}{2\sigma^2}\right)^2 \det \begin{pmatrix} \lambda_i^{\mathbf{\Lambda}} - \frac{||e_1||^2+||e_4||^2}{2\sigma^2} & \frac{\mathrm{Re}(e_1 e_4^*)}{\sigma^2} \\ \frac{\mathrm{Re}(e_1 e_4^*)}{\sigma^2} & \lambda_i^{\mathbf{\Lambda}} - \frac{||e_1||^2+||e_4||^2}{2\sigma^2} \end{pmatrix} \\
&\quad - \left(\frac{\mathrm{Re}(e_1 e_4^*)}{\sigma^2}\right)^2 \det \begin{pmatrix} \lambda_i^{\mathbf{\Lambda}} - \frac{||e_1||^2+||e_4||^2}{2\sigma^2} & \frac{\mathrm{Re}(e_1 e_4^*)}{\sigma^2} \\ \frac{\mathrm{Re}(e_1 e_4^*)}{\sigma^2} & \lambda_i^{\mathbf{\Lambda}} - \frac{||e_1||^2+||e_4||^2}{2\sigma^2} \end{pmatrix} \\
&= \left[\left(\lambda_i^{\mathbf{\Lambda}} - \frac{||e_1||^2 + ||e_4||^2}{2\sigma^2}\right)^2 - \left(\frac{\mathrm{Re}(e_1 e_4^*)}{\sigma^2}\right)^2\right]^2 = 0
\end{aligned} \tag{A.15}
$$

By solving (A.15), we have the eigenvalues of $\mathbf{\Lambda}$ as the following

$$\lambda_1^{\mathbf{\Lambda}} = \lambda_2^{\mathbf{\Lambda}} = \frac{1}{2\sigma^2}|e_1 + e_4|^2 \tag{A.16}$$

$$\lambda_3^{\mathbf{\Lambda}} = \lambda_4^{\mathbf{\Lambda}} = \frac{1}{2\sigma^2}|e_1 - e_4|^2 \tag{A.17}$$

A.4 Joint Probability Density Function of A and B

From (3.121), we know that the joint characteristic function of A and B is given as

$$\Phi_{A,B}(\omega_1, \omega_2) = [1 - j(\omega_1 - \omega_2)]^{-2}[1 - j(\omega_1 + \omega_2)]^{-2} \tag{A.18}$$

So the joint pdf of A and B is the inverse Fourier Fourier transform of (A.18) and given as

$$
\begin{aligned}
f_{A,B}(a,b) &= \mathcal{F}^{-1}\big(\,\Phi_{A,B}(\omega_1,\omega_2)\,\big) \\
&= \left(\frac{1}{2\pi}\right)^2 \int\int_{-\infty}^{+\infty} \frac{\exp[-j(a\omega_1 + b\omega_2)]}{[1 - j(\omega_1 - \omega_2)]^2[1 - j(\omega_1 + \omega_2)]^2}\, d\omega_1 d\omega_2
\end{aligned} \tag{A.19}
$$

We make the transformation as

$$\begin{cases} \omega_3 = \omega_1 - \omega_2 \\ \\ \omega_4 = \omega_1 + \omega_2 \end{cases} \tag{A.20}$$

then (A.19) changes to

$$\begin{aligned} f_{A,B}(a,b) &= \mathcal{F}^{-1}\big(\,\Phi_{A,B}(\omega_1,\omega_2)\,\big) \\ &= \Big(\frac{1}{2\pi}\Big)^2 \int\int_{-\infty}^{+\infty} \frac{\exp[-j(a\omega_1 + b\omega_2)]}{[1-j(\omega_1-\omega_2)]^2[1-j(\omega_1+\omega_2)]^2}\, d\omega_1 d\omega_2 \\ &= \frac{1}{2}\Big(\frac{1}{2\pi}\Big)^2 \int_{-\infty}^{+\infty} \frac{\exp[-j\omega_3(\frac{a-b}{2})]}{[1-j\omega_3]^2}\, d\omega_3 \int_{-\infty}^{+\infty} \frac{\exp[-j\omega_4(\frac{a+b}{2})]}{[1-j\omega_4]^2}\, d\omega_4 \end{aligned} \tag{A.21}$$

From the equations (3.382-6) and (3.382-7) listed in [39].

$$\int_{-\infty}^{+\infty} \frac{\exp[-j\omega_3(\frac{a-b}{2})]}{[1-j\omega_3]^2}\, d\omega_3 = \begin{cases} \pi(a-b)e^{-\frac{a-b}{2}}; & a-b>0 \\ \\ 0 & \text{otherwise} \end{cases} \tag{A.22}$$

$$\int_{-\infty}^{+\infty} \frac{\exp[-j\omega_4(\frac{a+b}{2})]}{[1-j\omega_4]^2}\, d\omega_4 = \begin{cases} \pi(a+b)e^{-\frac{a+b}{2}}; & a+b>0 \\ \\ 0 & \text{otherwise} \end{cases} \tag{A.23}$$

By using (A.22) and (A.23), in (A.21) we have

$$f_{A,B}(a,b) = \begin{cases} \frac{1}{8}(a+b)(a-b)e^{-\frac{a+b}{2}}e^{-\frac{a-b}{2}}; & a+b>0 \text{ and } a-b>0 \\ \\ 0 & \text{otherwise} \end{cases} \tag{A.24}$$

A.5 Joint Probability Density Function of U and V

From (3.123), we have the Jacobian as

$$J = \det \begin{pmatrix} \frac{\partial u}{\partial a} & \frac{\partial u}{\partial b} \\ \frac{\partial v}{\partial a} & \frac{\partial v}{\partial b} \end{pmatrix} = -2 \tag{A.25}$$

From (3.122) and (3.123), we have the joint pdf of U and V is

$$f_{U,V}(u,v) = \frac{1}{|J|} f_{A,B}(a,b)\Big|_{a=\frac{u+v}{2}, b=\frac{u-v}{2}} = \begin{cases} \frac{1}{16} uve^{-\frac{u}{2}} e^{-\frac{v}{2}}; & u > 0 \text{ and } v > 0 \\ 0; & \text{otherwise.} \end{cases} \tag{A.26}$$

A.6 Probability Distribution Function of W

From [36] (pp.195), we have that the probability distribution function of $W = \min(U, V)$ is given by

$$f_W(w) = f_U(w) + f_V(w) - f_U(w)F_V(w) - F_U(w)f_V(w) \tag{A.27}$$

From (3.126) and (3.127), we have that the cumulative probability distribution functions of U and V are given by

$$F_U(u) = \int_0^u f_U(u)du = \begin{cases} 4 - 4e^{-\frac{u}{2}} - 2ue^{-\frac{u}{2}}; & u > 0, \\ 0; & \text{otherwise} \end{cases} \tag{A.28}$$

and

$$F_V(v) = \int_0^v f_V(v)dv = \begin{cases} 4 - 4e^{-\frac{v}{2}} - 2ve^{-\frac{v}{2}}; & v > 0, \\ 0; & \text{otherwise} \end{cases} \tag{A.29}$$

respectively. By substituting (3.126), (3.127), (A.28) and (A.29) into (A.27), we have the the probability distribution function of W as

$$f_W(w) = \frac{1}{2}we^{-w} + \frac{1}{4}w^2e^{-w}; \quad w > 0 \tag{A.30}$$

A.7 Moment Generating Function of W

We take the Fourier transform of (3.131)

$$\begin{aligned} \Phi_W(\omega_1) &= \mathcal{F}(f_W(w)) = \int_0^{+\infty} (\frac{1}{2}we^{-w} + \frac{1}{4}w^2e^{-w})e^{jw\omega_1}\, dw \\ &= \int_0^{+\infty} (\frac{1}{2}we^{-w+jw\omega_1} + \frac{1}{4}w^2e^{-w+jw\omega_1})\, dw \end{aligned}$$

From equations (3.351-3) listed in [39], we have the characteristic function of W as

$$\begin{aligned} \Phi_W(\omega_1) &= \int_0^{+\infty} (\frac{1}{2}we^{-w(1-j\omega_1)} + \frac{1}{4}w^2e^{-w(1-j\omega_1)})\, dw \\ &= \frac{1}{2}(1 - j\omega_1)^{-2} + \frac{1}{2}(1 - j\omega_1)^{-3} \end{aligned}$$

and the moment generating function of W is

$$\Phi_W(s) = \Phi_W(\omega_1)\big|_{j\omega_1 = s} = \frac{1}{2}(1 - s)^{-2} + \frac{1}{2}(1 - s)^{-3} \tag{A.31}$$

A.8 Calculations Associated with Bounds of Decoding s_1 When $\hat{s_4}$ is From Decision Feedback

A.8.1 Evaluation of $P(\hat{s_4} = z_1^{'} \mid s_4 = z_1^{'})$ When σ^2 Approaches 0

As evaluated in (3.145) and (3.146), when σ^2 approaches 0, $P(\hat{s_4} = z_1^{'} \mid s_4 = z_1^{'})$ is upper bounded by

$$\begin{aligned} & \lim_{\sigma^2 \to 0} P_U(\hat{s_4} = z_1^{'} \mid s_4 = z_1^{'}) = \lim_{\sigma^2 \to 0} [1 - P_L(\hat{s_4} \neq s_4)] = 1 - \lim_{\sigma^2 \to 0} P_L(\hat{s_4} \neq s_4) \\ = \; & 1 - \frac{1}{2\pi}(8\sigma^2)^2 \int_0^{\frac{3\pi}{4}} \sin^4\theta \, d\theta - \frac{1}{2\pi}(8\sigma^2)^3 \int_0^{\frac{3\pi}{4}} \sin^6\theta \, d\theta \end{aligned} \tag{A.32}$$

and lower bounded by

$$\begin{aligned} & \lim_{\sigma^2 \to 0} P_L(\hat{s_4} = z_1^{'} \mid s_4 = z_1^{'}) = \lim_{\sigma^2 \to 0} [1 - P_U(\hat{s_4} \neq s_4)] = 1 - \lim_{\sigma^2 \to 0} P_U(\hat{s_4} \neq s_4) \\ = \; & 1 - \frac{1}{2\pi}(16\sigma^2)^2 \int_0^{\frac{3\pi}{4}} \sin^4\theta \, d\theta - \frac{1}{2\pi}(16\sigma^2)^3 \int_0^{\frac{3\pi}{4}} \sin^6\theta \, d\theta \end{aligned} \tag{A.33}$$

By combining (A.32) and (A.33), we conclude that when σ^2 approaches 0, $P(\hat{s_4} = z_1^{'} \mid s_4 = z_1^{'})$ approaches 1.

A.8.2 Evaluation of $P(\hat{s_1} \neq s_1 \mid \hat{s_4} = z_2^{'}; s_4 = z_1^{'})$ and $P(\hat{s_1} \neq s_1 \mid \hat{s_4} = z_4^{'}; s_4 = z_1^{'})$ When σ^2 Approaches 0

From (3.56), we have

$$r_{U\,1,1} = \grave{a}s_1 + \grave{b}s_4 + n_{U\,1,1} \tag{A.34}$$

When s_4 has been decoded as $\hat{s_4}$, then

$$r''_{U\,1,1} = r_{U\,1,1} - \grave{b}\hat{s_4} = \grave{a}s_1 + \grave{b}(s_4 - \hat{s_4}) + n_{U\,1,1} \tag{A.35}$$

where $n_{U\,1,1}$ is circularly symmetric complex Gaussian with zero mean and unit variance as mentioned in section 3.2.2. So

$$\begin{aligned}
& P(\hat{s_1} \neq s_1 \mid \hat{s_4} = z_2^{'}; s_4 = z_1^{'}; \alpha_{1,i};\ i = 1,2,3,4) \\
= \;& 1 - P\Big(\frac{\grave{a}}{\sqrt{8}} + \frac{\sqrt{3}\grave{b}}{\sqrt{8}} + \mathrm{Re}(n_{U\,1,1}) > 0\Big) P\Big(\frac{\grave{a}}{\sqrt{8}} + \frac{\grave{b}}{\sqrt{8}} + \mathrm{Im}(n_{U\,1,1}) > 0\Big) \\
= \;& 1 - \Big\{ P\Big(\frac{\grave{a}}{\sqrt{8}} + \frac{\sqrt{3}\grave{b}}{\sqrt{8}} + \mathrm{Re}(n_{U\,1,1}) > 0 \Big| \grave{a} + \sqrt{3}\grave{b} > 0\Big) P(\grave{a} + \sqrt{3}\grave{b} > 0) \\
& + P\Big(\frac{\grave{a}}{\sqrt{8}} + \frac{\sqrt{3}\grave{b}}{\sqrt{8}} + \mathrm{Re}(n_{U\,1,1}) > 0 \Big| \grave{a} + \sqrt{3}\grave{b} < 0\Big) P(\grave{a} + \sqrt{3}\grave{b} < 0) \Big\} \times \\
& \times \Big\{ P\Big(\frac{\grave{a}}{\sqrt{8}} + \frac{\grave{b}}{\sqrt{8}} + \mathrm{Im}(n_{U\,1,1}) > 0 \Big| \grave{a} + \grave{b} > 0\Big) P(\grave{a} + \grave{b} > 0) \\
& + P\Big(\frac{\grave{a}}{\sqrt{8}} + \frac{\grave{b}}{\sqrt{8}} + \mathrm{Im}(n_{U\,1,1}) > 0 \Big| \grave{a} + \grave{b} < 0\Big) P(\grave{a} + \grave{b} < 0) \Big\} \\
= \;& 1 - \Big\{ \Big[1 - Q\Big(\frac{(\grave{a} + \sqrt{3}\grave{b})}{2}\Big)\Big] P(\grave{a} + \sqrt{3}\grave{b} > 0) + Q\Big(\frac{-(\grave{a} + \sqrt{3}\grave{b})}{2}\Big) P(\grave{a} + \sqrt{3}\grave{b} < 0) \Big\} \times \\
& \times \Big\{ \Big[1 - Q\Big(\frac{(\grave{a} + \grave{b})}{2}\Big)\Big] P(\grave{a} + \grave{b} > 0) + Q\Big(\frac{-(\grave{a} + \grave{b})}{2}\Big) P(\grave{a} + \grave{b} < 0) \Big\}
\end{aligned} \tag{A.36}$$

and similarly,

$$\begin{aligned}
& P(\hat{s_1} \neq s_1 \mid \hat{s_4} = z_2^{'}; s_4 = z_1^{'}; \alpha_{1,i};\ i = 1,2,3,4) \\
= \;& 1 - P\Big(\frac{\grave{a}}{\sqrt{8}} + \frac{\sqrt{3}\grave{b}}{\sqrt{8}} + \mathrm{Im}(n_{U\,1,1}) > 0\Big) P\Big(\frac{\grave{a}}{\sqrt{8}} + \frac{\grave{b}}{\sqrt{8}} + \mathrm{Re}(n_{U\,1,1}) > 0\Big) \\
= \;& 1 - \Big\{ P\Big(\frac{\grave{a}}{\sqrt{8}} + \frac{\sqrt{3}\grave{b}}{\sqrt{8}} + \mathrm{Im}(n_{U\,1,1}) > 0 \Big| \grave{a} + \sqrt{3}\grave{b} > 0\Big) P(\grave{a} + \sqrt{3}\grave{b} > 0) \\
& + P\Big(\frac{\grave{a}}{\sqrt{8}} + \frac{\sqrt{3}\grave{b}}{\sqrt{8}} + \mathrm{Im}(n_{U\,1,1}) > 0 \Big| \grave{a} + \sqrt{3}\grave{b} < 0\Big) P(\grave{a} + \sqrt{3}\grave{b} < 0) \Big\} \times \\
& \times \Big\{ P\Big(\frac{\grave{a}}{\sqrt{8}} + \frac{\grave{b}}{\sqrt{8}} + \mathrm{Re}(n_{U\,1,1}) > 0 \Big| \grave{a} + \grave{b} > 0\Big) P(\grave{a} + \grave{b} > 0)
\end{aligned}$$

$$
\begin{aligned}
&+P\Big(\frac{\grave{a}}{\sqrt{8}}+\frac{\grave{b}}{\sqrt{8}}+\mathrm{Re}(n_{U\,1,1})>0\Big|\grave{a}+\grave{b}<0\Big)P(\grave{a}+\grave{b}<0)\Big\}\\
=\;& 1-\Big\{\Big[1-Q\Big(\frac{(\grave{a}+\sqrt{3}\grave{b})}{2}\Big)\Big]P(\grave{a}+\sqrt{3}\grave{b}>0)+Q\Big(\frac{-(\grave{a}+\sqrt{3}\grave{b})}{2}\Big)P(\grave{a}+\sqrt{3}\grave{b}<0)\Big\}\times\\
&\times\Big\{\Big[1-Q\Big(\frac{(\grave{a}+\grave{b})}{2}\Big)\Big]P(\grave{a}+\grave{b}>0)+Q\Big(\frac{-(\grave{a}+\grave{b})}{2}\Big)P(\grave{a}+\grave{b}<0)\Big\} \qquad \text{(A.37)}
\end{aligned}
$$

From (3.46), (3.50) and (3.51), we have

$$
P(\grave{a}+\grave{b}>0)=P\Big[\frac{1}{\sqrt{2\sigma^2}}\Big(\sqrt{A}+\frac{B}{\sqrt{A}}\Big)>0\Big]=P\Big(\frac{A+B}{\sqrt{A}}>0\Big) \qquad \text{(A.38)}
$$

According to (3.126), we get $U = A + B$ is non-negative with probability 1. And from the definition of A in (3.10), $A \geq 0$. Also $A = 0$ iff all the channel coefficients $\alpha_{1,i}$'s $(i = 1, 2, 3, 4)$ are equal to zero. From channel model given in section 2.1.1, the real and complex parts of $\alpha_{1,i}$'s, (i=1,2,3,4) are continuous Gaussian random variables. The probability that at least one of these values is not equal to zero is one. Accordingly, A is positive with probability one. Then from (A.38)

$$
P(\grave{a}+\grave{b}>0)=1 \qquad \text{(A.39)}
$$

According to (A.36), (A.37) and (A.39), by using Craig's formula, we have

$$
\begin{aligned}
&P(\hat{s_1}\neq s_1\;|\;\hat{s_4}=z_2';s_4=z_1';\alpha_{1,i};\;i=1,2,3,4)\\
=\;& P(\hat{s_1}\neq s_1\;|\;\hat{s_4}=z_4';s_4=z_1';\alpha_{1,i};\;i=1,2,3,4)\\
=\;& 1-P(\grave{a}+\sqrt{3}\grave{b}>0)+2P(\grave{a}+\sqrt{3}\grave{b}>0)\frac{1}{\pi}\int_0^{\frac{\pi}{2}}\exp\Big(-\frac{(\grave{a}+\sqrt{3}\grave{b})^2}{8\sin^2\theta}\Big)\;d\theta\\
&+P(\grave{a}+\sqrt{3}\grave{b}>0)\frac{1}{\pi}\int_0^{\frac{\pi}{2}}\exp\Big(-\frac{(\grave{a}+\grave{b})^2}{8\sin^2\vartheta}\Big)\;d\vartheta\\
&+[1-2P(\grave{a}+\sqrt{3}\grave{b}>0)]\frac{1}{\pi}\int_0^{\frac{\pi}{2}}\exp\Big(-\frac{(\grave{a}+\sqrt{3}\grave{b})^2}{8\sin^2\theta}\Big)\;d\theta\frac{1}{\pi}\int_0^{\frac{\pi}{2}}\exp\Big(-\frac{(\grave{a}+\grave{b})^2}{8\sin^2\vartheta}\Big)\;d\vartheta\\
&-\frac{1}{\pi}\int_0^{\frac{\pi}{2}}\exp\Big(-\frac{(\grave{a}+\sqrt{3}\grave{b})^2}{8\sin^2\theta}\Big)\;d\theta
\end{aligned}
$$

$$
\begin{aligned}
= \; & 1 - P(\grave{a} + \sqrt{3}\grave{b} > 0) + 2P(\grave{a} + \sqrt{3}\grave{b} > 0)\frac{1}{\pi}\int_0^{\frac{\pi}{2}} \exp\Big[-\frac{1}{16\sigma^2}\frac{(\sqrt{A} + \frac{\sqrt{3}B}{\sqrt{A}})^2}{\sin^2\theta}\Big]\, d\theta \\
& + P(\grave{a} + \sqrt{3}\grave{b} > 0)\frac{1}{\pi}\int_0^{\frac{\pi}{2}} \exp\Big[-\frac{1}{16\sigma^2}\frac{(\sqrt{A} + \frac{B}{\sqrt{A}})^2}{\sin^2\vartheta}\Big]\, d\vartheta \\
& + [1 - 2P(\grave{a} + \sqrt{3}\grave{b} > 0)]\frac{1}{\pi^2}\int\int_0^{\frac{\pi}{2}} \exp\Big[-\frac{1}{16\sigma^2}\Big(\frac{(\sqrt{A} + \frac{\sqrt{3}B}{\sqrt{A}})^2}{\sin^2\theta} + \frac{(\sqrt{A} + \frac{B}{\sqrt{A}})^2}{\sin^2\vartheta}\Big)\Big]\, d\theta\, d\vartheta \\
& - \frac{1}{\pi}\int_0^{\frac{\pi}{2}} \exp\Big[-\frac{1}{16\sigma^2}\frac{(\sqrt{A} + \frac{\sqrt{3}B}{\sqrt{A}})^2}{\sin^2\theta}\Big]\, d\theta
\end{aligned} \tag{A.40}
$$

where A and B are defined by (3.10) and (3.11), respectively. We know that

$$
P(\hat{s_1} \neq s_1 \mid \hat{s_4} = z_2^{'}; s_4 = z_1^{'}) = E\Big\{P(\hat{s_1} \neq s_1 \mid \hat{s_4} = z_2^{'}; s_4 = z_1^{'}; \alpha_{1,i};\ i = 1,2,3,4)\Big\} \tag{A.41}
$$

and

$$
P(\hat{s_1} \neq s_1 \mid \hat{s_4} = z_4^{'}; s_4 = z_1^{'}) = E\Big\{P(\hat{s_1} \neq s_1 \mid \hat{s_4} = z_4^{'}; s_4 = z_1^{'}; \alpha_{1,i};\ i = 1,2,3,4)\Big\} \tag{A.42}
$$

where E denotes the expectation with respect to $\alpha_{1,i};\ i = 1,2,3,4$. From (A.40)-(A.42), we have

$$
\begin{aligned}
& P(\hat{s_1} \neq s_1 \mid \hat{s_4} = z_2^{'}; s_4 = z_1^{'}) = P(\hat{s_1} \neq s_1 \mid \hat{s_4} = z_4^{'}; s_4 = z_1^{'}) \\
= \; & 1 - P(\grave{a} + \sqrt{3}\grave{b} > 0) \\
& + 2P(\grave{a} + \sqrt{3}\grave{b} > 0)\frac{1}{\pi}\int\int_{-\infty}^{+\infty}\int_0^{\frac{\pi}{2}} \exp\Big[-\frac{1}{16\sigma^2}\frac{(\sqrt{a} + \frac{\sqrt{3}b}{\sqrt{a}})^2}{\sin^2\theta}\Big] f_{A,B}(a,b)\ d\theta da db \\
& + P(\grave{a} + \sqrt{3}\grave{b} > 0)\frac{1}{\pi}\int\int_{-\infty}^{+\infty}\int_0^{\frac{\pi}{2}} \exp\Big[-\frac{1}{16\sigma^2}\frac{(\sqrt{a} + \frac{b}{\sqrt{a}})^2}{\sin^2\vartheta}\Big] f_{A,B}(a,b)\ d\vartheta da db \\
& + [1 - 2P(\grave{a} + \sqrt{3}\grave{b} > 0)]\times
\end{aligned}
$$

$$\times \frac{1}{\pi^2} \int \int_{-\infty}^{+\infty} \int \int_{0}^{\frac{\pi}{2}} \exp\Big[-\frac{1}{16\sigma^2} \Big(\frac{(\sqrt{a} + \frac{\sqrt{3}b}{\sqrt{a}})^2}{\sin^2\theta} + \frac{(\sqrt{a} + \frac{b}{\sqrt{a}})^2}{\sin^2\vartheta} \Big) \Big] f_{A,B}(a,b)\, d\theta\, d\vartheta da db$$

$$-\frac{1}{\pi} \int \int_{-\infty}^{+\infty} \int_{0}^{\frac{\pi}{2}} \exp\Big[-\frac{1}{16\sigma^2} \frac{(\sqrt{a} + \frac{\sqrt{3}b}{\sqrt{a}})^2}{\sin^2\theta} \Big] f_{A,B}(a,b)\, d\theta da db \tag{A.43}$$

In (A.43), $f_{A,B}(a,b)$ denotes the joint pdf of A and B. Because

$$\lim_{\sigma^2 \to 0} \Big\{ \exp\Big[-\frac{1}{16\sigma^2} \frac{(\sqrt{a} + \frac{\sqrt{3}b}{\sqrt{a}})^2}{\sin^2\theta} \Big] f_{A,B}(a,b) \Big\} = 0 \tag{A.44}$$

$$\lim_{\sigma^2 \to 0} \Big\{ \exp\Big[-\frac{1}{16\sigma^2} \frac{(\sqrt{a} + \frac{b}{\sqrt{a}})^2}{\sin^2\vartheta} \Big] f_{A,B}(a,b) \Big\} = 0 \tag{A.45}$$

and

$$\lim_{\sigma^2 \to 0} \Big\{ \exp\Big[-\frac{1}{16\sigma^2} \Big(\frac{(\sqrt{a} + \frac{\sqrt{3}b}{\sqrt{a}})^2}{\sin^2\theta} + \frac{(\sqrt{a} + \frac{b}{\sqrt{a}})^2}{\sin^2\vartheta} \Big) \Big] f_{A,B}(a,b) \Big\} = 0 \tag{A.46}$$

Also,

$$\Big| \exp\Big[-\frac{1}{16\sigma^2} \frac{(\sqrt{a} + \frac{\sqrt{3}b}{\sqrt{a}})^2}{\sin^2\theta} \Big] f_{A,B}(a,b) \Big| \leq f_{A,B}(a,b) \tag{A.47}$$

$$\Big| \exp\Big[-\frac{1}{16\sigma^2} \frac{(\sqrt{a} + \frac{b}{\sqrt{a}})^2}{\sin^2\vartheta} \Big] f_{A,B}(a,b) \Big| \leq f_{A,B}(a,b) \tag{A.48}$$

and

$$\Big| \exp\Big[-\frac{1}{16\sigma^2} \Big(\frac{(\sqrt{a} + \frac{\sqrt{3}b}{\sqrt{a}})^2}{\sin^2\theta} + \frac{(\sqrt{a} + \frac{b}{\sqrt{a}})^2}{\sin^2\vartheta} \Big) \Big] f_{A,B}(a,b) \Big] \Big| \leq f_{A,B}(a,b) \tag{A.49}$$

where $f_{A,B}(a,b)$ is integrable. According to Lebesgue's Dominated Convergence Theorem, as σ^2 approaches zero, we switch the sequence of integration and limitation and have

$$
\begin{aligned}
&\lim_{\sigma^2\to 0} P(\hat{s_1}\neq s_1 \mid \hat{s_4}=z_2^{'};s_4=z_1^{'}) = \lim_{\sigma^2\to 0} P(\hat{s_1}\neq s_1 \mid \hat{s_4}=z_4^{'};s_4=z_1^{'})\\
=\;& 1-P(\grave{a}+\sqrt{3}\grave{b}>0)\\
&+2P(\grave{a}+\sqrt{3}\grave{b}>0)\frac{1}{\pi}\lim_{\sigma^2\to 0}\int\int_{-\infty}^{+\infty}\int_0^{\frac{\pi}{2}}\exp\Big[-\frac{1}{16\sigma^2}\frac{(\sqrt{a}+\frac{\sqrt{3}b}{\sqrt{a}})^2}{\sin^2\theta}\Big]f_{A,B}(a,b)\;d\theta dadb\\
&+P(\grave{a}+\sqrt{3}\grave{b}>0)\frac{1}{\pi}\lim_{\sigma^2\to 0}\int\int_{-\infty}^{+\infty}\int_0^{\frac{\pi}{2}}\exp\Big[-\frac{1}{16\sigma^2}\frac{(\sqrt{a}+\frac{b}{\sqrt{a}})^2}{\sin^2\vartheta}\Big]f_{A,B}(a,b)\;d\vartheta dadb\\
&+[1-2P(\grave{a}+\sqrt{3}\grave{b}>0)]\frac{1}{\pi^2}\times\\
&\times\lim_{\sigma^2\to 0}\int\int_{-\infty}^{+\infty}\int\int_0^{\frac{\pi}{2}}\exp\Big[-\frac{1}{16\sigma^2}\Big(\frac{(\sqrt{a}+\frac{\sqrt{3}b}{\sqrt{a}})^2}{\sin^2\theta}+\frac{(\sqrt{a}+\frac{b}{\sqrt{a}})^2}{\sin^2\vartheta}\Big)\Big]f_{A,B}(a,b)d\theta d\vartheta dadb\\
&-\frac{1}{\pi}\lim_{\sigma^2\to 0}\int\int_{-\infty}^{+\infty}\int_0^{\frac{\pi}{2}}\exp\Big[-\frac{1}{16\sigma^2}\frac{(\sqrt{a}+\frac{\sqrt{3}b}{\sqrt{a}})^2}{\sin^2\theta}\Big]f_{A,B}(a,b)\;d\theta dadb\\
=\;& 1-P(\grave{a}+\sqrt{3}\grave{b}>0)\\
&+2P(\grave{a}+\sqrt{3}\grave{b}>0)\frac{1}{\pi}\int\int_{-\infty}^{+\infty}\int_0^{\frac{\pi}{2}}\lim_{\sigma^2\to 0}\exp\Big[-\frac{1}{16\sigma^2}\frac{(\sqrt{a}+\frac{\sqrt{3}b}{\sqrt{a}})^2}{\sin^2\theta}\Big]f_{A,B}(a,b)\;d\theta dadb\\
&+P(\grave{a}+\sqrt{3}\grave{b}>0)\frac{1}{\pi}\int\int_{-\infty}^{+\infty}\int_0^{\frac{\pi}{2}}\lim_{\sigma^2\to 0}\exp\Big[-\frac{1}{16\sigma^2}\frac{(\sqrt{a}+\frac{b}{\sqrt{a}})^2}{\sin^2\vartheta}\Big]f_{A,B}(a,b)\;d\vartheta dadb\\
&+[1-2P(\grave{a}+\sqrt{3}\grave{b}>0)]\frac{1}{\pi^2}\times\\
&\times\int\int_{-\infty}^{+\infty}\int\int_0^{\frac{\pi}{2}}\lim_{\sigma^2\to 0}\exp\Big[-\frac{1}{16\sigma^2}\Big(\frac{(\sqrt{a}+\frac{\sqrt{3}b}{\sqrt{a}})^2}{\sin^2\theta}+\frac{(\sqrt{a}+\frac{b}{\sqrt{a}})^2}{\sin^2\vartheta}\Big)\Big]f_{A,B}(a,b)d\theta d\vartheta dadb\\
&-\frac{1}{\pi}\int\int_{-\infty}^{+\infty}\int_0^{\frac{\pi}{2}}\lim_{\sigma^2\to 0}\exp\Big[-\frac{1}{16\sigma^2}\frac{(\sqrt{a}+\frac{\sqrt{3}b}{\sqrt{a}})^2}{\sin^2\theta}\Big]f_{A,B}(a,b)\;d\theta dadb\\
=\;& 1-P(\grave{a}+\sqrt{3}\grave{b}>0)=P(\grave{a}+\sqrt{3}\grave{b}<0)
\end{aligned}
\tag{A.50}
$$

A.8.3 Evaluation of $P(\hat{s_1}\neq s_1 \mid \hat{s_4}=z_3^{'};s_4=z_1^{'})$ When σ^2 Approaches 0

According to (A.35)

$$P(\hat{s_1}\neq s_1 \mid \hat{s_4}=z_3^{'};s_4=z_1^{'};\alpha_{1,i}\;i=1,2,3,4)$$

$$
\begin{aligned}
&= 1 - P\Big(\frac{\grave{a}}{\sqrt{8}} + \frac{(1+\sqrt{3})\grave{b}}{\sqrt{8}} + \mathrm{Re}(n_{U\,1,1}) > 0\Big) P\Big(\frac{\grave{a}}{\sqrt{8}} + \frac{(1+\sqrt{3})\grave{b}}{\sqrt{8}} + \mathrm{Im}(n_{U\,1,1}) > 0\Big) \\
&= 1 - \Big\{ P\Big(\frac{\grave{a}}{\sqrt{8}} + \frac{(1+\sqrt{3})\grave{b}}{\sqrt{8}} + \mathrm{Re}(n_{U\,1,1}) > 0 \Big| \grave{a} + (1+\sqrt{3})\grave{b} > 0\Big) P(\grave{a} + (1+\sqrt{3})\grave{b} > 0) \\
&\quad + P\Big(\frac{\grave{a}}{\sqrt{8}} + \frac{(1+\sqrt{3})\grave{b}}{\sqrt{8}} + \mathrm{Re}(n_{U\,1,1}) > 0 \Big| \grave{a} + (1+\sqrt{3})\grave{b} < 0\Big) P(\grave{a} + (1+\sqrt{3})\grave{b} < 0) \Big\}^2 \\
&= 1 - \Big\{ \Big[1 - Q\Big(\frac{(\grave{a} + (1+\sqrt{3})\grave{b})}{2}\Big)\Big] P(\grave{a} + (1+\sqrt{3})\grave{b} > 0) + Q\Big(\frac{-(\grave{a} + (1+\sqrt{3})\grave{b})}{2}\Big) \times \\
&\quad \times P(\grave{a} + (1+\sqrt{3})\grave{b} < 0) \Big\}^2 \\
&= 1 - P^2(\grave{a} + (1+\sqrt{3})\grave{b} > 0) - [2P(\grave{a} + (1+\sqrt{3})\grave{b} > 0) - 4P^2(\grave{a} + (1+\sqrt{3})\grave{b} > 0)] \times \\
&\quad \times Q\Big(\frac{(\grave{a} + (1+\sqrt{3})\grave{b})}{2}\Big) - [1 - 2P(\grave{a} + (1+\sqrt{3})\grave{b} > 0)]^2 Q^2\Big(\frac{(\grave{a} + (1+\sqrt{3})\grave{b})}{2}\Big) \qquad \text{(A.51)}
\end{aligned}
$$

From (A.51), by using Craig's formula, we have

$$
\begin{aligned}
&P(\hat{s_1} \neq s_1 \mid \hat{s_4} = z_3^{'}; s_4 = z_1^{'}) \\
&= 1 - P^2(\grave{a} + (1+\sqrt{3})\grave{b} > 0) - [2P(\grave{a} + (1+\sqrt{3})\grave{b} > 0) - 4P^2(\grave{a} + (1+\sqrt{3})\grave{b} > 0)] \times \\
&\quad \times \frac{1}{\pi} \int_0^{\frac{\pi}{2}} \exp\Big(- \frac{(\grave{a} + (1+\sqrt{3})\grave{b})^2}{8\sin^2\theta}\Big)\, d\theta \\
&\quad - [1 - 2P(\grave{a} + (1+\sqrt{3})\grave{b} > 0)]^2 \frac{1}{\pi} \int_0^{\frac{\pi}{4}} \exp\Big(- \frac{(\grave{a} + (1+\sqrt{3})\grave{b})^2}{8\sin^2\theta}\Big)\, d\theta \\
&= 1 - P^2(\grave{a} + (1+\sqrt{3})\grave{b} > 0) - \\
&- [2P(\grave{a} + (1+\sqrt{3})\grave{b} > 0) - 4P^2(\grave{a} + (1+\sqrt{3})\grave{b} > 0)] \frac{1}{\pi} \int_0^{\frac{\pi}{2}} \exp\Big[- \frac{1}{16\sigma^2} \frac{(\sqrt{A} + \frac{(1+\sqrt{3})B}{\sqrt{A}})^2}{\sin^2\theta}\Big]\, d\theta \\
&- [1 - 2P(\grave{a} + (1+\sqrt{3})\grave{b} > 0)]^2 \frac{1}{\pi} \int_0^{\frac{\pi}{4}} \exp\Big[- \frac{1}{16\sigma^2} \frac{(\sqrt{A} + \frac{(1+\sqrt{3})B}{\sqrt{A}})^2}{\sin^2\theta}\Big]\, d\theta \qquad \text{(A.52)}
\end{aligned}
$$

then

$$
\begin{aligned}
&P(\hat{s_1} \neq s_1 \mid \hat{s_4} = z_3; s_4 = z_1) = E\Big\{ P(\hat{s_1} \neq s_1 \mid \hat{s_4} = z_3; s_4 = z_1; \alpha_{1,i}\, i = 1,2,3,4) \Big\} \\
&= 1 - P^2(\grave{a} + (1+\sqrt{3})\grave{b} > 0) \\
&- [2P(\grave{a} + (1+\sqrt{3})\grave{b} > 0) - 4P^2(\grave{a} + (1+\sqrt{3})\grave{b} > 0)] \times
\end{aligned}
$$

$$
\begin{aligned}
&\times\frac{1}{\pi}E\Big\{\int_0^{\frac{\pi}{2}}\exp\Big[-\frac{1}{16\sigma^2}\frac{(\sqrt{A}+\frac{(1+\sqrt{3})B}{\sqrt{A}})^2}{\sin^2\theta}\Big]\,d\theta\Big\}\\
-\;&[1-2P(\grave{a}+(1+\sqrt{3})\grave{b}>0)]^2\frac{1}{\pi}E\Big\{\int_0^{\frac{\pi}{4}}\exp\Big[-\frac{1}{16\sigma^2}\frac{(\sqrt{A}+\frac{(1+\sqrt{3})B}{\sqrt{A}})^2}{\sin^2\theta}\Big]\,d\theta\Big\}\\
=\;&1-P^2(\grave{a}+(1+\sqrt{3})\grave{b}>0)-[2P(\grave{a}+(1+\sqrt{3})\grave{b}>0)-4P^2(\grave{a}+(1+\sqrt{3})\grave{b}>0)]\frac{1}{\pi}\times\\
&\times\int\int_{-\infty}^{+\infty}\int_0^{\frac{\pi}{2}}\exp\Big[-\frac{1}{16\sigma^2}\frac{(\sqrt{a}+\frac{(1+\sqrt{3})b}{\sqrt{a}})^2}{\sin^2\theta}\Big]f_{A,B}(a,b)\,d\theta dadb\\
-\;&[1-2P(\grave{a}+(1+\sqrt{3})\grave{b}>0)]^2\times\\
&\times\frac{1}{\pi}\int\int_{-\infty}^{+\infty}\int_0^{\frac{\pi}{4}}\exp\Big[-\frac{1}{16\sigma^2}\frac{(\sqrt{a}+\frac{(1+\sqrt{3})b}{\sqrt{a}})^2}{\sin^2\theta}\Big]f_{A,B}(a,b)\;d\theta dadb
\end{aligned}
\tag{A.53}
$$

From (A.53), by using similar analysis in Appendix A.8.2, according to Lebesgue's Dominated Convergence Theorem, we switch the sequence of integration and limitation and have

$$
\begin{aligned}
&\lim_{\sigma^2\to 0}P(\hat{s_1}\neq s_1\mid\hat{s_4}=z_3;s_4=z_1)\\
=\;&1-P^2(\grave{a}+(1+\sqrt{3})\grave{b}>0)-[2P(\grave{a}+(1+\sqrt{3})\grave{b}>0)-P^2(\grave{a}+(1+\sqrt{3})\grave{b}>0)]\frac{1}{\pi}\times\\
&\times\lim_{\sigma^2\to 0}\int\int_{-\infty}^{+\infty}\int_0^{\frac{\pi}{2}}\exp\Big[-\frac{1}{16\sigma^2}\frac{(\sqrt{a}+\frac{(1+\sqrt{3})b}{\sqrt{a}})^2}{\sin^2\theta}\Big]f_{A,B}(a,b)\,d\theta dadb\\
-\;&[1-2P(\grave{a}+(1+\sqrt{3})\grave{b}>0)]^2\times\\
&\times\lim_{\sigma^2\to 0}\frac{1}{\pi}\int\int_{-\infty}^{+\infty}\int_0^{\frac{\pi}{4}}\exp\Big[-\frac{1}{16\sigma^2}\frac{(\sqrt{a}+\frac{(1+\sqrt{3})b}{\sqrt{a}})^2}{\sin^2\theta}\Big]f_{A,B}(a,b)\;d\theta dadb\\
=\;&1-P^2(\grave{a}+(1+\sqrt{3})\grave{b}>0)-[2P(\grave{a}+(1+\sqrt{3})\grave{b}>0)-P^2(\grave{a}+(1+\sqrt{3})\grave{b}>0)]\frac{1}{\pi}\times\\
&\times\int\int_{-\infty}^{+\infty}\int_0^{\frac{\pi}{2}}\lim_{\sigma^2\to 0}\exp\Big[-\frac{1}{16\sigma^2}\frac{(\sqrt{a}+\frac{(1+\sqrt{3})b}{\sqrt{a}})^2}{\sin^2\theta}\Big]f_{A,B}(a,b)\,d\theta dadb\\
-\;&[1-2P(\grave{a}+(1+\sqrt{3})\grave{b}>0)]^2\times\\
&\times\frac{1}{\pi}\int\int_{-\infty}^{+\infty}\int_0^{\frac{\pi}{4}}\lim_{\sigma^2\to 0}\exp\Big[-\frac{1}{16\sigma^2}\frac{(\sqrt{a}+\frac{(1+\sqrt{3})b}{\sqrt{a}})^2}{\sin^2\theta}\Big]f_{A,B}(a,b)\;d\theta dadb\\
=\;&1-P^2[\grave{a}+(1+\sqrt{3})\grave{b}>0]
\end{aligned}
\tag{A.54}
$$

A.9 Evaluation of $\min\{1 - P^2[\grave{a} + (1+\sqrt{3})\grave{b} > 0]\ ;\ P(\grave{a} + \sqrt{3}\grave{b} < 0)\}$

A.9.1 Mathematical Preliminaries

Consider a random variable G expressed in quadratic form as

$$G = \boldsymbol{\alpha}^H \mathbf{Q_G} \boldsymbol{\alpha} \tag{A.55}$$

where $\boldsymbol{\alpha}$ is defined by (3.98) and $\mathbf{Q_G}$ is Hermitian. From (3.79), (3.99) and (3.100), we have the characteristic function of G as

$$\Phi_G(\omega) = \Phi_G(s)\big|_{s=j\omega} = \frac{1}{|\mathbf{I} - j\omega\mathbf{Q_G}|} = \frac{1}{\Pi_{i=1}^{I}(1 - j\omega\lambda_i)} \tag{A.56}$$

where λ_i's $(i = 1, 2, ..., I)$ are eigenvalues of $\mathbf{Q_G}$. We know that

$$P(G < 0) = \int_{-\infty}^{0} f_G(g)\, dg \tag{A.57}$$

where $f_G(g)$ denotes the pdf of G. Since $f_G(g)$ is the inverse Fourier transform of $\Phi_G(\omega)$, (A.57) changes to

$$P(G < 0) = -\frac{1}{j2\pi}\int_{-\infty+j\epsilon}^{+\infty+j\epsilon} \frac{\Phi_G(\omega)}{\omega} d\omega = -\frac{1}{j2\pi}\int_{-\infty+j\epsilon}^{+\infty+j\epsilon} \frac{1}{\Pi_{i=1}^{I}(1 - j\omega\lambda_i)\omega} d\omega \tag{A.58}$$

In (A.58), a small positive number ϵ is inserted to avoid the evaluation of integration at the singularity point $\omega = 0$. With the substitution $x = j\omega$, (A.58) changes to

$$P(G < 0) = -\frac{1}{j2\pi}\int_{-\epsilon-j\infty}^{-\epsilon+j\infty} \frac{1}{\Pi_{i=1}^{I}(1 - x\lambda_i)x} dx = -\frac{1}{j2\pi}\int_{-\epsilon-j\infty}^{-\epsilon+j\infty} g(x)dx \tag{A.59}$$

where

$$g(x) = \frac{1}{\Pi_{i=1}^{I}(1 - x\lambda_i)x} \tag{A.60}$$

We calculate (A.59) with the aid of the residue theorem [43]. By choosing a counter-clockwise contour C as shown in Fig.A.1, (A.59) changes to

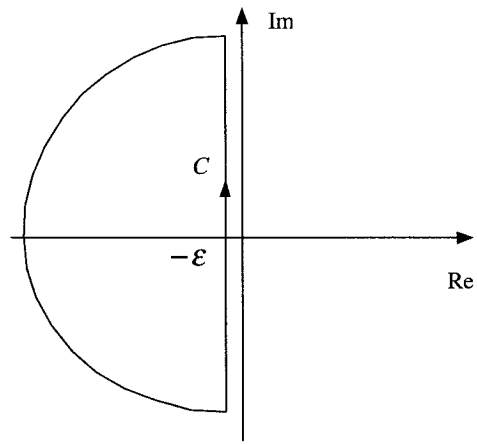

Fig. A.1 Contour of Integration

$$P(G < 0) = -\frac{1}{j2\pi} \oint_C g(x)dx = -\sum_C \text{Res}[g(x)] \tag{A.61}$$

where $\sum_C$ means that only the residues at the poles lying inside the contour C are taken into account. According to [43], for the Laurels series of a function $f(z)$

$$f(z) = \sum_{n=0}^{\infty} a_n(z - z_0)^n + \frac{b_1}{z - z_0} + \frac{b_2}{(z - z_0)^2} + \ldots \tag{A.62}$$

the coefficient b_1 of the term $\frac{1}{z-z_0}$ is called the residue at $z = z_0$. For a pole of order M, the residue at $z = z_0$ is given by

$$\text{Res}_{z=z_0}[f(z)] = \frac{1}{(M-1)!} \lim_{z \to z_0} \left\{ \frac{d^{M-1}}{dz^{M-1}} [(z - z_0)^M f(z)] \right\} \tag{A.63}$$

Here we only consider the special case we encountered in this thesis. For this case, $g(x)$ has two distinct double poles. We re-write $g(x)$ defined in (A.60) in the form

$$\begin{aligned} g(x) &= \frac{1}{(1-x\lambda_1)^2(1-x\lambda_3)^2 x} = \frac{\lambda_1^{-2}\lambda_3^{-2}}{(x-\frac{1}{\lambda_1})^2(x-\frac{1}{\lambda_3})^2 x} \\ &= \frac{R_1}{x-\frac{1}{\lambda_1}} + \frac{R_2}{(x-\frac{1}{\lambda_1})^2} + \frac{R_3}{x-\frac{1}{\lambda_3}} + \frac{R_4}{(x-\frac{1}{\lambda_3})^2} + \frac{R_5}{x} \end{aligned} \tag{A.64}$$

From (A.63) and (A.64), the residues of $g(x)$ are

$$R_1 = \lim_{x \to \frac{1}{\lambda_1}} \frac{d}{dx} \left\{ g(x)(x - \frac{1}{\lambda_1})^2 \right\} = -\frac{3\lambda_3\lambda_1^2 - \lambda_1^3}{(\lambda_3 - \lambda_1)^3} \tag{A.65}$$

and

$$R_3 = \lim_{x \to \frac{1}{\lambda_3}} \frac{d}{dx} \left\{ g(x)(x - \frac{1}{\lambda_3})^2 \right\} = -\frac{3\lambda_1\lambda_3^2 - \lambda_3^3}{(\lambda_1 - \lambda_3)^3} \tag{A.66}$$

A.9.2 Calculation of $P[\grave{a} + (1+\sqrt{3})\grave{b} < 0]$ and $P(\grave{a} + \sqrt{3}\grave{b} < 0)$

From (3.46), (3.50) and (3.51), we know that

$$\begin{aligned} P[\grave{a} + (1+\sqrt{3})\grave{b} < 0] &= P\Big[\frac{1}{\sqrt{2\sigma^2}}\big(\sqrt{A} + (1+\sqrt{3})\frac{B}{\sqrt{A}}\big) < 0\Big] = P\big(\frac{A + (1+\sqrt{3})B}{\sqrt{A}} < 0\big) \\ &= P\big[A + (1+\sqrt{3})B < 0\big] \end{aligned} \tag{A.67}$$

and

$$\begin{aligned} P[\grave{a}+\sqrt{3}\grave{b}<0] &= P\Big[\frac{1}{\sqrt{2\sigma^2}}\big(\sqrt{A}+\frac{\sqrt{3}B}{\sqrt{A}}\big)<0\Big] = P\big(\frac{A+\sqrt{3}B}{\sqrt{A}}<0\big) \\ &= P\big[A+\sqrt{3}B<0\big] \end{aligned} \tag{A.68}$$

According to (3.10) and (3.11), we write $A+(1+\sqrt{3})B$ and $A+\sqrt{3}B$ in quadratic forms

$$A+(1+\sqrt{3})B = \boldsymbol{\alpha}^H \mathbf{Q}_{\mathbf{G1}} \boldsymbol{\alpha} \tag{A.69}$$

and

$$A+\sqrt{3}B = \boldsymbol{\alpha}^H \mathbf{Q}_{\mathbf{G2}} \boldsymbol{\alpha} \tag{A.70}$$

where

$$\mathbf{Q}_{\mathbf{G1}} = \begin{pmatrix} 1 & 0 & 0 & 1+\sqrt{3} \\ 0 & 1 & -(1+\sqrt{3}) & 0 \\ 0 & -(1+\sqrt{3}) & 1 & 0 \\ 1+\sqrt{3} & 0 & 0 & 1 \end{pmatrix} \tag{A.71}$$

and

$$\mathbf{Q}_{\mathbf{G2}} = \begin{pmatrix} 1 & 0 & 0 & \sqrt{3} \\ 0 & 1 & -\sqrt{3} & 0 \\ 0 & -\sqrt{3} & 1 & 0 \\ \sqrt{3} & 0 & 0 & 1 \end{pmatrix} \tag{A.72}$$

The eigenvalues of $\mathbf{Q_{G1}}$ and $\mathbf{Q_{G2}}$ are

$$\lambda_1 = \lambda_2 = \sqrt{3}; \quad \lambda_3 = \lambda_4 = 2 + \sqrt{3} \tag{A.73}$$

and

$$\lambda_1^{'} = \lambda_2^{'} = 1 - \sqrt{3}; \quad \lambda_3^{'} = \lambda_4^{'} = 1 + \sqrt{3} \tag{A.74}$$

respectively. In the calculation of $P\big[A + (1+\sqrt{3})B < 0\big]$ and $P\big[A + \sqrt{3}B < 0\big]$, we only consider the residues at the poles lying inside the contour indicated in Fig.A.1, which are

$$R_1 = -\frac{3\lambda_3\lambda_1^2 - \lambda_1^3}{(\lambda_3 - \lambda_1)^3} = -0.2377 \tag{A.75}$$

and

$$R_1^{'} = -\frac{3\lambda_3^{'}\lambda_1^{'2} - \lambda_1^{'3}}{(\lambda_3^{'} - \lambda_1^{'})^3} = -0.1151 \tag{A.76}$$

respectively. According to (A.61),

$$P\big[A + (1+\sqrt{3})B < 0\big] = 0.2377 \tag{A.77}$$

and

$$P\big[A + \sqrt{3}B < 0\big] = 0.1151 \tag{A.78}$$

So

$$\begin{aligned} & \min\{1 - P^2[\grave{a} + (1+\sqrt{3})\grave{b} > 0]\,;\; P(\grave{a} + \sqrt{3}\grave{b} < 0)\} \\ = \;& \min\{1 - (1 - 0.2377)^2\,;\; 0.1151\} = 0.1151 \end{aligned} \tag{A.79}$$

Appendix B

Computer Simulations Software

In this chapter, we present the software used for computer simulations associated with this thesis. The parameters required for simulations are:

- the length of information bit sequence;
- the frame length;
- the SNR range for simulation;

For the spatially correlated channels, further parameters need be specified.

- the wavelength of carrier λ;
- the distance between base station and mobile R;
- the radius of scatters around mobile D;
- the distance between adjacent transmit antennas d'.

B.1 Simulation Steps

B.1.1 Information Source and Encoder

The input of the simulation is a sequence of information bits generated by Matlab function **randint()**. By using Gray mapping illustrated in Fig.3.2, every two bits are mapped to an information-bearing symbol. With the employment of Quasi-Orthogonal [28] or Improved Quasi-Orthogonal coding scheme [29], we get the a sequence of codewords with the code matrix (3.2), which is denoted as **mat_InputQuOr** in the routine.

program B.1.1 Information Source, Gray Mapping and Encoder

```
% Constellations for Improved Quasi-Orthogonal code
% Symbol Energy is 1/4 ; Gray Mapping
vec_Costl=[1+j,-1+j,1-j,-1-j]./(2*sqrt(2));
vec_CostlRot=[1+j,-1+j,1-j,-1-j].*exp(j*pi/6)./(2*sqrt(2));
% For Quasi-Orthogonal code
% vec_CostlRot=[1+j,-1+j,1-j,-1-j]./(2*sqrt(2));

% Information Bits Sequence
num_real=2*randint(1,num_length,2)-1;
num_Imag=2*randint(1,num_length,2)-1;
num_Sent(1:2:2*num_length-1)=num_real;
num_Sent(2:2:2*num_length)=num_Imag;

% Index of Symbols in Gray Mapping
num_SentDec=num_real+num_Imag./2+2.5;

% Sequence of Information Bearing Symbols
num_Input(1:4:num_length-3)=vec_Costl(num_SentDec(1:4:num_length-3));
num_Input(2:4:num_length-2)=vec_Costl(num_SentDec(2:4:num_length-2));
num_Input(3:4:num_length-1)=vec_CostlRot(num_SentDec(3:4:num_length-1));
num_Input(4:4:num_length-0)=vec_CostlRot(num_SentDec(4:4:num_length-0));

% Improved Quasi-Orthogonal Encoder
% Row 1
mat_InputQuOr(1,1:4:num_length-3)=num_Input(1:4:num_length-3);
mat_InputQuOr(1,2:4:num_length-2)=-conj(num_Input(2:4:num_length-2));
mat_InputQuOr(1,3:4:num_length-1)=-conj(num_Input(3:4:num_length-1));
mat_InputQuOr(1,4:4:num_length-0)=num_Input(4:4:num_length-0);
% Row 2 ... Row 3 ... Row 4 ... (Omitted)
```

B.1.2 Independent and Spatially Correlated Rayleigh Fading Channels

In this work we consider two types of fading channels: independent and spatially correlated Rayleigh fading channels.

For independent Rayleigh fading channels described in section 2.1.1, the real parts and the imaginary parts of the elements in channel coefficient matrix, which is denoted as **mat_FadingG** in the routine, are simulated by Matlab function **randn()** with zero mean and variance 0.5.

In the realization of spatially correlated channels discussed in the chapter 4, we need more steps. By using (4.2), we get the correlation matrix among four channels, which is denoted as **mat_Correlation** in the routine. By calling Matlab function **sqrtm()**, we get the root of **mat_Correlation**, which is denoted as **mat_RootCorrl** in the routine. The product of mat_RootCorrl and **mat_FadingG**, denoted as **mat_CorFading**, represents the spatially correlated channels we simulate.

B.1.3 Additive Complex Gaussian Noise

The real part and imaginary part of additive complex Gaussian noise at the receiver are simulated by Matlab function **randn()** with zero mean and variance σ^2. The relationship between σ^2 and SNR/bit (in dB) is expressed by (3.73).

B.1.4 Independence Among the Random Generators

We know that the Matlab random generators produce pseudo-random numbers, where the sequence of numbers generated is determined by the state of the generator. Since Matlab resets the state at start-up, the sequence of numbers generated will be the same unless the state is changed. We also notice that in the implementation of computer simulations, all the random generators are independent. In order to realize the independence among the random generators, a command **rand**('state' , sum $(100 * \text{clock})$) is employed to reset the state each time.

program B.1.2 Independent and Correlated Fading Channels

```
% 4 Tx antennas
int_NumberOfTx=4;
% Distance Between Adjacent Antennas is 5 Lambda
int_DistanceBetTx=5;
% asin(R/D)
int_Delta=asin(100*3/18/500);

% Matrix Cs
mat_Correlation=zeros(4,4);
for iRow=1:int_NumberOfTx
 for iCol=1:int_NumberOfTx
  mat_Correlation(iRow,iCol)=besselj(0,int_Delta*2*pi*
       abs(iRow-iCol)*int_DistanceBetTx);
 end
end

% Root of Cs
mat_RootCorrl=sqrtm(mat_Correlation);
% For Independent Channels CR is Identical Matrix as
% mat_RootCorrl=eye(4);

% Fading Channel
mat_FadingG=randn(4,num_length/4)/sqrt(2)
      +(randn(4,num_length/4)/sqrt(2)).*j;
mat_CorFading(1,1:num_length/4)=mat_RootCorrl(1,1)*
  mat_FadingG(1,1:num_length/4)+mat_RootCorrl(1,2)*
  mat_FadingG(2,1:num_length/4)+mat_RootCorrl(1,3)*
  mat_FadingG(3,1:num_length/4)+mat_RootCorrl(1,4)*
  mat_FadingG(4,1:num_length/4);
... (Omitted)

% quasi-static
mat_Fading=reshape(repmat(mat_CorFading,4,1),4,num_length);
```

program B.1.3 Additive Complex Gaussian Noise

```
% Additive Complex Gaussian Noise
% Relation Between Variance and SNR
num_Var=(10^(-GAMAbforAll(iSNR)/20))/2;
mat_Received=mat_SumAfterFading+num_Var*randn(1,num_length)
            +num_Var*randn(1,num_length).*j;
```

B.1.5 Optimal Decoding

From section 3.2.1, optimal decoding can be decoupled into symbol pair joint decoding. In decoding symbol pair s_1 and s_4, the decoder chooses the values for $\tilde{s_1}$ and $\tilde{s_4}$ that minimize the metric **mat_Dis14** in the implementation. In decoding symbol pair s_2 and s_3, the decoder chooses the values for $\tilde{s_2}$ and $\tilde{s_3}$ that minimize the metric **mat_Dis23** in the implementation. The associated routine is included in the program B.1.4. In the program, the Matlab function **min()** is employed to return the index of the pair of symbols that minimize metrics (3.30) and (3.31).

B.1.6 Simplified Decoding

Simplified decoding consists of the following steps:

Noise Decorrelation: The associated operations have be presented in (3.28) and (3.29). The implementation is included in program B.1.5.

QR Decomposition: The associated operations have be presented in (3.48) – (3.55). The implementation is included in program B.1.6.

Symbol-by-Symbol with Decision Feedback Decoding: The implementation is included in program B.1.7. The Matlab function **min()** is employed to return the indexes of the symbols that minimize metrics (3.67)-(3.70).

B.2 Complete Computer Simulation Program

The complete computer simulation program associated with this thesis is included in the program B.2.1.

program B.1.4 Optimal Decoder

```
% mat_Di Corresponds to rH_i,1 in the Thesis
mat_D1=mat_Received(1:4:num_length-3)
      .*(conj(mat_Fading(1,1:4:num_length-3)))
      +(conj(mat_Received(2:4:num_length-2)))
      .*mat_Fading(2,1:4:num_length-3)
      +(conj(mat_Received(3:4:num_length-1)))
      .*mat_Fading(3,1:4:num_length-3)
      +mat_Received(4:4:num_length-0)
      .*(conj(mat_Fading(4,1:4:num_length-3)));
mat_D2=...
mat_D3=...
mat_D4=... (Omitted)

for iHex=1:16
 %D1-AS1-BS4
 mat_M14= mat_D1-mat_A.*mat_Symbol16(1,iHex)-mat_B.*mat_Symbol16(2,iHex);
 %D4-BS1-AS4
 mat_N14= mat_D4-mat_B.*mat_Symbol16(1,iHex)-mat_A.*mat_Symbol16(2,iHex);
 mat_Dis14(iHex,:)=(1/2/(num_Var)^2)*(mat_C14N_11.*(abs(mat_M14).^2
          +abs(mat_N14).^2)+2*mat_C14N_12.*real(conj(mat_M14).*(mat_N14)));
 % D1-AS2+BS3
 mat_M23= mat_D2-mat_A.*mat_Symbol16(1,iHex)+mat_B.*mat_Symbol16(2,iHex);
 % D4+BS2-AS3
 mat_N23= mat_D3+mat_B.*mat_Symbol16(1,iHex)-mat_A.*mat_Symbol16(2,iHex);
 mat_Dis23(iHex,:)=(1/2/(num_Var)^2)*(mat_C14N_11.*(abs(mat_M23).^2
         +abs(mat_N23).^2)-2*mat_C14N_12.*real(conj(mat_M23).*(mat_N23)));
end

% Index of the Symbol Pair that Minimizes the Metric
[K,mat_Min14]=min(mat_Dis14,[],1);
[K,mat_Min23]=min(mat_Dis23,[],1);
% Convert Index to Information Bit
mat_Result14=(2*(fliplr(de2bi(mat_Min14-1)))-1).';
mat_Result23=(2*(fliplr(de2bi(mat_Min23-1)))-1).';
```

program B.1.5 Noise Decorrelation

```
% Calculation of C1^{-1/2} and C2^{-1/2}
% A and B
mat_A=(abs(mat_Fading(1,1:4:num_length-3))).^2
                    +(abs(mat_Fading(2,1:4:num_length-3))).^2
                    +(abs(mat_Fading(3,1:4:num_length-3))).^2
                    +(abs(mat_Fading(4,1:4:num_length-3))).^2;
mat_B=2*real(mat_Fading(1,1:4:num_length-3)
      .*conj(mat_Fading(4,1:4:num_length-3))
     -mat_Fading(2,1:4:num_length-3)
      .*conj(mat_Fading(3,1:4:num_length-3)));

%A^2-B^2
mat_Mo=mat_A.^2-mat_B.^2;

%Before Considering Variance
mat_C14N_11=mat_A./mat_Mo;
mat_C14N_12=-mat_B./mat_Mo;

% lambda1^(-1/2)
mat_Lambda1=((mat_A-mat_B).*(2*num_Var^2)).^(-1/2);
% lambda2^(-1/2)
mat_Lambda2=((mat_A+mat_B).*(2*num_Var^2)).^(-1/2);

% Elements of C1^(-1/2)  C11, C22
mat_C11=(mat_Lambda1+mat_Lambda2).*(1/2);
% Elements of C1^(-1/2)  C12, C21
mat_C12=(mat_Lambda2-mat_Lambda1).*(1/2);

% Elements of C2^(-1/2)  C211, C222
mat_C211=mat_C11;
% Elements of C2^(-1/2)  C212, C221
mat_C212=-mat_C12;

% Elements of H1
mat_h1=mat_C11.*mat_A+mat_C12.*mat_B;
mat_h2=mat_C12.*mat_A+mat_C11.*mat_B; %% h2

% Elements of H2
mat_h3=mat_C211.*mat_A-mat_C212.*mat_B;  %% h3
mat_h4=mat_C212.*mat_A-mat_C211.*mat_B;  %% h4

% Decorrelation
mat_D1p=mat_C11.*mat_D1+mat_C12.*mat_D4;
mat_D4p=mat_C12.*mat_D1+mat_C11.*mat_D4;
mat_D2p=mat_C211.*mat_D2+mat_C212.*mat_D3;
mat_D3p=mat_C212.*mat_D2+mat_C211.*mat_D3;
```

program B.1.6 QR Decomposition

```
% QR Decomposition
mat_a=sqrt((mat_h1.^2+mat_h2.^2));
mat_b=(mat_h1.*mat_h2).*2./mat_a;
mat_c=sqrt((mat_h2-(mat_b./(mat_a)).*mat_h1).^2
     +(mat_h1-(mat_b./(mat_a)).*mat_h2).^2);

mat_W1(1,1:2:num_length/2-1)=mat_h1./mat_a;
mat_W1(2,1:2:num_length/2-1)=mat_h2./mat_a;
mat_W1(1,2:2:num_length/2-0)=(mat_h2-(mat_b./(mat_a)).*mat_h1)./mat_c;
mat_W1(2,2:2:num_length/2-0)=(mat_h1-(mat_b./(mat_a)).*mat_h2)./mat_c;

% QR Decomposition
mat_d=sqrt((mat_h3.^2+mat_h4.^2));
mat_e=(mat_h3.*mat_h4).*2./mat_d;
mat_f=sqrt((mat_h4-(mat_e./(mat_d)).*mat_h3).^2
     +(mat_h3-(mat_e./(mat_d)).*mat_h4).^2);

mat_W2(1,1:2:num_length/2-1)=mat_h3./mat_d;
mat_W2(2,1:2:num_length/2-1)=mat_h4./mat_d;
mat_W2(1,2:2:num_length/2-0)=(mat_h4-(mat_e./(mat_d)).*mat_h3)./mat_f;
mat_W2(2,2:2:num_length/2-0)=(mat_h3-(mat_e./(mat_d)).*mat_h4)./mat_f;
```

program B.1.7 Symbol-by-Symbol with Decision Feedback Decoding

```
for iQ34=1:4
 mat_Distance4(iQ34,:)=abs(mat_D4ppp-mat_Symbol4_34(1,iQ34)*mat_c).^2;
 mat_Distance3(iQ34,:)=abs(mat_D3ppp-mat_Symbol4_34(1,iQ34)*mat_f).^2;
end

[K,mat_Min4]=min(mat_Distance4,[],1);
[K,mat_Min3]=min(mat_Distance3,[],1);

...

for iQ12=1:4
 mat_Distance1(iQ12,:)=abs(mat_D1ppp-mat_b.*mat_Symbol4_34(1,mat_Min4)
                      -mat_Symbol4_12(1,iQ12)*mat_a).^2;
 mat_Distance2(iQ12,:)=abs(mat_D2ppp-mat_e.*mat_Symbol4_34(1,mat_Min3)
                      -mat_Symbol4_12(1,iQ12)*mat_d).^2;
end

[K,mat_Min1]=min(mat_Distance1,[],1);
[K,mat_Min2]=min(mat_Distance2,[],1);
```

program B.2.1 Complete Computer Simulation Program

```
clear all;
% 128 Symbols/Frame
framelength=128;
% Number of Symbols for Inner-most Iteration
num_length=framelength*1000;
GAMAbforAll=[0:2:30];
num_Tx=4;
num_Rx=1;

% Constellations for Improved Quasi-Orthogonal code
% Symbol Energy is 1/4
% Gray Mapping
vec_Costl=[1+j,-1+j,1-j,-1-j]./(2*sqrt(2));
vec_CostlRot=[1+j,-1+j,1-j,-1-j].*exp(j*pi/6)./(2*sqrt(2));

mat_Symbol4_12=[1+j,-1+j,1-j,-1-j]./(2*sqrt(2));
mat_Symbol4_34=[1+j,-1+j,1-j,-1-j].*exp(j*pi/6)./(2*sqrt(2));

%% All Possible combination for two symbols
mat_Bin(1:16,1:4)=fliplr((de2bi(0:15)));
mat_Symbol16(1,:)=vec_Costl(mat_Bin(1:16,1)*2+mat_Bin(1:16,2)+1);
mat_Symbol16(2,:)=vec_CostlRot(mat_Bin(1:16,3)*2+mat_Bin(1:16,4)+1);
clear mat_Bin;

% 4 Tx Antennas
int_NumberOfTx=4;
% Distance Between Adjacent Antennas is 5 Lambda
int_DistanceBetTx=5;
% asin(R/D)
int_Delta=asin(100*3/18/500);
% Matrix Cs
mat_Correlation=zeros(4,4); for iRow=1:int_NumberOfTx
 for iCol=1:int_NumberOfTx
  mat_Correlation(iRow,iCol)=besselj(0,int_Delta*2*pi*abs(iRow-iCol)
                              *int_DistanceBetTx);
 end
end
% Root of Cs
mat_RootCorrl=sqrtm(mat_Correlation); mat_RootCorrl=eye(4);

for m=1:1e6
 for n=1:50
  rand('state',sum(100*clock));

  % Information Bits Sequence
```

```
num_real=2*randint(1,num_length,2)-1;
num_Imag=2*randint(1,num_length,2)-1;
num_Sent(1:2:2*num_length-1)=num_real;
num_Sent(2:2:2*num_length)=num_Imag;

% Index of Symbols in Gray Mapping
num_SentDec=num_real+num_Imag./2+2.5;

% Sequence of Information Bearing Symbols
num_Input(1:4:num_length-3)=vec_Costl(num_SentDec(1:4:num_length-3));

num_Input(2:4:num_length-2)=vec_Costl(num_SentDec(2:4:num_length-2));
num_Input(3:4:num_length-1)=vec_CostlRot(num_SentDec(3:4:num_length-1));
num_Input(4:4:num_length-0)=vec_CostlRot(num_SentDec(4:4:num_length-0));

% Improved Quasi-Orthogonal Encoder
% Row  1
mat_InputQuOr(1,1:4:num_length-3)=num_Input(1:4:num_length-3);
mat_InputQuOr(1,2:4:num_length-2)=-conj(num_Input(2:4:num_length-2));
mat_InputQuOr(1,3:4:num_length-1)=-conj(num_Input(3:4:num_length-1));
mat_InputQuOr(1,4:4:num_length-0)=num_Input(4:4:num_length-0);

% Row  2
mat_InputQuOr(2,1:4:num_length-3)=num_Input(2:4:num_length-2);
mat_InputQuOr(2,2:4:num_length-2)=conj(num_Input(1:4:num_length-3));
mat_InputQuOr(2,3:4:num_length-1)=-conj(num_Input(4:4:num_length-0));
mat_InputQuOr(2,4:4:num_length-0)=-num_Input(3:4:num_length-1);

% Row  3
mat_InputQuOr(3,1:4:num_length-3)=num_Input(3:4:num_length-1);
mat_InputQuOr(3,2:4:num_length-2)=-conj(num_Input(4:4:num_length-0));
mat_InputQuOr(3,3:4:num_length-1)=conj(num_Input(1:4:num_length-3));
mat_InputQuOr(3,4:4:num_length-0)=-num_Input(2:4:num_length-2);

% Row  4
mat_InputQuOr(4,1:4:num_length-3)=num_Input(4:4:num_length-0);
mat_InputQuOr(4,2:4:num_length-2)=conj(num_Input(3:4:num_length-1));
mat_InputQuOr(4,3:4:num_length-1)=conj(num_Input(2:4:num_length-2));
mat_InputQuOr(4,4:4:num_length-0)=num_Input(1:4:num_length-3);

% Fading Channel
mat_FadingG=randn(4,num_length/4)/sqrt(2)
            +(randn(4,num_length/4)/sqrt(2)).*j;
mat_CorFading(1,:)=mat_RootCorrl(1,1)*mat_FadingG(1,:)
                   +mat_RootCorrl(1,2)*mat_FadingG(2,:)
                   +mat_RootCorrl(1,3)*mat_FadingG(3,:)
                   +mat_RootCorrl(1,4)*mat_FadingG(4,:);
```

```
mat_CorFading(2,:)=mat_RootCorrl(2,1)*mat_FadingG(1,:)
                   +mat_RootCorrl(2,2)*mat_FadingG(2,:)
                   +mat_RootCorrl(2,3)*mat_FadingG(3,:)
                   +mat_RootCorrl(2,4)*mat_FadingG(4,:);
mat_CorFading(3,:)=mat_RootCorrl(3,1)*mat_FadingG(1,:)
                   +mat_RootCorrl(3,2)*mat_FadingG(2,:)
                   +mat_RootCorrl(3,3)*mat_FadingG(3,:)
                   +mat_RootCorrl(3,4)*mat_FadingG(4,:);
mat_CorFading(4,:)=mat_RootCorrl(4,1)*mat_FadingG(1,:)
                   +mat_RootCorrl(4,2)*mat_FadingG(2,:)
                   +mat_RootCorrl(4,3)*mat_FadingG(3,:)
                   +mat_RootCorrl(4,4)*mat_FadingG(4,:);
mat_Fading=reshape(repmat(mat_CorFading,4,1),4,num_length);

% Fading
mat_AfterFading=mat_InputQuOr.*mat_Fading;
mat_SumAfterFading=mat_AfterFading(1,:)+mat_AfterFading(2,:)
                   +mat_AfterFading(3,:)+mat_AfterFading(4,:);

% Calculation of C1^{-1/2} and C2^{-1/2}
% A and B
mat_A=(abs(mat_Fading(1,1:4:num_length-3))).^2
     +(abs(mat_Fading(2,1:4:num_length-3))).^2
     +(abs(mat_Fading(3,1:4:num_length-3))).^2
     +(abs(mat_Fading(4,1:4:num_length-3))).^2;
mat_B=2*real(mat_Fading(1,1:4:num_length-3)
      .*conj(mat_Fading(4,1:4:num_length-3))
       -mat_Fading(2,1:4:num_length-3)
      .*conj(mat_Fading(3,1:4:num_length-3)));
mat_Mo=mat_A.^2-mat_B.^2;

%Before Considering Variance
mat_C14N_11=mat_A./mat_Mo;
mat_C14N_12=-mat_B./mat_Mo;

  for iSNR=1:length(GAMAbforAll)
   % Additive Complex Gaussian Noise
   % Relation Between Variance and SNR
   num_Var=(10^(-GAMAbforAll(iSNR)/20))/2;
   mat_Received=mat_SumAfterFading+num_Var*randn(1,num_length)
               +num_Var*randn(1,num_length).*j;
```

```
% mat_Di Corresponds to rH_i,1 in the Thesis
mat_D1=mat_Received(1:4:num_length-3)
       .*(conj(mat_Fading(1,1:4:num_length-3)))
       +(conj(mat_Received(2:4:num_length-2)))
       .*mat_Fading(2,1:4:num_length-3)
       +(conj(mat_Received(3:4:num_length-1)))
       .*mat_Fading(3,1:4:num_length-3)
       +mat_Received(4:4:num_length-0)
       .*(conj(mat_Fading(4,1:4:num_length-3)));
 mat_D2=mat_Received(1:4:num_length-3)
       .*(conj(mat_Fading(2,1:4:num_length-3)))
       -(conj(mat_Received(2:4:num_length-2)))
       .*mat_Fading(1,1:4:num_length-3)
       +(conj(mat_Received(3:4:num_length-1)))
       .*mat_Fading(4,1:4:num_length-3)
       -mat_Received(4:4:num_length-0)
       .*(conj(mat_Fading(3,1:4:num_length-3)));
 mat_D3=mat_Received(1:4:num_length-3)
       .*(conj(mat_Fading(3,1:4:num_length-3)))
       +(conj(mat_Received(2:4:num_length-2)))
       .*mat_Fading(4,1:4:num_length-3)
       -(conj(mat_Received(3:4:num_length-1)))
       .*mat_Fading(1,1:4:num_length-3)
       -mat_Received(4:4:num_length-0)
       .*(conj(mat_Fading(2,1:4:num_length-3)));
 mat_D4=mat_Received(1:4:num_length-3)
       .*(conj(mat_Fading(4,1:4:num_length-3)))
       -(conj(mat_Received(2:4:num_length-2)))
       .*mat_Fading(3,1:4:num_length-3)
       -(conj(mat_Received(3:4:num_length-1)))
       .*mat_Fading(2,1:4:num_length-3)
       +mat_Received(4:4:num_length-0)
       .*(conj(mat_Fading(1,1:4:num_length-3)));

 for iHex=1:16
  %D1-AS1-BS4
  mat_M14=mat_D1-mat_A.*mat_Symbol16(1,iHex)
          -mat_B.*mat_Symbol16(2,iHex);
  %D4-BS1-AS4
  mat_N14=mat_D4-mat_B.*mat_Symbol16(1,iHex)
          -mat_A.*mat_Symbol16(2,iHex);
  mat_Dis14(iHex,:)=(1/2/(num_Var)^2)*(mat_C14N_11
         .*(abs(mat_M14).^2+abs(mat_N14).^2)
         +2*mat_C14N_12.*real(conj(mat_M14).*(mat_N14)));
  %D1-AS2+BS3
  mat_M23=mat_D2-mat_A.*mat_Symbol16(1,iHex)
          +mat_B.*mat_Symbol16(2,iHex);
```

```
%D4+BS2-AS3
    mat_N23=mat_D3+mat_B.*mat_Symbol16(1,iHex)
            -mat_A.*mat_Symbol16(2,iHex);
    mat_Dis23(iHex,:)=(1/2/(num_Var)^2)*(mat_C14N_11.*(abs(mat_M23).^2
        +abs(mat_N23).^2)-2*mat_C14N_12.*real(conj(mat_M23).*(mat_N23)));
    end

    clear mat_M14 mat_N14 mat_M23 mat_N23 iHex
    % Index of the Symbol Pair that Minimizes the Metric
    [K,mat_Min14]=min(mat_Dis14,[],1);
    [K,mat_Min23]=min(mat_Dis23,[],1);
    clear mat_Dis14 mat_Dis23



    % Convert Index to Information Bit
    mat_Result14=(2*(fliplr(de2bi(mat_Min14-1)))-1).';
    mat_Result23=(2*(fliplr(de2bi(mat_Min23-1)))-1).';

    mat_Last1234=reshape([mat_Result14(1:2,:);mat_Result23
                        ;mat_Result14(3:4,:)],1,2*num_length);
    clear mat_Result14 mat_Result23
    BERNIQOOptN(n,iSNR)=sum((num_Sent-mat_Last1234).^2)/4/2/num_length;
    SERNIQOOptN(n,iSNR)=sum(sum(reshape(((num_Sent-mat_Last1234).^2)
                        ,2,num_length),1)~=0,2)/(num_length);
    FERNIQOOptN(n,iSNR)=sum(sum(reshape(((num_Sent-mat_Last1234).^2)
                        ,2*framelength,num_length/framelength),1)~=0,2)
                         /(num_length/framelength);

    % Lambda1^(-1/2)
    mat_Lambda1=((mat_A-mat_B).*(2*num_Var^2)).^(-1/2);
    % lambda2^(-1/2)
    mat_Lambda2=((mat_A+mat_B).*(2*num_Var^2)).^(-1/2);

    % Elements of C1^(-1/2)  C11, C22
    mat_C11=(mat_Lambda1+mat_Lambda2).*(1/2);
    % Elements of C1^(-1/2)  C12, C21
    mat_C12=(mat_Lambda2-mat_Lambda1).*(1/2);

    % Elements of C2^(-1/2)  C211, C222
    mat_C211=mat_C11;
    % Elements of C2^(-1/2)  C212, C221
    mat_C212=-mat_C12;

    % Elements of H1
    mat_h1=mat_C11.*mat_A+mat_C12.*mat_B;
    mat_h2=mat_C12.*mat_A+mat_C11.*mat_B; %% h2
```

```
% Elements of H2
mat_h3=mat_C211.*mat_A-mat_C212.*mat_B;  %% h3
mat_h4=mat_C212.*mat_A-mat_C211.*mat_B;  %% h4

% Decorrelation
mat_D1p=mat_C11.*mat_D1+mat_C12.*mat_D4;
mat_D4p=mat_C12.*mat_D1+mat_C11.*mat_D4;
mat_D2p=mat_C211.*mat_D2+mat_C212.*mat_D3;
mat_D3p=mat_C212.*mat_D2+mat_C211.*mat_D3;

mat_a=sqrt((mat_h1.^2+mat_h2.^2));
mat_b=(mat_h1.*mat_h2).*2./mat_a;
mat_c=sqrt((mat_h2-(mat_b./(mat_a)).*mat_h1).^2
     +(mat_h1-(mat_b./(mat_a)).*mat_h2).^2);

mat_W1(1,1:2:num_length/2-1)=mat_h1./mat_a;
mat_W1(2,1:2:num_length/2-1)=mat_h2./mat_a;
mat_W1(1,2:2:num_length/2-0)=(mat_h2-(mat_b./(mat_a)).*mat_h1)./mat_c;
mat_W1(2,2:2:num_length/2-0)=(mat_h1-(mat_b./(mat_a)).*mat_h2)./mat_c;

% Inverse of W1
mat_W1Det(1:num_length/4)=mat_W1(1,1:2:num_length/2-1)
                          .*mat_W1(2,2:2:num_length/2-0)
                          -mat_W1(1,2:2:num_length/2-0)
                          .*mat_W1(2,1:2:num_length/2-1);
mat_W1Inv(1,1:2:num_length/2-1)=mat_W1(2,2:2:num_length/2-0)
                                ./mat_W1Det(1:num_length/4);
mat_W1Inv(2,1:2:num_length/2-1)=-mat_W1(2,1:2:num_length/2-1)
                                ./mat_W1Det(1:num_length/4);
mat_W1Inv(1,2:2:num_length/2-0)=-mat_W1(1,2:2:num_length/2-0)
                               ./mat_W1Det(1:num_length/4);
mat_W1Inv(2,2:2:num_length/2-0)=mat_W1(1,1:2:num_length/2-1)
                               ./mat_W1Det(1:num_length/4);

mat_d=sqrt((mat_h3.^2+mat_h4.^2));
mat_e=(mat_h3.*mat_h4).*2./mat_d;
mat_f=sqrt((mat_h4-(mat_e./(mat_d)).*mat_h3).^2
     +(mat_h3-(mat_e./(mat_d)).*mat_h4).^2);

mat_W2(1,1:2:num_length/2-1)=mat_h3./mat_d;
mat_W2(2,1:2:num_length/2-1)=mat_h4./mat_d;
mat_W2(1,2:2:num_length/2-0)=(mat_h4-(mat_e./(mat_d)).*mat_h3)./mat_f;
mat_W2(2,2:2:num_length/2-0)=(mat_h3-(mat_e./(mat_d)).*mat_h4)./mat_f;

% Inverse of W2
mat_W2Det(1:num_length/4)=mat_W2(1,1:2:num_length/2-1)
                          .*mat_W2(2,2:2:num_length/2-0)
                          -mat_W2(1,2:2:num_length/2-0)
                          .*mat_W2(2,1:2:num_length/2-1);
```

```
mat_W2Inv(1,1:2:num_length/2-1)=mat_W2(2,2:2:num_length/2-0)
                                ./mat_W2Det(1:num_length/4);
mat_W2Inv(2,1:2:num_length/2-1)=-mat_W2(2,1:2:num_length/2-1)
                                ./mat_W2Det(1:num_length/4);
mat_W2Inv(1,2:2:num_length/2-0)=-mat_W2(1,2:2:num_length/2-0)
                                ./mat_W2Det(1:num_length/4);
mat_W2Inv(2,2:2:num_length/2-0)=mat_W2(1,1:2:num_length/2-1)
                                ./mat_W2Det(1:num_length/4);

% Cancellation of W1 W2
mat_D1ppp=mat_W1Inv(1,1:2:num_length/2-1).*mat_D1p
         +mat_W1Inv(1,2:2:num_length/2-0).*mat_D4p;
mat_D4ppp=mat_W1Inv(2,1:2:num_length/2-1).*mat_D1p
         +mat_W1Inv(2,2:2:num_length/2-0).*mat_D4p;
mat_D2ppp=mat_W2Inv(1,1:2:num_length/2-1).*mat_D2p
        +mat_W2Inv(1,2:2:num_length/2-0).*mat_D3p;
mat_D3ppp=mat_W2Inv(2,1:2:num_length/2-1).*mat_D2p
        +mat_W2Inv(2,2:2:num_length/2-0).*mat_D3p;

for iQ34=1:4
 mat_Distance4(iQ34,:)=abs(mat_D4ppp-mat_Symbol4_34(1,iQ34)*mat_c).^2;
 mat_Distance3(iQ34,:)=abs(mat_D3ppp-mat_Symbol4_34(1,iQ34)*mat_f).^2;
end

[K,mat_Min4]=min(mat_Distance4,[],1);
[K,mat_Min3]=min(mat_Distance3,[],1);

mat_Min4Temp=num_SentDec(4:4:num_length);
mat_Min3Temp=num_SentDec(3:4:num_length-1);

S4ERNImprQuaOrSubOpt(n,iSNR)=sum((mat_Min4Temp-mat_Min4)~=0)
                             /(num_length/4);
S3ERNImprQuaOrSubOpt(n,iSNR)=sum((mat_Min3Temp-mat_Min3)~=0)
                             /(num_length/4);

for iQ12=1:4
 mat_Distance1(iQ12,:)=abs(mat_D1ppp-mat_b.*mat_Symbol4_34(1,mat_Min4)
                       -mat_Symbol4_12(1,iQ12)*mat_a).^2;
 mat_Distance2(iQ12,:)=abs(mat_D2ppp-mat_e.*mat_Symbol4_34(1,mat_Min3)
                       -mat_Symbol4_12(1,iQ12)*mat_d).^2;
end

[K,mat_Min1]=min(mat_Distance1,[],1);
[K,mat_Min2]=min(mat_Distance2,[],1);

mat_Min1Temp=num_SentDec(1:4:num_length-3);
mat_Min2Temp=num_SentDec(2:4:num_length-2);
```

```
S1ERNImprQuaOrSubOpt(n,iSNR)=sum((mat_Min1Temp-mat_Min1)~=0)
                             /(num_length/4);
S2ERNImprQuaOrSubOpt(n,iSNR)=sum((mat_Min2Temp-mat_Min2)~=0)
                             /(num_length/4);

    % When s_4 s_3 is Known
    for iQ12p=1:4
     mat_Distance1p(iQ12p,:)=abs(mat_D1ppp-mat_b
                             .*mat_Symbol4_34(1,mat_Min4Temp)
                             -mat_Symbol4_12(1,iQ12p)*mat_a).^2;
     mat_Distance2p(iQ12p,:)=abs(mat_D2ppp-mat_e
                             .*mat_Symbol4_34(1,mat_Min3Temp)
                             -mat_Symbol4_12(1,iQ12p)*mat_d).^2;
    end

    [K,mat_Min1p]=min(mat_Distance1p,[],1);
    [K,mat_Min2p]=min(mat_Distance2p,[],1);

    S1pERNImprQuaOrSubOpt(n,iSNR)=sum((mat_Min1Temp-mat_Min1p)~=0)
                                  /(num_length/4);
    S2pERNImprQuaOrSubOpt(n,iSNR)=sum((mat_Min2Temp-mat_Min2p)~=0)
                                  /(num_length/4);

    mat_QRResult1234=2*reshape(fliplr(de2bi([mat_Min1;
                               mat_Min2;mat_Min3;mat_Min4]-1)).',
                               1,2*num_length)-1;
    BERNImprQuaOrSubOpt(n,iSNR)=sum((num_Sent-mat_QRResult1234).^2)
                                /8/num_length;
    SERNImprQuaOrSubOpt(n,iSNR)=sum(sum(reshape(((num_Sent
                                -mat_QRResult1234).^2),2,num_length),1)
                                ~=0,2)/(num_length);
    FERNImprQuaOrSubOpt(n,iSNR)=sum(sum(reshape(((num_Sent
                                -mat_QRResult1234).^2),2*framelength,
                                num_length/framelength),1)~=0,2)
                               /(num_length/framelength);
   end
  end
  BERNIQOOptM(m,:)=sum(BERNIQOOptN,1)/n;
  SERNIQOOptM(m,:)=sum(SERNIQOOptN,1)/n;
  FERNIQOOptM(m,:)=sum(FERNIQOOptN,1)/n;

  S4ERM(m,:)=sum(S4ERNImprQuaOrSubOpt)/n;
  S3ERM(m,:)=sum(S3ERNImprQuaOrSubOpt)/n;
  S2ERM(m,:)=sum(S2ERNImprQuaOrSubOpt)/n;
  S1ERM(m,:)=sum(S1ERNImprQuaOrSubOpt)/n;

  S2pERM(m,:)=sum(S2pERNImprQuaOrSubOpt)/n;
  S1pERM(m,:)=sum(S1pERNImprQuaOrSubOpt)/n;
```

```
  BERMSub(m,:)=sum(BERNImprQuaOrSubOpt,1)/n;
  SERMSub(m,:)=sum(SERNImprQuaOrSubOpt,1)/n;
  FERMSub(m,:)=sum(FERNImprQuaOrSubOpt,1)/n;

save rsimul0119.mat m n BERNIQOOptM SERNIQOOptM FERNIQOOptM
                  S1ERM S2ERM S3ERM S4ERM S2pERM S1pERM BERMSub
                  SERMSub FERMSub GAMAbforAll mat_RootCorrl
end BERNIQOOpt=sum(BERNIQOOptM,1)/m;
SERNIQOOpt=sum(SERNIQOOptM,1)/m; FERNIQOOpt=sum(FERNIQOOptM,1)/m;

BERImprQuaOrSubOpt=sum(BERMSub,1)/m;
SERImprQuaOrSubOpt=sum(SERMSub,1)/m;
FERImprQuaOrSubOpt=sum(FERMSub,1)/m;

SERS1p=sum(S1pERM,1)/m; SERS2p=sum(S2pERM,1)/m;
SERS1=sum(S1ERM,1)/m; SERS2=sum(S2ERM,1)/m; SERS4=sum(S4ERM,1)/m;
SERS3=sum(S3ERM,1)/m;

% Plot
semilogy(GAMAbforAll,BERNIQOOpt,'r',GAMAbforAll,BERImprQuaOrSubOpt,'r',
         GAMAbforAll,FERNIQOOpt,'b',GAMAbforAll,FERImprQuaOrSubOpt,'b',
         GAMAbforAll,SERNIQOOpt,'k',GAMAbforAll,SERImprQuaOrSubOpt,'k');
figure; semilogy(GAMAbforAll,SERS1,'r',GAMAbforAll,SERS2,'b',
        GAMAbforAll,SERS3,'k',GAMAbforAll,SERS4,'g',
        GAMAbforAll,SERS1p,'c',GAMAbforAll,SERS2p,'m')
grid
```

Appendix C

Numerical Evaluation Software

C.1 Numerical Evaluation of Error Probability of Decoding s_4

program C.1.1 Numerical Evaluation of Error Probability of Decoding s_4

```
clear all;
GAMAb=[0:2:30]; %SNR Range
% Upper Bound
for iSNR=1:length(GAMAb)
    M=2;
    phi=pi/2;   %Phi
    part1=phi/pi;
    part2=0;
    part3=0;
    var=(10^(-GAMAb(iSNR)/10))/4; %sigma^2
    c=1/(16*var);                 % c
    N=2*sqrt(c*(1+c))*sin(2*phi); % N
    D=(1+2*c)*cos(2*phi)-1;       % D
    T=0.5*atan(N/D)+(pi/2)*(1-((1+sign(D))/2)*sign(N)); %T
    for k1=0:M-1
        part2=part2
         +(factorial(2*k1)/factorial(k1)/factorial(k1))/((4+4*c)^(k1));
    end
    part2=part2*T*sqrt(c/(1+c))/pi;
```

```
    for k2=1:M-1
        for j=0:k2-1
            part3=part3+(factorial(2*k2)/factorial(2*k2-j)/factorial(j))
                *(-1)^(k2+j)*sin(2*T*(k2-j))/((4+4*c)^(k1))/(2*k2-2*j);
        end
    end
    part3=part3*2*sqrt(c/(1+c))/pi;
    EQ(iSNR)=part1-part2-part3;
    SER11(iSNR)=-EQ(iSNR).^2+2*EQ(iSNR);
end
for iSNR=1:length(GAMAb)
    M=3;
    phi=pi/2;   %Phi
    part1=phi/pi;
    part2=0;
    part3=0;
    var=(10^(-GAMAb(iSNR)/10))/4; %sigma^2
    c=1/(16*var);                 % c
    N=2*sqrt(c*(1+c))*sin(2*phi); % N
    D=(1+2*c)*cos(2*phi)-1;       % D
    T=0.5*atan(N/D)+(pi/2)*(1-((1+sign(D))/2)*sign(N)); %T
    for k1=0:M-1
        part2=part2
            +(factorial(2*k1)/factorial(k1)/factorial(k1))/((4+4*c)^(k1));
    end
    part2=part2*T*sqrt(c/(1+c))/pi;
for k2=1:M-1
        for j=0:k2-1
            part3=part3+(factorial(2*k2)/factorial(2*k2-j)/factorial(j))
                *(-1)^(k2+j)*sin(2*T*(k2-j))/((4+4*c)^(k1))/(2*k2-2*j);
        end
    end
    part3=part3*2*sqrt(c/(1+c))/pi;
    EQ(iSNR)=part1-part2-part3;
    SER12(iSNR)=-EQ(iSNR).^2+2*EQ(iSNR);
end SER1=(SER11+SER12)/2;
% Lower Bound
for iSNR=1:length(GAMAb)
    M=2;
    phi=pi/2;   %Phi
    part1=phi/pi;
    part2=0;
    part3=0;
    var=(10^(-GAMAb(iSNR)/10))/4; %sigma^2
```

```
    c=1/(8*var);                    % c
    N=2*sqrt(c*(1+c))*sin(2*phi); % N
    D=(1+2*c)*cos(2*phi)-1;        % D
    T=0.5*atan(N/D)+(pi/2)*(1-((1+sign(D))/2)*sign(N)); %T
    for k1=0:M-1
        part2=part2
             +(factorial(2*k1)/factorial(k1)/factorial(k1))/((4+4*c)^(k1));
    end
    part2=part2*T*sqrt(c/(1+c))/pi;
    for k2=1:M-1
        for j=0:k2-1
             part3=part3+(factorial(2*k2)/factorial(2*k2-j)/factorial(j))
                   *(-1)^(k2+j)*sin(2*T*(k2-j))/((4+4*c)^(k1))/(2*k2-2*j);
        end
    end
    part3=part3*2*sqrt(c/(1+c))/pi;
    EQ(iSNR)=part1-part2-part3;
    SER21(iSNR)=-EQ(iSNR).^2+2*EQ(iSNR);
end for iSNR=1:length(GAMAb)
    M=3;
    phi=pi/2;   %Phi
    part1=phi/pi;
    part2=0;
    part3=0;
    var=(10^(-GAMAb(iSNR)/10))/4; %sigma^2
    c=1/(8*var);                    % c
    N=2*sqrt(c*(1+c))*sin(2*phi); % N
    D=(1+2*c)*cos(2*phi)-1;        % D
    T=0.5*atan(N/D)+(pi/2)*(1-((1+sign(D))/2)*sign(N)); %T
   for k1=0:M-1
        part2=part2
            +(factorial(2*k1)/factorial(k1)/factorial(k1))/((4+4*c)^(k1));
    end
    part2=part2*T*sqrt(c/(1+c))/pi;
    for k2=1:M-1
        for j=0:k2-1
             part3=part3+(factorial(2*k2)/factorial(2*k2-j)/factorial(j))
                  *(-1)^(k2+j)*sin(2*T*(k2-j))/((4+4*c)^(k1))/(2*k2-2*j);
        end
    end
    part3=part3*2*sqrt(c/(1+c))/pi;
    EQ(iSNR)=part1-part2-part3;
    SER22(iSNR)=-EQ(iSNR).^2+2*EQ(iSNR);
end SER2=(SER21+SER22)/2;
%Plot
semilogy(GAMAb,SER1,GAMAb,SER2) grid
```

C.2 Numerical Evaluation of Error Probability of Decoding s_1 Assuming s_4 Has Been Decoded Correctly

program C.2.1 Numerical Evaluation of Error Probability of Decoding s_1 Assuming s_4 Has Been Decoded Correctly

```
clear all; M=4;
GAMAb=[0:2:30]; %SNR Range
for iSNR=1:length(GAMAb)
    phi=pi/2;   %Phi
    part1=phi/pi;
    part2=0;
    part3=0;
    var=(10^(-GAMAb(iSNR)/10))/4; %sigma^2
    c=1/(16*var);                 % c
    N=2*sqrt(c*(1+c))*sin(2*phi); % N
    D=(1+2*c)*cos(2*phi)-1;       % D
    T=0.5*atan(N/D)+(pi/2)*(1-((1+sign(D))/2)*sign(N)); %T
    for k1=0:M-1
        part2=part2+
          (factorial(2*k1)/factorial(k1)/factorial(k1))/((4+4*c)^(k1));
    end
    part2=part2*T*sqrt(c/(1+c))/pi;
    for k2=1:M-1
        for j=0:k2-1
            part3=part3+(factorial(2*k2)/factorial(2*k2-j)
                /factorial(j))*(-1)^(k2+j)
                *sin(2*T*(k2-j))/((4+4*c)^(k1))/(2*k2-2*j);
        end
    end
    part3=part3*2*sqrt(c/(1+c))/pi;
    EQ(iSNR)=part1-part2-part3;
    SER(iSNR)=-EQ(iSNR).^2+2*EQ(iSNR);
end Plot semilogy(GAMAb,SER,'k') grid
```

References

[1] T.Ojanpera and R.Prasad, *An Overview of Third-Generation Wireless Personal Communications: A European Perspective*, IEEE Personal Communications, Vol.5, No.6, pp. 59-65, December, 1998.

[2] D.Gesbert, L.Haumonte, H.Bölcskei, R.Krishnamoorthy, and A.J.Paulraj, *Technologies and Performance for Non-Line-of-Sight Broadband Wireless Access Networks*, IEEE Communications Magazine, Vol.40, No.4, pp. 86-95, April, 2002.

[3] N.Al-Dhahir, C.Fragouli, A.Stamoulis, W.Younis and R.Calderbank, *Space-Time Processing for Broadband Wireless Access*, IEEE Communications Magazine, Vol.40, No.9, pp. 136-142, September, 2002.

[4] S.D.Blostein and H.Leib, *Multiple Antenna Systems: Their Role and Impact in Future Wireless Access*, IEEE Communications Magazine, Vol.41, No.7, pp. 94-101, July, 2003.

[5] V.Tarokh, N.Seshadri and A.R.Calderbank, *Space-Time Codes for High Data Rate Wireless Communication: Performance Criterion and Code Construction*, IEEE Transactions on Information Theory, Vol.44, No.2, pp. 744-765, March, 1998.

[6] P.W.Wolniansky, G.J.Foschini, G.D.Golden and R.A.Valenzuela, *V-BLAST: An Architecture for Realizing Very High Data Rates Over the Rich-Scattering Wireless Channel*, Signals,

Systems, and Electronics, 1998. ISSSE 98. 1998 URSI International Symposium on, pp. 295-300, September - October, 1998.

[7] V.Tarokh, H.Jafarkhani and A.R.Calderbank, *Space-Time Block Codes from Orthogonal Designs*, IEEE Transactions on Information Theory, Vol.45, No.5, pp. 1456-1467, July, 1999.

[8] C.Heegard and S.B.Wicker, *Turbo Coding*, Kluwer Academic Publishers, Boston, MA, 1999.

[9] A.Paulraj, *MIMO Wireless for Fixed Broadband Service*, Communications and Vehicular Technology, 2000. SCVT-200. Symposium on, pp. 263-297, October, 2000.

[10] X.Lin and R.S.Blum, *Improved Space-Time Codes Using Serial Concatenation*, IEEE Communications Letters, Vol.4, Issue 7, pp. 221-223, March, 2000.

[11] J.D.Terry and J.T.Heiskala *Spherical Space-Time Codes (SSTC)*, IEEE Communications Letters, Vol.5, Issue 3, pp. 107-109, March, 2001.

[12] H.E.Gamal and A.R.Hammons Jr., *On the Design and Performance of Algebraic Space-Time Codes for BPSK and QPSK Modulation*, IEEE Transactions on Communications, Vol.50, Issue 6, pp. 907-913, June, 2002.

[13] E.Biglieri, G.Taricco and A.Tulino, *Performance of Space-Time Codes for a Large Number of Antennas*, IEEE Transactions on Information Theory, Vol.48, Issue 7, pp. 1794-1803, July, 2002.

[14] D.M.Ionescu, *On Space-Time Code Design*, IEEE Transactions on Wireless Communications, Vol.2, Issue 1, pp. 20-28, January, 2003.

[15] G.Caire and G.Colavolpe, *On Low-Complexity Space-Time Coding for Quasi-Static Channels*, IEEE Transactions on Information Theory, Vol.49, Issue 6, pp. 1400-1416, June, 2003.

[16] E.Telatar, *Capacity of Multi-antenna Gaussian Channels*, AT&T Bell Labs, Tech. Rep., June, 1995.

[17] G.J. Foschini and M.J.Gans, *On Limits of Wireless Communications in a Fading Environment when Using Multiple Antennas*, Wireless Pers. Commun., Vol.6, pp. 311-335, 1998.

[18] S.Alamouti, *A Simple Transmit Diversity Technique for Wireless Communication*, IEEE Journal on Select Areas in Communications, Vol.16, No.8, pp. 1451-1458, July, 1998.

[19] A.V.Geramita and J.Seberry, *Orthogonal Design, Quadratic Forms and Hadamard Matrices*, Lecture Notes in Pure and Applied Mathematics, Vol.43. New York and Basel: Marcel Dekker,1979.

[20] J.F.Adams,P.D.Lax and R.S.Phillips, *On matrices whose real linear combinations are non-singular*, in Proc. Amer. Math. Soc., Vol. 16, pp. 945-947, 1965.

[21] J.Radon, *Lineare scharen orthogonaler matrizen*, Abhandlungen aus dem Mathematischen Seminar der Hamburgishen Universität, Vol. I, pp. 1-14, 1922.

[22] A.Hurwitz, *Über die Komposition der quadratischen Formen*, Math. Ann., Vol. 88, pp. 1-25, 1923.

[23] G.Ganesan and P.Stoica, *Space-Time Block Codes: A Maximum SNR Approach*, IEEE Transactions on Information Theory, Vol.47, No.4, pp. 1650-1656, November, 2003.

[24] O.Tirkkonen, A.Boariu and A.Hottinen, *Tradeoffs Between Rate, Puncturing and Orthogonality in Space-Time Block Codes*, Communications, IEEE International Conference on, Vol.4, pp. 1117-1121, June, 2001.

[25] X.Liang, *Orthogonal Designs With Maximal Rates*, IEEE Transactions on Information Theory, Vol.49, No.10, pp. 2468-2503, October, 2003.

[26] X.Liang and X.Xia, *On the Nonexistence of Rate-One Generalized Complex Orthogonal Designs*, IEEE Transactions on Information Theory, Vol.49, No.11, pp. 2984-2988, November, 2003.

[27] O.Tirkkonen, A.Boariu and A.Hottinen, *Minimal non-orthogonality rate 1 space-time block code for 3+ antennas*, Spread Spectrum Techniques and Applications, 2000 IEEE Sixth International Symposium on, Vol.2, pp. 429-432, September, 2000.

[28] H.Jafarkhani, *A Quasi-Orthogonal Space-Time Block Code*, IEEE Transactions on Communications, Vol.9, No.1, pp. 42-45, January, 2001.

[29] N.Sharma and C.B.Papadias, *Improved Quasi-Orthogonal Codes Through Constellation Rotation*, IEEE Transactions on Communications, Vol.51, No.3, pp. 332-335, March, 2003.

[30] M. Pohst, *On the computation of lattice vectors of minimal length, successive minima and reduced basis with applications*, ACM SIGSAM Bull., Vol. 15, pp. 37C44, 1981.

[31] O.Damen, A.Chkeif and J.C.Belfiore, *Lattice Code Decoder for Space-Time Codes*, IEEE Communications Letters, Vol. 4, No. 5, MAY, 2000.

[32] B.Noble and J.W.Daniel, *Applied Linear Algebra 3rd Edition*, pp. 236-239, Prentice Hall, 1998.

[33] A.M.Mathai and Serge.B.Provost, *Quadratic Forms in Random Variables* Marcel Dekker, 1992.

[34] G.L.Turin, *The characteristic function of Hermitian quadratic forms in complex normal variables* Biometrika Vol. 47, pp. 199-201 1960.

[35] F.Oberhettinger, *Table of Fourier Transforms and Fourier Transforms of Distributions* Springer-Verlag, 1990.

[36] A.Papoulis and S.U.Pillai, *Probability, Random Variables, and Stochastic Processes 4th Edition* McGraw-Hill Education, 2002.

[37] M.K.Simon and M.Alouini, *Digital Communication over Fading Channels, A Unified Approach to Performance Analysis*, pp. 198, John Wiley & Sons, Inc. 2000.

[38] A.Browder, *Mathematical Analysis: An Introduction* Springer-Verlag, 1996.

[39] G.Ryzhik, *Tables of Integrals, Series, and Products*, Academic Press, Inc. 1980.

[40] Craig.J.W, *A New Simple and Exact Result for Calculating the Probability of Error for Two-Dimensional Signal Constellations*, IEEE MILCOM'91 Conf. Record, Boston, pp. 25.5.1-25.5.5, 1991.

[41] W.C.Jakes, *Micorwave Mobile Communications*, New York: Wiely, 1974, pp. 60-65.

[42] D.Shiu, G.J.Foschini, M.J. Gans and J.M. Kahn, *Fading Correlation and Its Effect on the Capacity of Multielement Antenna Systems*, IEEE Transactions on Communications, Vol.48, NO.3 pp. 502-513, March, 2000.

[43] E.Kreyszig, *Advanced Engineering Mathematics 7th Edition* pp. 837-844 John Wiley & Sons, Inc. 1993.